ISSN 1810-0384

ADVANCES IN ELECTROMETALLURGY

No. 1 Volume 8 2010

CAMBRIDGE INTERNATIONAL SCIENCE PUBLISHING

Advances in Electrometallurgy is a cover-to-cover English translation of *Sovremennaya Elektrometallurgiya*, published four times a year by International Association 'Welding' at the E.O. Paton Electric Welding Institute, National Academy of Sciences of Ukraine, 11 Bozhenko Street, 03680 Kyiv, Ukraine

Published by

Cambridge International Science Publishing Ltd
7 Meadow Walk, Great Abington, Cambridge CB21 6AZ, England
Tel: +44 (0) 1223 893295; Fax: +44 (0) 1223 894539
email: cisp@cisp-publishing.com; http://www.cisp-publishing.com

Advances in Electrometallurgy 2010 ***8*** *(1) 5–9*
Translated from Sovremennaya Elektrometallurgiya 2010 ***8*** *(1) 8–11*

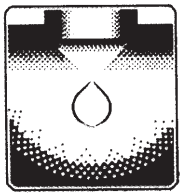

ELECTROSLAG TECHNOLOGY

Selecting fluxes for arc slag remelting in production of titanium billets

L.B. Medovar, V.Ya. Saenko and V.A. Ryabinin

E.O. Paton Electric Welding Institute, Kiev

The specifics of selection of flux systems for producing titanium ingots by the ASR method is considered. The data obtained in experimental ASR melts using salt compositions are presented.

The method of arc slag remelting (ASR), developed at the E.O. Paton Electric Welding Institute, Kiev in the 1970s [1], combines the treatment of molten metal with the electric arc, burning in a controlled gas atmosphere and in a liquid synthetic slag through each of the current passes in the process of remelting of the consumable electrode. The layer of the synthetic slags, covering the metallic pool, results in the de-concentration of heat of the cross-section of the pool and reduces the depth of the metal pool making it flatter in comparison with vacuum-arc (VAR) and electron beam remelting (EBR). In addition, as a result of the formation of the slag skull, the billets produced by ASR in contrast to VAR are characterised by a smooth side surface and no machining is required prior to subsequent processing.

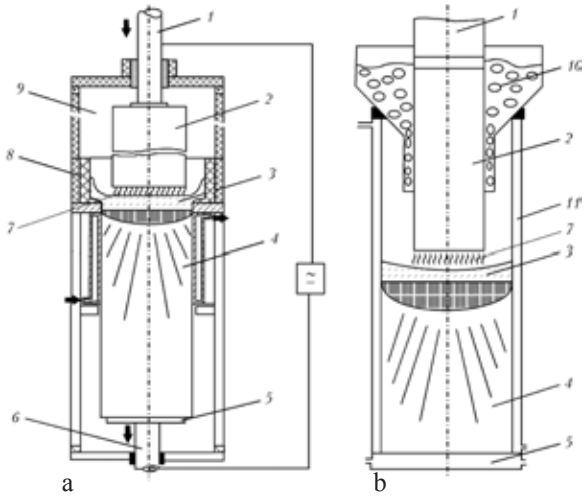

Fig. 1. Technology of ASR in a chamber furnace with withdrawal of the billet from a short solidification mould (a) and in a conventional ESR furnace in a stationary solidification mould using a flux gate (b): 1) the head of the consumable electrode, 2) the consumable electrode, 3) the slag pool, 4) the billet, 5) the water-cooled baseplate, 6) the mechanism for withdrawing the billet from the solidification mould, 7) the arc, 8) the lined slag attachment, 9) the furnace chamber, 10) the flux gate, 11) water-cooled solidification mould.

To apply the method of ASR to the production of titanium billets, it was necessary to ensure isolation of the arc from contact with air and produce a controlled gas atmosphere in the arcing zone. It was also necessary to reduce the cost of titanium and its alloys and made them fully capable of competition with stainless nickel-containing steels and alloys [2, 3].

Two methods were tested (Fig. 1): ASR using a flux gate – the simplest device placed directly on the upper end of the solidification mould; ASR in a chamber furnace.

In the latter case, experiments were carried out with the existing furnaces for vacuum-arc remelting with the vacuum system switched off and also in specially designed chamber furnaces for ASR in which the process can be realised in a controlled gas atmosphere.

In ASR, the electric arc burns in a shielding gas or slag vapours. The presence of the slag vapours, containing chemical elements with low ionisation potentials, results in the stabilisation and stable burning of the arc. In contrast to VAR, in ASR the metallic corona does not form on the billet. This is explained by the fact that in ASR the metal splashes (small droplets) fall either into the slag pool or the edge of the slag, distributed around the perimeter of the slag pool.

The depth of the metal pool in melting the billets by ASR is smaller in comparison with EBR and the pool is flatter. This is explained by the fact that the surface of the pool is heated more uniformly. The dissipation of heat through the pool is also supported by the transfer of droplets into the pool by several flows throughout the entire cross-section of the electrode.

In ASR the surface of the liquid slag pool is one of the electrodes. The slag pool is an electrolyte melt with a large number of complex and simple ions. The temperature of the slag pool may reach 2000°C. Some components of the slag evaporate at these temperatures, others breakup (dissociate) into the component ions and in this form may take part in the current transfer process. However, since the temperature of the arc discharge is considerably higher than the temperature of the slag pool, the intensity of the evaporation, dissociation and ionisation processes is greatly higher in this case.

It should be mentioned that the components included in the composition of ASR slags exert different effects on the arcing conditions. The positive effect is exerted by alkali and alkali-earth metals with a low ionisation potential [4–7]. They are easily ionised, form cations and free electrons which take part subsequently in charge transfer.

The total ionisation potential of a mixture of different gases and vapours, present in ASR, is determined by the component with the lowest ionisation potential and depends on the concentration of this component.

For example, the ionisation potentials of potassium, sodium, calcium and argon are equal to 4.33, 5.11, 6.10 and 15.7 V. Thus, the chemical composition of the fluxes has a strong effect on the electrical characteristics of the process (stability of arcing, the height of ignition peaks, the presence of breaks in the current curve, open circuit voltage of the power source, etc).

The presence of easily ionised elements in the slag results in a large decrease of the voltage gradient in the arc column, increase of the strength of the effect of elements with low ionisation potential on the effective ionisation potential of the gas mixture. The latter tends to the potential of the most easily ionised element in the arc atmosphere.

In most cases, ASR of titanium is carried out using ESR (electroslag remelting) fluxes, containing CaF_2 and a number of halides of alkali and rare-earth materials (Table 1). The role of the fluxes in ASR slightly differs from the conventional role of the refining component in ESR and ASR of steels and iron-based alloys. The role of the slag as the heat carrier is almost completely balanced.

The main zone of energy generation is the arc. The investigations, including those carried out in the plant conditions [4], show that in comparison with ESR, ASR used in melting of billets of steels and alloys reduces the consumption of energy by a factor of 1.5 and also halves the requirement on the synthetic flux per 1 t of metal.

The main functions of the slag in ASR of titanium, in addition to stabilising the arc, include the formation of the surface, formation of a skull layer, protection of the metal against the surrounding atmosphere, formation of a protective condensate coating on the consumable electrode. If the flux composition is correctly selected, slag regeneration may take place.

Electroslag metal with a homogeneous chemical composition is produced using fluxes

not containing the oxides of easily reduced elements of chromium, manganese, silicon, etc. Special attention has been paid to fluorides used as components of the flux. However, some of these compounds (fluorides of lithium, potassium, sodium) are characterised by high conductivity and susceptibility to the formation of complex compounds with titanium, chromium, zirconium, etc.

As a result of the low melting and boiling point of the chlorides of alkali-earth metals which is lower than that of the identical fluorides, the majority of them cannot be used as the base of the flux in ASR. In addition, some of these compounds (for example, potassium chloride) are susceptible to hydration [8]. The properties of the compounds, included in the fluxes, are shown in Table 1.

The highest chemical activity in relation to the molten metal and the simplest structure are typical of salt slags. They do not contain any oxides contaminating the metal with non-metallic inclusions and oxidising the metal.

In the middle of the 1950s, B.I. Medovar and S.M. Gurevich proposed for the first time in the world and used halide-type fluxes for welding of high-alloyed steels, with the fluxes containing no oxidation compounds [3]. The boiling point of the flux should be sufficiently high (not lower than 2000°C) to ensure that the slags can be superheated above the melting point of titanium. The basic component of these fluxes is CaF_2.

Table 1. Properties of the materials used for flux compositions in ASR titanium [8]

Component	Temperature, °C		Density, g/cm³, at T, °C		
	melting	boiling	20	$1000/T_m$	$1000/T_{boil}$
LiCl	606	1382	—	1.50	1.33
LiF	842	1676	1.80	1.73	–
MgF2	1263	2227	3.14	—	2.19
CaF2	1418	2500	3.20	2.60	2.40
SrCl	868	1950	3.20	2.70	2.65
SrF2	1486	2477	4.24	—	3.28
BaCl2	958	1560	3.14	3.11	—
BF2	1320	2200	4.91	4.22	3.78
NaF	995	1700	1.963	1.96	–
NaCl	800	1440	—	1.42 1.55	–
YF3	1152	2227	5.07	—	–
LaF3	1493	2327	5.94	—	4.43
AlF3	1040	1260	—	—	–
Na_3AlF_6	1000		—	3.036 3.036	–
Ti	1671	3260	4.54	—	4.08

One of the first welding fluxes based on CaF_2 was ANF-1, i.e., fluorspar refined to the required grain size and baked at a high temperature. Similar fluxes appeared abroad and were used only after a delay of a number of years. Almost immediately the fluoride fluxes were also used in ESR of steels alloyed with easily oxidised elements. The experimental investigations, carried out at the E.O. Paton Electric Welding Institute, show that the flux for ESR of titanium can consist of special purity refractory fluorides of alkali-earth metals: calcium fluoride, strontium fluoride and barium fluoride [5], and also the fluorides of rare-earth metals (FREM) based on LaF_4. The fluorides of alkali-earth metals are characterised by high melting (more than 1200°C) and boiling (higher than 2200°C) points. The fluxes based on CaF_2 were tested experimental conditions for ASR of titanium: CaF_2–FREM; CaF_2–BaF_2CaCl_2; CaF_2–BaF_2–$CaCl_2$–SrF_2. They are also used efficiently for the production of titanium billets by ASR.

The new possibilities of producing defect-free titanium billets by ASR are offered by a new method developed on the basis of the application of a current-conducting solidification mould combined with active slags, containing metallic calcium. Consequently, hard high-nitrogen inclusions, if they are present in the consumable electrodes, can be dissolved to a greater extent during remelting.

However, according to [5], this method can be applied only in a chamber furnace with a controlled atmosphere and using new flux compositions because the method is associated with the problems with withdrawal of the billets and, in addition to this, there are new requirements on the fluxes used. New data on the application of chamber furnaces

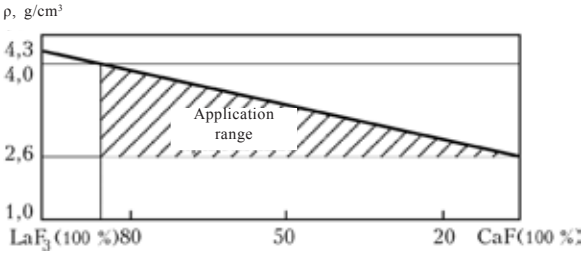

Fig. 2. Region of application of the flux based on FREM compounds and CaF_2 for the ASR process.

Fig. 3. A flux gate with a device for blowing with argon.

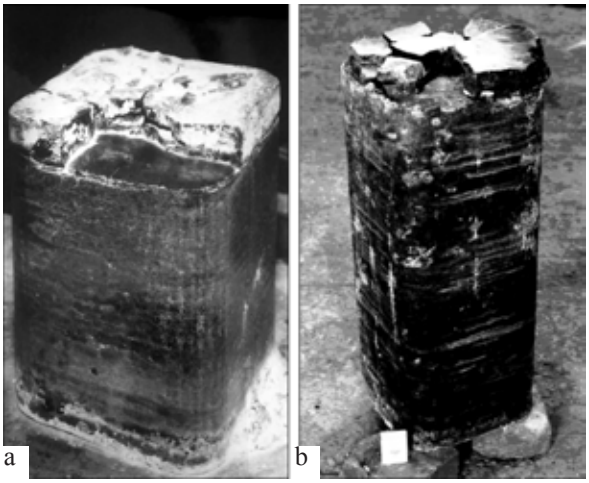

Fig. 4. Titanium ASR ingots produced from VT1-0 titanium with a square cross-section of 200 × 200 mm, melted under CaF_2 (a) and CaF_2+FREM (b) fluxes.

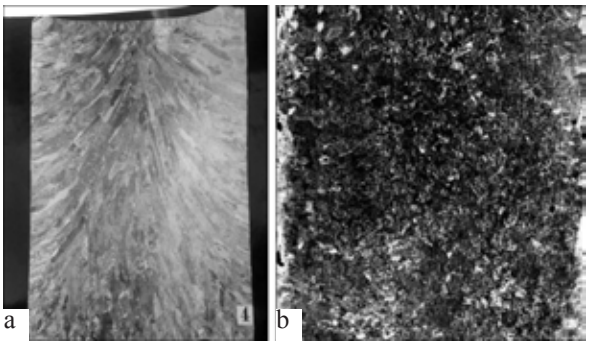

Fig. 5. Templates of ASR billets of VT1-0 titanium produced using fluxes CaF_2 (a) and CaF_2+ FREM (b).

in the production of titanium billets were published in [6, 7].

When using FREM as flux components, it is necessary to calculate accurately the density of the produced flux compositions, otherwise the density of the slag is higher than the density of the metal. The nomogram for the application of FREM and calcium fluoride is shown in Fig. 2. The nomogram was spotted using the experimental results obtained and the E.O. Paton Electric Welding Institute, Kiev with the application of FREM in the production of ASR titanium billets.

ASI was used for producing a pilot-plant batch of billets of VT1-0 titanium using new flux compositions. ASR was carried out in a R-951 furnace using stationary solidification moulds with the square cross-section of 200 × 200 mm with a flux gate. The flux was poured in through a siphon. The melting zone was shielded with a flux gate and by argon blowing (Fig. 3). After removing the slag skull, the billets were characterised by a satisfactory surface. The external appearance of the produced ASI billets is shown in Fig. 4. The results of chemical analysis of the produced metal are presented in Table 2.

The hardness HB of the ASR metal, melted using the flux with the FREM addition, is higher than that produced using pure CaF_2, evidently as a result of the alloying of titanium with rare-earth metals leading to the production of these elements from the slag during ASR.

Figure 5 shows fragments of the longitudinal macrosections of the upper part of the ASR billets, melted in accordance with the technological conditions of the melts No. 1 and 2, and also the external appearance

Table 2. Results of ASR of VT1-0 titanium in a square solidification mould 200×200 mm with a flux gate

Melt No.	Electrical regime of melt		Flux	[O], %			[N], %			Hardness, HB		
	I, kA	*U*, V		Bottom	Middle	Top	Bottom	Middle	Top	Bottom	Middle	Top
1	3.0	98	CaF_2	0.097	0.08	0.12	0.021	0.024	0.025	133	135	139
2	2.5	100	CaF_2+FREM (30%)	0.099	0.10	0.11	0.030	0.030	0.035	151	152	157

Comment. According to the requirements of GOST 19807-77, the oxygen content of VT1-0 is ≤0.12%

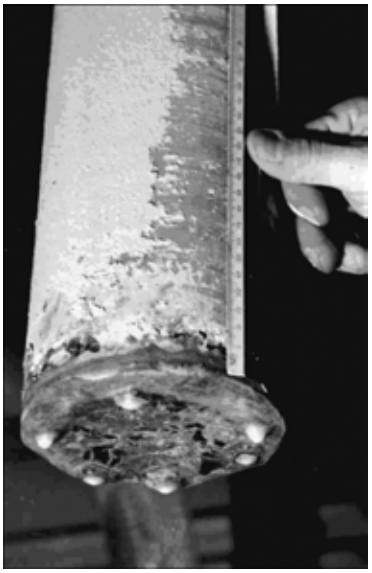

Fig. 6. The end of a consumable electrode with a diameter of 10 mm, VT1-0 titanium, after melting.

of the end of a consumable electrode after completing melting. Melting of the electrode is characterised by the distinctive uniform droplet formation of the metal throughout the entire cross-section of the electrode (Fig. 6).

The experimental results show that the production of the titanium billets by the ASI method may be realised in the existing ESR furnaces using conventional ESR solidification moulds, fitted with a flux gate. The application of fluxes with the additions of FREM (up to 30%) in ASR titanium results in the high quality of the billets surface and a high density macrostructure with no defects.

References

1. Paton B.E., et al., A method of remelting consumable electrode, Author's Cert. No. 520784, SSSR, MPK S 21 c 5/56, 07.07.82.
2. Paton B.E., et al., Probl. Spets. Elektrometall., 1995, No. 4, 3–6.
3. Medovar B.I. and Gurevich S.M., Avt Svarka, 1955, 31–41.
4. Paton B.E., et al., Probl. Spets. Elektrometall., 2000, No. 4, 18–20.
5. Medovar L.B., et al., Probl. Spets. Elektrometall., 2000, No. 4, 80–29.
6. Troyanskii A.A. and Ryabtsev A.D., Elektrometallurgiya, 2005, No. 1, 11–17.
7. Troyanskii A.A. and Ryabtsev A.D., Lit. Proiz., 2007, No. 1, 11–17.
8. Gurevich S.M., et al., Production of ingots and cast billets from titanium alloys by electroslag remelting, in: Electroslag remelting, Proceedings of the Second national conference on electroslag remelting, Metallurgiya, Moscow, 1964, 184–188.

Advances in Electrometallurgy 2010 ***8*** *(1) 10–13*
Translated from Sovremennaya Elektrometallurgiya 2010 ***8*** *(1) 12–14*

Special features of equipment for the continuous production of centrifugal electroslag castings

S.V. Skripnik

Titan NPF Company, Kiev

New design solutions of a system for centrifugal electroslag casting for continuous production of centrifugal electroslag castings are described. A 3 t furnace is equipped with a mechanism for rotating non-consumable electrodes. If necessary, they occupy periodically the working position during heating of slag and metal pools, and then they are removed from the melting zone. Their place is occupied by consumable electrodes. Metal with slag is poured periodically into a rotary mould of the centrifugal machine of a new design.

The method of centrifugal electroslag casting (CESC) with the vertical axis of rotation, developed at the E.O. Paton Electric Welding Institute, can be used to produce cast billets of high-quality with the properties not inferior to those of forgings [1, 2]. The advantages of the method in comparison with the deformation production methods include the possibility of producing large and shaped billets from steels and alloys, including from alloys with low deformability.

As a result of the relatively simple procedure, the method is used on an increasing scale in engineering production. At the same time, the productivity of this method is considerably lower than that of the deformation methods as a result of both the specific features and existing practice with the production of a single casting from a single melt which delays the application of the method in series production.

To increase the productivity of the process and, consequently, reduce the cost of production of the billets, it is necessary to change the nature of production in transition to semi-continuous or continuous casting. This production can be realised using the CESC complex fitted with an electroslag furnace with non-consumable and consumable electrodes [3]. In this system, the consumable electrodes can be replaced during melting.

The concept of the construction of electroslag furnaces with the replacement of consumable electrodes during melting with preheating of the lower ends of the changeable electrodes, immersed in the slag pool, has been included in a number of foreign and domestic electroslag remelting furnaces [4]. However, these furnaces are unjustifiably cumbersome and expensive. At the same time, the problem of producing defect-free billets in the ESR furnaces with the change of the consumable electrodes has not been completely solved.

Many investigators oppose even short-term breaks in supply of energy into the slag pool which are unavoidable in operation with the replacement of the electrodes during melting, assuming that even short-term disruptions of the heat balance in ESR which leads to the formation of micro- and macrosegregation bands in the billets have a detrimental effect on the fatigue strength of the metal containing these defects [4].

Since the CESC processes use crucible melting, the liquid metal temperature and

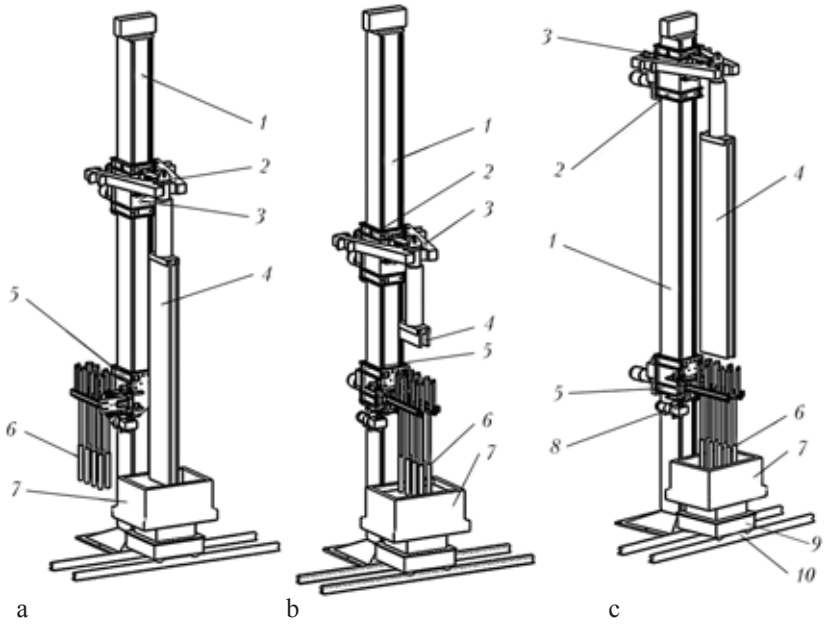

Fig. 1. Distribution of the consumable and nonconsumable electrode in the process of production of billets: a) remelting of consumable electrodes, b) heating of the slag during replacement of the electrodes, c) positioning new electrodes during heating of the slag; 1) the column with the base, 2) the clamping device for consumable electrodes, 3) the upper carriage, 4) electrodes, 5) lower carriage, 6) the block of non-consumable electrodes, 7) the crucible, 8) the rotating mechanism, 9) rail track; 10) roll-out carriage with the electromechanical drive.

the condition of the bottom surface of the crucible can be easily regulated by the ESR parameters prior to and after replacing the electrodes. Therefore, the task of the application of the furnace with the replacement of the electrode for CESC is greatly simplified.

The proposed equipment with the change of consumable electrodes during electrode melting (Fig. 1) consists of a stationary column with the base, an upper carriage with a mechanism for clamping consumable electrodes and a lower carriage with a rotating mechanism carrying non-consumable electrodes, and also current-carrying busbars and connectors of the flexible water-cooled cables with couplings. The current-carrying busbars and the cables of the upper and lower carriages are connected to the same current source. The use of the lower carriage with the rotating mechanism which carries the non-consumable electrodes an rotates of them into the non-working position and back during melting, widens the technological parameters of equipment.

Another special feature of this equipment is the possibility of regulation in the lower carriage of the distance between the non-consumable electrodes in two coordinates in the horizontal plane and also selection of the number and dimensions of these electrodes. The variation of the disposition of the non-consumable electrode in the slag pool makes it possible to use changeable ceramic crucibles of different dimensions.

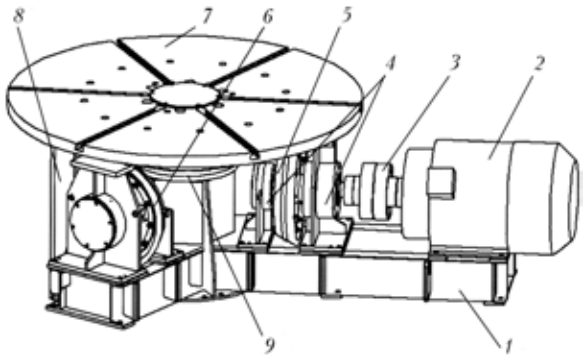

Fig. 2. Design of the centrifugal machine: 1) stand, 2) electric motor, 3) connecting coupling, 4) varying section, 5) drive roll, 6) driven roll, 7) faceplate, 8) protective shield, 9) the central bearing section.

Figure 2 shows the design of a centrifugal machine with the vertical axis of rotation which can be used in the centrifugal electroslag casting system**.** The machine has the following characteristics:

External diameter of the mould, mm	1800
Height of the mould, mm	1200
Total load on the faceplate, kg	up to 12 000
Nominal frequency of rotation, 1/min	1500
Frequency of rotation of the mould, 1/min	80-800
Power of the electric drive, kW	110
Weight of the casting, kg	up to 3000
Weight of the centrifugal machine, kg	4950

The centrifugal equipment has the form of a frame welded from channels and secured to the base using anchoring bolts. The drive consists of an asynchronous motor and a microprocessor frequency converter L300P (Hitachi). The driver transfers the torque to the drive roll connected with the clutch. Three bearing sections are secured in the frame under the angle of 120°. The bearing sections contain one drive and two driven rolls without the possibility of radial displacement. The faceplate with the diameter of 2000 mm is rotated using the drive roll by a friction pair. All the rolls are covered with protective shields. The central bearing section fixes the faceplate in the axial position.

This design greatly reduces the load on the shaft and the bearings of the central bearing section from disbalance in rotation. The centre of gravity of the mould and the casting, i.e., the point of application of the perturbing centrifugal forces, is situated between the drive and driven rolls. Another special feature is the fact that the central shaft can be deflected during operation from the vertical axis through some angle which compensates the inaccuracy of positioning the faceplate and the horizontal plane.

To ensure safety, the centrifugal machine is positioned at some distance from the crucible furnace in a container and its working space is restricted by a roll-away protective jacket. The machine is fitted with systems for water-air cooling and lubricating of the bearings with a liquid lubricant.

The CESC operates as follows. A slag pool is produced in a ceramic crucible by the dry start or by pouring a portion of slag prepared in a separate flux-melting furnace. This is followed by the ESR of consumable electrodes. During this period, the non-consumable electrodes occupy the non-working deposition (Fig. 1a). After building up the required portion of liquid metal in the crucible the consumable electrodes are removed from the melting zone. The liquid metal together with the slag are transported using a rolling carriage to the centrifugal machine positioned 5 m from the furnace, and they are poured into the rotating mould of the centrifugal machine. A small portion of liquid metal (10–15%) is left in the crucible. After pouring in a new portion of slag, the rotating mechanism, fitted with the electromechanical drive, is used for rotating the block of non-consumable electrodes into the working position (Fig. 1b). The slag pool is preheated with non-consumable electrodes.

Preheating of the slag is accompanied by replacing the consumable electrodes (Fig. 1c). The non-consumable electrodes are subsequently removed from the melting zone and consumable electrodes are introduced. Removal from the melting zone is ensured using the rotating mechanism (Fig. 3).

A special feature of the rotating mechanism is the optimum design of the current-carrying busbars in the form of hinges. Consequently, the minimum break in the process of replacing the electrodes can be efficiently ensured. A break in the electroslag process taking into account the transport time of the crucible to the centrifugal machine and back is 2–3 min.

In addition to remelting the new consumable electrodes, the first casting is solidified and removed from the mould. After building up the required portion of liquid metal, the operations are repeated.

Relatively small blanks for components are produced efficiently by CESC whose productivity is lower than that of the deformation methods. Therefore, the centrifugal electroslag casting systems should be fitted

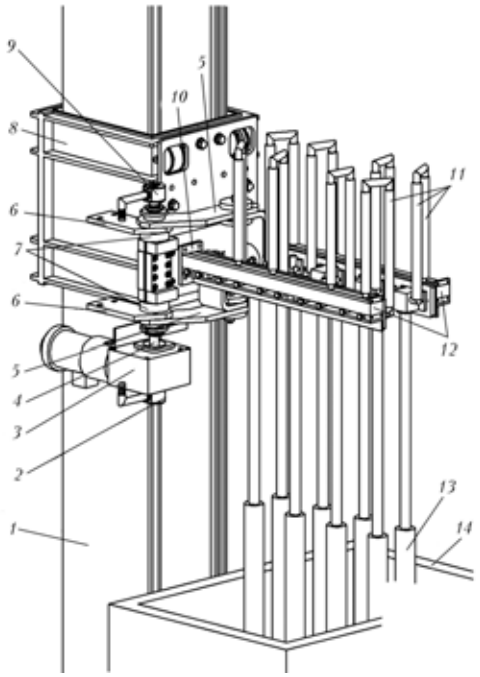

Fig. 3. Design of the rotating mechanism: 1) the column, 2) the coupling, 3) electromechanical drive; 4) the shaft of the rotational mechanism, 5) current-conducting busbars, 6) connectors, 7) busbar hinges, 8) the lower carriage, 9) couplings, 10) the flanges for the supply of water, 11) elements of the willing system, 12) the stationary brackets, 13) non-consumable electrodes, 4) the crucible.

with a centrifugal machine with a relatively high power.

This method can be used to produce large seamless blanks, for example in ring and wheel rolling production which have present are produced by deformation-welding methods. In alternating loading, the welded joint is a weak link of the entire structure.

When using the centrifugal electroslag casting system fitted with a crucible furnace and a centrifugal machine with a relatively high power, productivity can be increased by increasing the weight of the casting and by using multi-position moulds.

With transition to continuous production of castings, the proposed centrifugal electroslag casting system increases the productivity of the process and also the economic parameters and efficiency as a result of improving the heat balance of the melting process in a constantly heated crucible, increasing the service life of the lining working without thermal cycles of heating and cooling, reducing the duration of preparatory operations carried out previously prior to every melt (dressing of the bottom surface of the crucible to remove the remnants of the solidified slag, repair of a bottom electrode in the mono-filar scheme, verification of the elements of the water cooling systems, etc).

References

1. Goryachek A.V., et al., Metallurgyia mashinostroeniya, 2008, No. 1, 26–28.
2. Skripnik S.V., et al., Sovremen. Elektrometall., 2008, No. 3, 15-17.
3. Goryachek O.V., Equipment for electroslag remelting of metals and alloys, Patent No. 74472, Ukraine, MPC S 22 V 9/18.9/187, 15.12.2005.
4. Paton B.E. and Medovar B.I., Electroslag furnaces, Naukova Dumka, Kiev, 1976.

Advances in Electrometallurgy 2010 ***8*** *(1) 14–20*
Translated from Sovremennaya Elektrometallurgiya 2010 ***8*** *(1) 15–19*

ELECTRON BEAM PROCESSES

Production of titanium ingots and slabs by electron beam melting in equipment constructed at Antares International Company

A.Ya. Derecha. O.E. Sobko-Nesteruk and S.A. Sukhin

Antares International Company

10-year experience of the Antares International Company with the establishment and development of metallurgical production of titanium is generalized. Some technical and technological aspects of organizing the production of ingots and slabs (rectangular ingots) by the electron beam melting technology are considered. The physical parameters of the produced ingots and slabs and their quality characteristics are given.

Increasing requirements on the quality of titanium by the users in aerospace technology and also the tendency for reducing the cost of titanium production for commercial applications stimulate the development of new processes of production of titanium billets. Special attention is given to the electron beam melting (EBM) which is one of the most efficient methods of processing titanium scrap [1]. In some cases. the cold-bottom

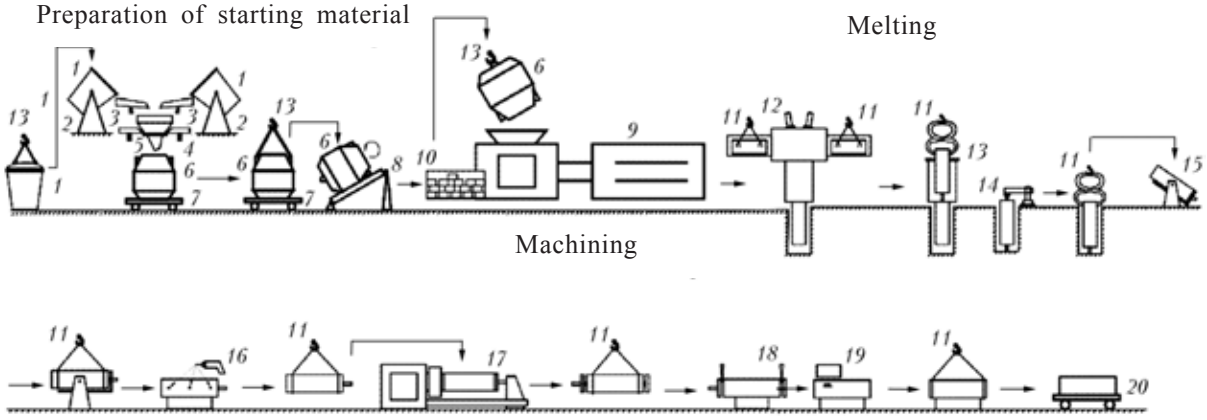

Fig. 1. Technological flow lines of production of titanium billets: 1) container with sponge; 2) tilting device; 3) vibrational feeder; 4) balance-dosing device; 5) dosing bunker; 6) the drum of the mixer; 7) the carriage; 8) the mixture; 9) briquette presser; 10) container with briquettes; 11) bridge crane; 12) the furnace; 13) loading equipment; 14) radial-drilling machine; 15) tilting device; 16) sampling device; 17) lathe; 18) strip-cutting machine; 19) ultrasound inspection equipment; 20) transfer carriage.

electron beam melting of titanium combined with vacuum-arc remelting (VAR) is an inseparable technological process of production of titanium for rotors [2].

Leading producers of titanium in the USA. China. Japan and Western Europe have expressed interest in the method of cold-bottom technology of electron beam remelting. Powerful electron beam furnaces have been constructed which are capable of melting the largest titanium billets and slabs and of processing titanium sponge and scrap [3].

In 1999. as a result of merging the financial and investment resources in the Antares International Company. and taking into account the practical experience of a team of experts working for a long period of time in the area of electron beam technology. it was decided to organise the industrial production of titanium on the basis of electron beam melting. A project of metallurgical production with the annual volume of production of 5000 t titanium billets was set up. The main aim of the project was the development and economical production of high-quality titanium and processing titanium in the production systems of billets and slabs with the highest economic parameters.

The project was realised in several stages over a period of 2.5 years. The foundations for assembling systems were laid in 2000. The production complex started production at the end of 2002 in the following composition:

– the lines for the preparation of charge materials.

– two units of electron beam melting equipment.

– equipment for mechanical cutting and dressing of billets.

– a plant laboratory for investigations and controlling the quality of metal.

A technology and equipment used in the production of billets were developed (Fig. 1). In this technology. various titanium initial materials (crap or titanium sponge separately or in mixtures in any proportion) are used. and alloying additions are added if necessary.

The process of preparation of the charge includes purification. grading. dosing and charging the titanium starting material for remelting. The line for the preparation of the charge contains devices for automatic dosing in the composition of two strip feeders and an electronic balance with the output to a computer interface. Consequently. it is possible to produce charge mixtures from several components in the required proportions. A conical drum mix with the capacity of 0.65 m^3 is used for averaging out the charge mixture.

The prepared mixture of the bulk component of the charge is compacted into briquettes in a hydraulic press with a force of 6.3 MN. Each of the two briquetting presses is used for producing 8 t of briquettes from titanium sponge or 4 t of briquettes for savings per shift.

Prior to loading into the equipment. the charge materials for remelting are placed in usual steel containers. The required amount of the starting material for producing large billets is ensured by cassette loading from 2 to 6 containers. The capacity of the containers and the number are such that it is possible to load up to approximately 12 t of briquetting sponge. shavings or melting scrap per each melt.

Production is based (Fig. 2) on two industrial electron beam systems VT01. Specialised equipment of a new generation (Fig. 3). designed for melting titanium. was designed. produced and introduced into service over a very short period of time. All the systems

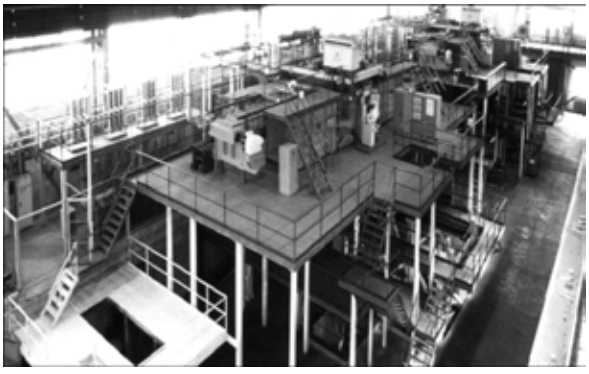

Fig. 2. Production shop for electron beam melting at the Antares International Company.

for production equipment where produced at the Antares International Company and in various Ukrainian plants.

Technical characteristics of VT01 electron beam equipment

Power of the electron beam gun. kW	2800
Accelerating voltage. kV	30
Number of electron beam guns.	seven
Working vacuum. Pa	0.133–1.330
Productivity of the vacuum system. l/s	70.000
Largest dimensions of the billets. m:	
Length	4.0
Diameter	0.82
Width/thickness	0.86/0.60
Number of loading systems	2
Number of containers for loading	4–6
Size of the billets. m:	
Diameter	0.82; 0.64; 0.40; 0.38
Length	4.0
Width/thickness	1.31/0.19; 1.31/0.26; 1.31/0.42
Dimensions of the equipment.m	20×20×16

The design and production capacity of single VT01 equipment is 2500 t of titanium ingots and slabs per annum.

Electron beam equipment VT01 consists of a hermetically sealed chamber within a diameter of 3 m which is in contact in the upper part with a seven-gun electron beam heater (EBH) on a carriage; the lower part there is the modulus of technological equipment and the billets chamber with the brittle mechanism on a moving platform; on two sides there are two loading chamber is in the

Fig. 3. VT01 electron beam equipment.

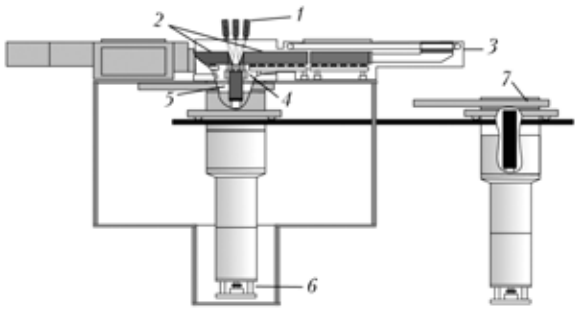

Fig. 4. Diagram of VT01 equipment: 1) VTR electron beam gun; 2) remelting blanks; 3) the mechanism for feeding the blanks; 4) the water-cooled solidification mould; 5) the billets; 6) the withdrawal mechanism; 7) the vacuum gate.

horizontal position with the feed mechanisms and replaceable charge containers.

To simplify servicing the chamber in the period between the individual melts. and also to unload large billets. the electron beam heaters and the billet chamber are separated in relation to the melting chamber. The equipment. combining in a single unit the solidification mould and the copper cold baseplate. can be rapidly replaced in transition to another standard size of the billets. and two solidification moulds can also be used for parallel casting of two billets simultaneous live. The diagram of VT01 equipment is shown in Fig. 4.

This design of VT01 equipment ensures high functional properties. reliability and economic efficiency of operation. with the duration of non-productive periods minimised.

In the process of electron beam melting of the charge containing titanium sponge main difficulties form as a result of splashing of metal and due to a high rate of gas generation which disrupts the stable operation of the electron beam guns.

Electron beam guns working on the basis of high-voltage glow discharge (HVGD) are characterised by high stability in these conditions [4]. A number of powerful HVGD guns (unit power of 400 and 600 kW) were constructed at the Antares company with participation of the experts of the Kiev National Technical University of Ukraine. A special feature of these guns is that high vacuum is not required for their stable operation. The

level of the working pressure of the gases of these gases higher than the residual pressure in the volume of the melting chamber of equipment and is in the range 0.133–6.660 Pa.

The application of the powerful electron beam guns VTR and VT01 electron beam systems next it possible to produce large titanium billets at high melting rates comparable with vacuum arc remelting in the industrial conditions. Consequently. the energy losses and the losses of metal as a result of evaporation are reduced. the problem of producing titanium billets and billets of titanium alloys of the required precision composition is simplified.

The VTR electron beam guns are characterised by simple design and servicing and are produced from relatively cheap materials. The cathode is made of aluminium. the operating life is 1000 h.

For the given melting methods. the VT01 equipment contains seven VTR electron beam guns distributed on the cover of the chamber in groups depending on the functional principle: two electron beam guns per for each billets; one – for maintaining pouring on the cold base; two – for heating the metal in the solidification mould.

Each gun has a separate high-voltage power source with a power of 630 kW. assembled on the thyristor converters. With this power system. the oscillatory processes in a discharge in the individual guns (and in the cathode–anode gap) have no effect on the stable operation of other guns.

The electron beams on the heated surface are controlled by a upper level microprocessor and controllers with a set of lower level devices. The programmed distribution of power and of the trajectory of the electron beams produces the required optimum configuration of the heating zones. The safe movement of the beams is restricted within the limits of the equipment.

VT01 equipment is fitted with a system for controlling and recording the parameters of the melting process. The actual parameters obtained from a set of sensors are recorded by a computer with a specific periodicity and printed in the form of a melting report. Figure 5 and 6 shows the diagrams of the variation of the length of the billets. vacuum and the electrical conditions of the guns during melting.

The vacuum diagram shows that the initial period is characterised by the increase of pressure in the chamber determined by the release of adsorbed gases from the screens and internal walls of the chamber. When the stationary regime is established. the vacuum is restored. the operation of the electron beam guns is stabilised (Fig. 6). and the melting rate is constant.

Another important factor. improving the economic parameters of the method of production of the billets. is the cold-bottom remelting with the counter feed of two blanks simultaneously. The development and surface of each blank create suitable conditions for mutual 'screening' and 'accumulation' of part of the radiant energy. and also the products of splashing and evaporation of titanium. This is accompanied by reduced energy losses

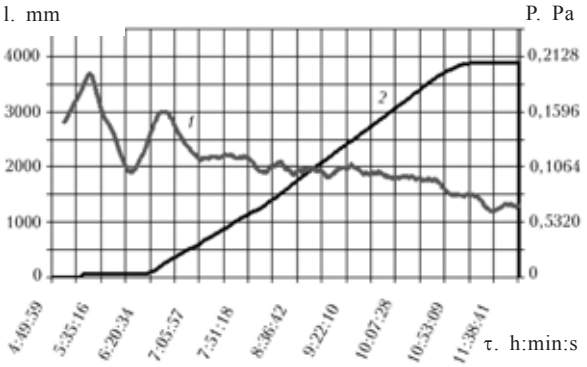

Fig. 5. Variation of vacuum (1) and length l of the billet (2) during melting.

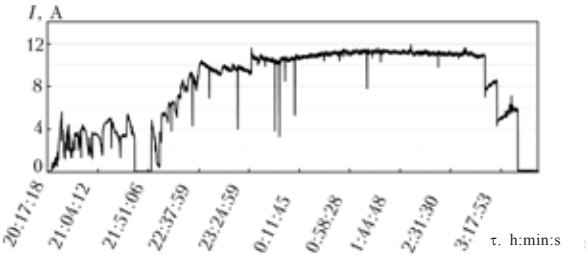

Fig. 6. Variation of the current of the electron beam during melting.

for melting of billets and irreversible metal losses. The dependence of the energy and mass parameters of the process of melting of titanium sponge in the production of billets with a diameter of 825 mm and rectangular billets with the size of 190 × 1325 mm is shown in Fig. 7 and 8.

For example. when the power of the electron beam supplied in melting is increased and the melting rate also increases. the consumption of electric energy per production unit decreases and the yield of suitable metal increases (Fig. 9).

The chemical composition of the titanium billets. produced from TG100-TG130 titanium sponge. is presented in Table 1. As regards the content of the controlled elements. titanium corresponds to the grades Grade1 and Grade2. ASTM B348.

The low oxygen content of the billets. produced from titanium sponge. is not always justify from the viewpoint of the user. especially because of mechanical strength. At the same time. at a specific content. oxygen is an effective hardening agent of titanium. To increase the strength properties of titanium

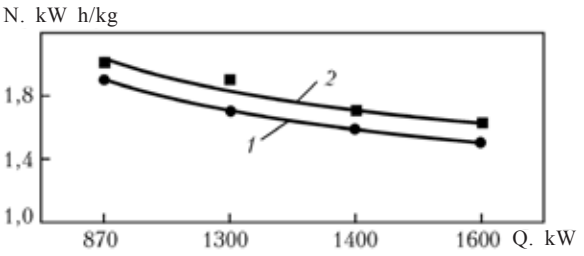

Fig. 7. The dependence of consumption *N* of electric energy on the supplied power *Q*; here and in Fig. 8. 9:1) a billet with a diameter of 825 mm; 2) rectangular billets 190 × 1325 mm.

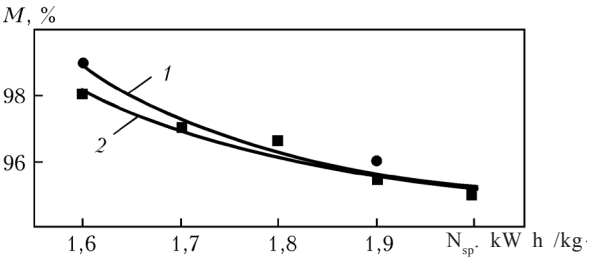

Fig. 8. Dependence of the yield of metal *M* on specific consumption of electrical energy N_{sp}.

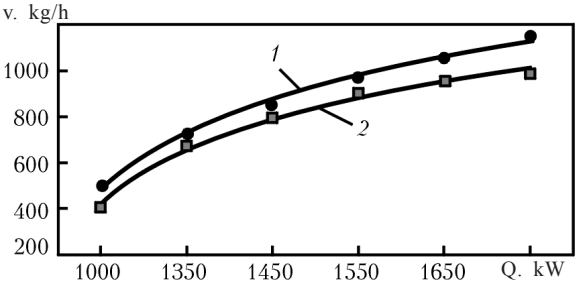

Fig. 9. Dependence of the melting rate *v* on the supplied power.

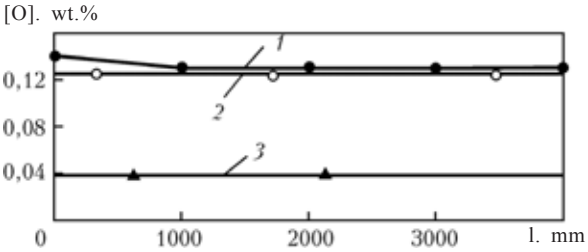

Fig. 10. Distribution of oxygen in a 190 × 1325 mm rectangular ingot. alloyed with TiO_2: 1) experimental; 2) calculated; 3) in titanium sponge.

of commercial purity. investigations were carried out to develop an effective alloying technology. Additions of non-pigment titania TiO2 are added in the stage of preparation of briquettes from the sponge.

The results of analysis of the oxygen content in the rectangular billets. alloyed with oxygen. are presented in Fig. 10. The oxygen content corresponds to the calculated content of 0.13 wt.% at the initial content in the sponge of 0.0 38–0.0 42 wt.%. The distribution of oxygen along the length of the billets is almost uniform. A number of orders has been received to produce titanium billets weighing 9t with the oxygen content of 0.22–0.24%.

In the as-received condition. the surface of the billets and slabs is machined. Cylindrical billets are machined in an 1A660 lathe. and rectangular ones in 6M616 milling cutters.

The surface is machined with hard-alloy tools without using any cooling liquid so that there is no contamination of the resultant shavings. Fine defects are removed by abrasive dressing. On the basis of agreement with the customer the ends of the billets can be cut off.

Table 1. Chemical composition of billets produced from titanium sponge. wt.%

Billet size. mm	Sampling area	Fe	O	N	H	C	Remainder (max)	
							Each	Total
∅830	Head	0.05	0.04	0.011	0.0017	0.01	≤0.1	≤0.4
	Bottom	0.05	0.05	0.012	0.0018	0.01	≤0.1	≤0.4
∅640	Head	0.05	0.05	0.011	0.0019	0.01	≤0.1	≤0.4
	Bottom	0.05	0.06	0.012	0.0019	0.01	≤0.1	≤0.4
190×1325	Head	0.05	0.04	0.010	0.0015	0.01	≤0.1	≤0.4
	Bottom	0.05	0.05	0.011	0.0018	0.01	≤0.1	≤0.4
ASTM B 348-00		0.30	0.25	0.030	0.0100	0.10	0.1	0.4

Comment. Titanium - base

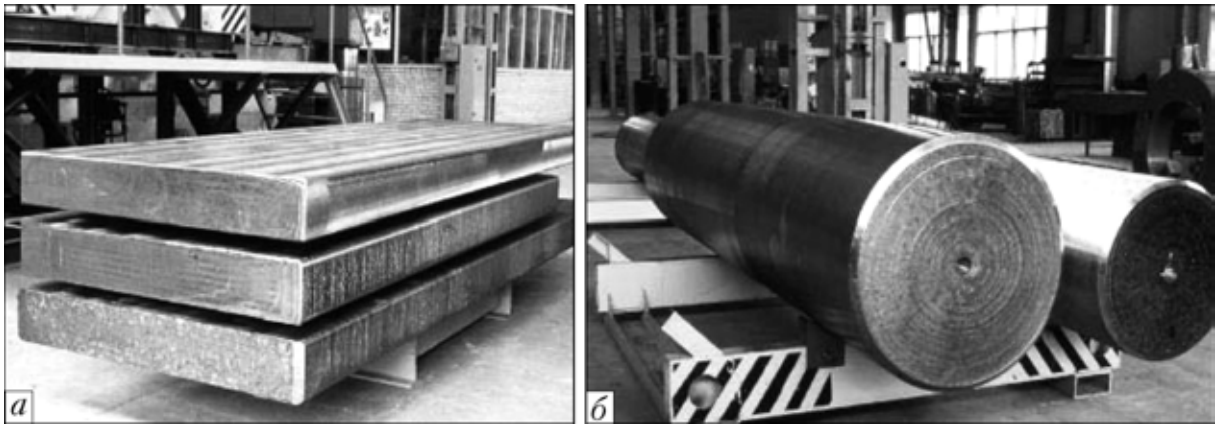

Fig. 11. External appearance of billets produced at the Antares company: a) rectangular cross-section 190 × 1325 mm; cylindrical billets diameter 825 mm.

To reduce the production losses and consumption of metal in cutting it is recommended to use a strip-cutting machine produced by company Everising (Taiwan) used for high productivity cutting of billets. The width of cut is 1.6 mm. The maximum capacity of the machine with respect to the machined billet is 1300 × 1300 mm.

The titanium based in the form of shavings and cut-offs. formed after machining. are returned to processing in melting of billets. Prior to use the shavings are crushed and shaped into briquettes.

The produced billets and slabs are subjected to 100% ultrasound inspection to determine the presence of internal defects.

The quality of the titanium billets is controlled in the plant laboratory by analysis of the chemical composition of the metal to determine whether the results satisfy the requirements of the customer and standard norms. The laboratory has devices for spectral analysis Spectromax of the Spectra company (Germany) and equipment for the analysis of the content of gases (oxygen. nitrogen. hydrogen) and carbon (LECO USA).

From the start of service the equipment has been used for remelting several thousand tons of titanium starting material. The profile and range of the produced billets asre as follows: cylindrical billets with a diameter of 825 and 640 mm, rectangular billets 190 × 1325; 250 × 1325; 420 × 1325 mm. The external appearance of the billets is shown in Fig. 11.

The development plans of Antares Inter-

tem for producing titanium billets and slabs weighing up to 14 t.

References

1. Musatov M.N., et al., Tekhnol. Legkikh Splavov, 1990, No. 8, 60–75.
2. Froes F.H. and Senkov O.N., Titanium today and tomorrow. in: Electron beam melting and refining, state-of-the-art, 1977, 2–27.
3. Ritchie M., et al., Melting and refining, State of the art, 1997, 252–261.
4. Tikhonovskii A.L., et al., Probl. Spets. Elektrometall., 1993. No. 1. 70–73.

Advances in Electrometallurgy 2010 ***8*** *(1) 21–30*
Translated from Sovremennaya Elektrometallurgiya 2010 ***8*** *(1) 20–27*

Erosion-resisting multilayer coatings based on titanium carbides and nitrides with ductile interlayers

E.V. Dabizha, A.A. Leshchuk, I.V. Bondar' and N.N. Borisova

Institute of Superhard Materials, National Academy of Sciences, Kiev

Prospects for the application of ion-plasma methods for deposition of wear- and erosion-resistant multilayer protective coatings are discussed. It is shown that the methods of microelectric arc plasma vacuum and magnetron vacuum coating deposition which refer to the given group, are most multifunctional. The results of updating the vacuum installation VU-700D(M), in which three peripheral sources of microelectric arc deposition and one source of magnetron sputtering are mounted, are given. New technological and hardware solutions have been developed, allowing deposition of protective erosion-resistant multilayer coatings with a total thickness of up to 30 μm on compressor blades of gas turbine engines. The effect of the thickness of a soft cobalt interlayer and the temperature of the deposition process on the critical thickness of multilayer coatings of carbide and titanium nitride as well as on the nanohardness of the coatings was investigated.

The application of coatings is one of the advanced methods of modification of the surface of components and of improving the surface properties in engineering and instrument making, increasing the service characteristics of the tools, and it is an important member of many technological cycles of production of new materials. Therefore, special attention is paid to the development of methods and technologies of depositing coatings and to extensive examination of these coatings.

At present, there is a large number of methods of depositing coatings realised in a number of vacuum systems designed for depositing coatings from different materials on different components.

In the group of the advanced methods of producing coatings, the most efficient and promising are the methods of depositing coatings in low-temperature gas discharge plasma which produce, in addition to the metal vapours, ionised particles which can be controlled by electrical and magnetic fields. In comparison with more energy-consuming methods of thermal and electron beam evaporation, these methods are characterised by the higher efficiency (i.e., with lower energy consumption and consumption of various reagents) of the dispersion of materials to the atomic, molecular, cluster state, and can be used for depositing the surface of components with thin (up to 10 μm) functional, auxiliary or decorative coatings [1].

In ion-plasma deposition of coatings, the high adhesion of the coatings to the base is ensured by the physical–chemical interaction of the plasma flow with the surface of the substrate which is under a given potential and, consequently, ion bombardment of the surface of the component and activation of the surface take place in addition to condensation and this leads to the extensive annotation of the atoms of the required material into the surface layer of the substrate.

The ion-plasma coating methods include

magnetron sputtering, micro-electric arc evaporation (sputtering), and activated reactive evaporation [2–4]. The first two methods are most promising in this group. The last method is a modification of thermal evaporation extending the possibilities of the method but does not fully remove the existing shortcomings of thermal evaporation.

Main advantages of these coating methods are determined by the physical principles forming the basis of these methods. The possibility of sputtering (evaporation) of the material from the solid phase of the zone of partial melting results in the situation in which it is necessary to use expensive evaporating elements produced usually from refractory scarce materials. The absence of the evaporating elements with the restricted service life and the relatively small load greatly increase the rate of growth of the coating and its thickness and also the total surface of the coated components. The possibilities of growing thicker coatings is the controlling condition for the application of this method in the deposition of thick erosion-resisting coatings on different components.

The sputtering with the ions of the cathode material or explosive microevaporation of the material is utilised in the formation of coatings in the form of an alloy with the retention of the stoichiometric composition of the initial material, and the introduction of a chemically active gases – the production of chemical compounds. As a result of the presence of the ionic component in the sputtered material it is possible to accelerate the component in the supply on the substrate with a negative potential. Therefore, processes of activation of the surface atoms take place on the substrate and increase the adhesion of the coating to the substrate, the degree of sputtering of the atoms from the surface (ionic etching) and implantation of the ions.

The dimensions of the ion-plasma sputtering systems can be varied in a wide range so that coatings can be deposited on components of various dimensions resulting in high reproducibility of the results and the relative simple control of the sputtering process.

It is well known that the method of microarc evaporation with ion bombardment is based on the initiation of a microarc discharge in vacuum on the cathode surface and the subsequent formation of cathode spots having exceptionally high density and temperature [5–7].

The generation of high power is determined by the bombardment of the zone of the cathode spot with the ions of the sputtered material. As a result of high temperature and ion bombardment, the droplets of molten metal, atoms and ions are included in the composition of the products of erosion of the cathode in the zone of the spot. The dimensions and number of the droplets are determined by the thermophysical properties of the cathode material and the arc discharge current [5].

As shown in [8] the consumption of the cathode mass in the ion phase per unit transferred charge for the given material is a constant value, whereas the erosion of the cathode in the droplet phase (in droplets) depends on the technological conditions and increases with increasing charge transferred through the unit area (microarc discharge current).

The droplets emitted by the cathode are additionally heated during transfer from the cathode to the substrate as a result of the bombardment of the surface of the droplets with ions. The droplets subsequently evaporate and act as the main source of neutral vapours in the volume of the discharge gap. If the alloy containing metals whose tension greatly differs from the elasticity of the vapour is sputtered, evaporation of the more volatile component takes place at a higher rate resulting in changes in both the composition of the droplet and the deposited coating, in comparison with the composition of the cathode material [5].

Ion bombardment of the evaporating vapour is also accompanied by additional ionisation of the atoms of the vapour and, consequently, the fraction of the ions is 30–50% of the total flow, condensed on the surface of the component [8].

When a reaction gas (nitrogen, methane or

oxygen) is added into the discharge gap, the gas interacts with the products of sputtering of the cathode material and this is accompanied by the deposition of a coating in the form of compounds (nitrides, carbides oxides of transition metals), characterised by high hardness, strength, and they can be used as protective wear- and erosion-resisting coatings on different components.

The processes of microelectric arc reactive sputtering are realised by a simple method using, as the power source, standard welding rectifiers. This is a considerable advantage of the method in comparison with other methods [4]. However, this method has also considerable disadvantages, for example, the presence of the droplet phase in the coating.

Magnetron sputtering does not have this shortcoming because in this method deposition takes place in the form of atoms of the sputtered material (partially in the form of ions of this material). The magnetron sputtering system is the modification of the extensively used systems for diode sputtering. In addition to the positive properties of diode sputtering, magnetron sputtering as other advantages: high rate of condensation of the materials; lower degree of contamination of the condensate with the gas inclusions; decrease of the temperature to which the substrate is heated during coating.

The physical basis of the magnetron sputtering system is an independent anomalous glow discharge in a rarefied gas in crossed electrical and magnetic fields. The magnetic system generates a magnetic field with the arched configuration and the strength of 0.03-0.13 T above the cathode surface [3].

The electrons, present in this zone, carry out complicated cycloidal motion and in collision with the gas molecules cause ionisation of the latter, generating positive ions which are accelerated in the electrical field, bombard the surface of the target–cathode and knockout material particles from the surface.

There are two main effect in bombardment of the cathode surface with the ions of the sputtering gas – secondary electronic emission and ion sputtering of the cathode target. Secondary emission of the electrons is used to maintain the discharge and the sputtered atoms condense on the substrate in the form of a coating.

The presence of the concentrated plasma zone in the near-cathode space results in the higher ionic current density and higher sputtering rate in comparison with diode sputtering. This is associated with the change of the sputtering mechanism from direct collision in bombardment with the ions for diode sputtering in the mechanism of thermal peaks for magnetron sputtering [9]. In contrast to the mechanism of sputtering by direct collisions, magnetron sputtering is characterised by the linear dependence of the deposition rate on the power of the magnetron discharge so that it is possible to automate quite easily the supply of the reaction gas in deposition of the coatings in the form of chemical compounds of the sputtered metal and the reaction gas.

The working gas in magnetron sputtering systems is usually argon in the DC regime. These systems operate at the argon pressure of 0.01–100 Pa and the discharge voltage of 300–800 V [3].

The magnetron sputtering systems can be used to produce coatings of almost any metals, and semiconductor materials without disrupting the stoichiometric composition. Consequently, these systems are highly promising for application in a number of areas of science and technology.

The presence in this method of the electron trap formed in the cross magnetic and electrical fields ensures a high degree of ionisation of the gas atoms. Therefore, the addition of other reaction gases (nitrogen, methane, oxygen) to the discharge gas volume makes it possible to produce, as a result of the high degree of ionisation and activation of these gases, fields of compounds of transition metals (nitrides, carbides and oxides).

The most widely used compositions of the shielding wear- and erosion-resisting coatings and the properties of these coatings are presented in Table 1 [10].

The vacuum system of the Smorgonskii Plant of Optical Machine Construction VY-

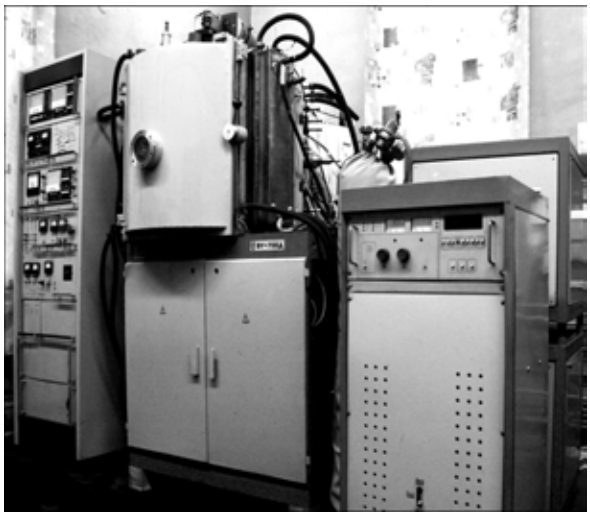

Figure 1. General view of the VU-700-D (M) modernised vacuum equipment.

700-D (M), Belarus, was modernised for vacuum technologies of depositing coatings. The general appearance of the system is shown in Fig. 1.

The basic system has the form of a cylindrical vacuum chamber with a diameter and a height of up to 700 mm, with the magnetron with indirect cooling of the target in stock in the left wall in a pocket, whereas the right-hand side contains the electrode for cleaning the surface of the sprayed components is the indirect glow discharge. On the top of the chamber varies a vacuum rotational drive with a six-deposition attachment for the double planetary rotation of the components up to

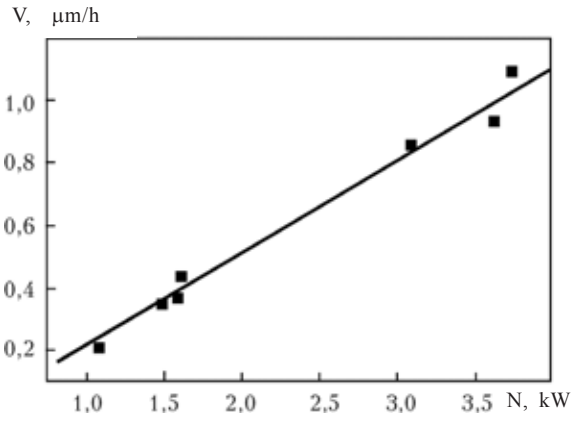

Fig. 2. Dependence of the deposition rate *v* of titanium on the power *N* applied to the magnetron with indirect cooling of the target-cathode.

Table 1. Composition of wear-resisting coatings and properties of these coatings

Composition of coating	Microhardness, GPa	Oxidation resistance at highest surface temperature	Friction coefficient
TiN	19.3...22.0	600	0.50
TiC	28.0...30.0	400	No data
TiCN	30.0	400	0.40
TiAlN	30.0...35.0	540	0.40
TiAlCrN	35.0	920	0.40
TiAlCrYN	27.0	950	No data
CrN	16.5...21.5	700	0.50
Al_2O_3	21.0...30.0	1200	No data
ZrN	28.0	600	0.60
MoS_2	15.0	—	0.02
WC/C	15.0	300	0.20

500 mm long and with a diameter of up to 140 mm for exposure of the surface of the components in the vapour flow.

The characteristics of this sputtering system were investigated in sputtering of a titanium target (working pressure of argon was 0.08 Pa). The dependence of the deposition rate of the titanium coating on the power supply to the magnetron is shown in Fig. 2.

As shown by the figure, the deposition rate of the coating has the form of a linear dependence on the applied power. At a power of N = 3.5 kW with indirect cooling of the target is no longer combined with cooling of the target and when the power supply to the magnetron is switched off the chamber shows slight rasberry-like glow of the cathode target.

The deposition rate at a high powers investigated with cyclic activation of the magnetron (five minutes of operation and cooling of the target of the magnetron). According to the experimental results, the increase of the power, supplied to the magnetron, above 3.5 kW results in even faster heating of the target and slight distortion of the latter impairing the efficiency of cooling and increasing the temperature to which the target is heated.

Heating of the target to a temperature above 700°C is accompanied by a decrease

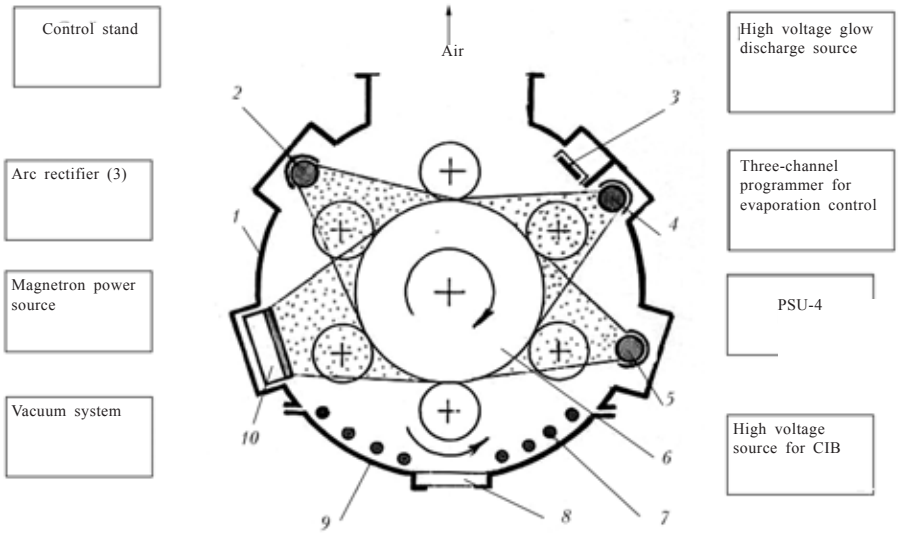

Fig. 3. Flow diagram of VU-700-D (M) modernised equipment: 1) vacuum chamber; 2, 5) arc evaporators (with a titanium cathode); 3) the electrode of indirect glow discharge; 4) arc evaporator (with a cobalt cathode); 6) holder of the double planetary rotational drive; 7) electrode heaters; 8) inspection system; 9) the door; 10) the magnetron.

of the efficiency of sputtering of the atoms of the titanium cathode by the argon atoms. Since the deposition rate of the coating of 0.9 μm/h does not solve the problem with the growth of the thick multilayer erosion-resisting coatings, it was necessary to develop a magnetron with direct water cooling of the cathode–target and modernise the vacuum chamber of equipment for installing additional evaporation and sputtering devices.

Figure 3 shows the flow diagram of the modernised equipment VU-700-D (M). As indicated by the figure, the modernised system is fitted with heating elements installed on the doors. The closed heaters are designed for heating the chamber and components in vacuum prior to depositing coatings and for maintaining the required temperature during deposition of the coatings.

The total power of the heaters is 5 kW. On the left-hand side of the cylindrical wall of the vacuum chamber there is a 'pocket' containing a linear modernised magnetron with direct cooling of the cathode–target.

The diagram of assembling of the cathode section of the modernise magnetron with direct cooling of the target–cathode is shown in Fig. 4.

The general view of the modernised magnetron is shown in Fig. 5. The size of the target–cathode is 145 × 520 mm. The figure shows that the length of the sputtering zone is slightly smaller than the length of the target–cathode (460 mm).

The dependence of the deposition rate of the titanium coating on the power applied to the magnetron for the modernised system is shown in Fig. 6. The deposition rate of the coating has a linear dependence also at a power higher than 5 kW, indicating that the efficiency of cooling of the target is sufficiently high. The structure of the magnetron enables operation at a power of up to 10 kW.

As shown by Fig. 3, in the modernised variant the vacuum chamber has three additional watercooled pockets containing two specially developed linear peripheral arcotrons with

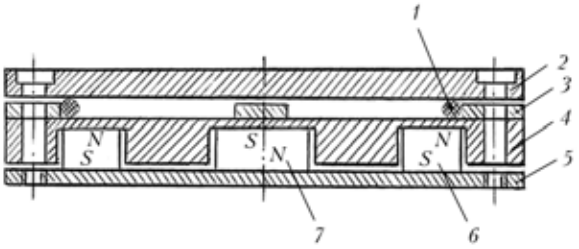

Fig. 4. Assembling of the cathode section of the modernised magnetron with direct cooling of the target-cathode: 1) rubber vacuum sealing bead; 2) the target-cathode; 3) the copper sheet for water cooling; 4) the copper separator for the magnets; 5) the lower 'shoe' of the magnetic system; 6, 7) peripheral and central magnets of the magnetron, respectively.

Fig. 5. General view of the modernised magnetron with direct cooling of the target-cathode.

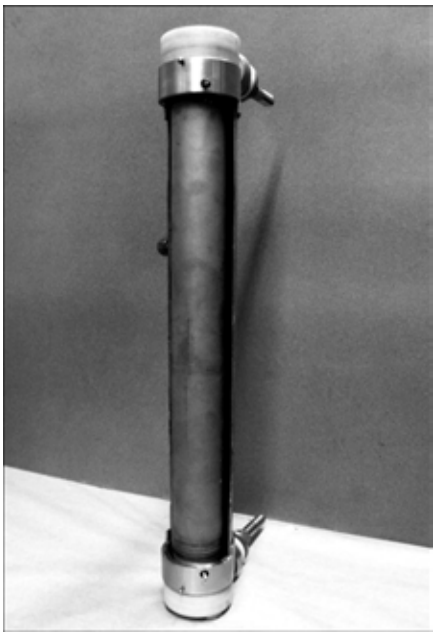

Fig. 7. General view of a linear peripheral arcotron with a titanium cathode.

a titanium cathode and one arcotron with a copper cathode, and also with cathode sections for preliminary cleaning of components in glow discharge. The general view of the arcotrons with titanium and cobalt cathodes is shown in Fig. 7 and 8, respectively.

According to the investigations, the arcotrons and the control and power units developed for them operate efficiently at a current of the microelectric arc discharge of 120–200 A. The efficient cooling of the walls of the pockets with the arcotrons was ensured during operation at a discharge current of 200 A. The deposition rate of the coating of titanium nitride and the current of the microelectric arc discharge of 165 A and operation of a single arcotron is 3.1, in the case of two arcotrons it is 6 μm/h.

Modernised equipment is fitted with a BPM-25 high-power unit for the magnetron with the total power of 25 kW. An additional power unit with a total power of 25 kW, designed for heating components to 500°C, was produced for the process of cathode ion

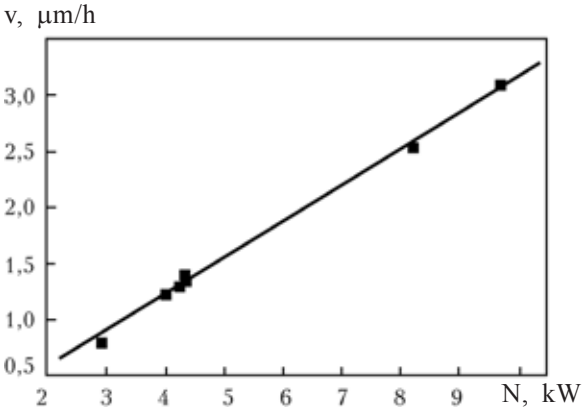

Fig. 6. Dependence of the cooling rate v of titanium on the power N, applied to the magnetron with direct cooling of the target-cathode.

Fig. 8. General view of a cathode section for glow discharge and the arcotron with a cobalt cathode.

treatment. For the automatic mixing of the gases (sputtering gas argon and the reaction gas) in the given proportion in the magnetron reaction deposition of the coatings, the system is also fitted with a spectral analysis system and automatic control of the gas supply PSU-4.

Using the methods of microelectric arc or magnetron sputtering it is possible to produce different shielding erosion-resisting coatings (Table 1). The experiments show that there is some critical thickness of these coatings (5–7 μm) at which the coatings start to soften and fail partially or completely after cooling to room temperature. This is caused by the high level of internal stresses formed as a result of differences in the coefficient of thermal expansion of the materials of the coating and the substrate [11].

The formation of the coatings of the carbides or nitrides of titanium by the method of microarc vacuum ion-plasma evaporation is associated with difficulties because they separate from the substrate. This method of deposition of coatings ensures efficient cleaning of the surface of the component with high energy ions and also parallel heating and activation of the surface resulting in high strength of adhesion of the coating to the substrate.

To determine more accurately the mechanism of separation of the coatings from the substrate, the specimens of Cr18Ni9Ti steel with the size of 20×10×1.5 mm were deposited with a suspension of graphite mixed with acetone. After drying, a thin layer of dispersed graphite remained on the surface of the specimen and in deposition of a coating on this layer it was possible to ensure the low adhesion strength of the coating to the surface of the specimen. The specimen prepared in this manner was deposited with a coating of titanium nitride, thickness 5 μm. The temperature to which the specimen was heated during deposition of the coating was (500±20°C); after cooling in the vacuum chamber in a vacuum of 0.008 Pa the specimen was taken out of the chamber. The coating separated from the surface by swelling of a continuous film which did not fail in this case.

Earlier investigations into the deposition of such a coating on pure sheets of Cr18Ni9Ti steel showed that the coating also separates but separation from the surface of the specimen was accompanied by simultaneous breakup of the coating into the finest particles.

This indicates that the resultant coating has high bonding strength of the surface of the specimen. The non-compensated force, required for separation and failure of the coating into the smallest fragments, transfers to the fragments the energy with which they fly away from the surface of the specimen.

The separation force generates stresses which builds up in the coating layer during its strong bonding with the surface.

As mentioned previously, in the absence of adhesion the coating only separated from the substrate without breaking up. The breaking up of the coating indicate the level of stresses built up in the coating and the strength of adhesion of the coating to the substrate. Therefore, the critical thickness of the coating at which the force additionally applied to the surface of the coating for separation from the substrate decreases to such an extent that the coating separates spontaneously from the substrate can be regarded as a suitable complex technological characteristic for evaluating the strength of bonding of the coating with the substrate. In most cases, separation takes place after cooling of the specimen with a coating and sometimes also in the deposition process, and the thickness of the produced coating is considerably higher than the critical value.

The deposition of coatings on the thin sheets of Cr18Ni9Ti stainless steel with the size of 40×10×0.4 mm results in bending of the sheets indicating the presence of high stresses in the coating layer.

According to the experimental results, the level of the internal stresses in the produced layer increases with increasing thickness of the layer. The results also show that of the stresses are higher in the coatings of titanium nitride in comparison with titanium carbide

and, correspondingly, the critical thickness of the titanium nitride coatings also lower. To grow a thicker layer of the coating it is necessary to utilise the effect of decrease of the stresses as a result of alternation of the layers in which the thickness is considerably smaller than the critical thickness for the given material and conditions, with thin interlayer of a ductile material [12]. All these factors were taken into account in the formation of multilayer coatings of these materials with a soft interlayer.

VU-700-D (M) modernised equipment was used for the development of new technological and apparatus solutions for depositing protective corrosion-resisting multilayer coatings. Taking into account the critical thickness of the coatings of titanium carbide or nitride the calculated thickness of the layers in the multilayer coating of titanium carbide was 3.4 μm and in the case of titanium nitride it was 2.9 μm.

According to the experimental results, the soft interlayer can be represented by thin layers of Cr18Ni9Ti steel or cobalt, although the latter is a more efficient material of the interlayer.

The effect of the thickness of the cobalt interlayer and the critical thickness of the Co/TiC multilayer coating was investigated. The specimens were in the form of 20×10×1.5 mm sheets of Cr18Ni9Ti steel.

In the vacuum chamber the sheets were cleaned by condensation with ion bombardment at a voltage of 60 and 1200 V and heated in ion bombardment to (400±20) °C. The pressure of the reaction gas methane CH4 during deposition of the TiC coating was (0.18±0.05) Pa.

After depositing each coating of TiC the specimen was cooled in the vacuum chamber in a vacuum of 0.008 Pa to a temperature of 100°C and then taken out of the chamber and cooled to room temperature in air.

If the multilayer coating after depositing the next layer did not separate, the specimen was placed again in the vacuum chamber for additional growth of the next layer. When the critical thickness of the multilayer coating was reached there were cases of separation and breakup of the coating from part or the entire sprayed surface. The thickness of the multilayer coating at which this took place was assumed to be critical.

The dependence of the critical thickness of the multilayer coating Co/TiC, formed at a temperature of (400+20) °C, on the thickness of the cobalt interlayers is shown in Fig. 9. As indicated by the figure, the critical thickness did not increase linearly with the increase of the thickness of the cobalt interlayer but increased along a rising curve. At the thickness of the soft interlayer of 0.27 μm the critical thickness of the multilayer Co/TiN coating was 15 μm.

Because no saturation was recorded at the given thickness of the ductile interlayer on the dependence shown in Fig. 9, it was interesting to investigate the effect of cobalt layers of a considerably greater thickness of the critical thickness of the multilayer coating.

The experimental results show that the temperature resulting in the formation of the coating is a very important process parameter. Since the rate of increase of the stresses in the growing layer of the TiN coating is higher than in the case of titanium carbide coatings, it was important to investigate the effect of temperature on the formation of a multilayer coating based on TiN. For this purpose, specimens of Cr18Ni19Ti steel with the size of 20×10×1.5 mm were deposited in layers, as in the previous case, with a multilayer Co/TiN coating at different process temperatures. The thickness of the TiN layers was 2.9 μm, and that of the cobalt layers 0.27 μm.

The temperature of formation of the coating of 300–500°C is very important because this temperature range is characterised by the formation of the structure of columnar or filament-like crystals which are characteristic of the processes of growth of the coatings [13, 14]. At a higher temperature, volume diffusion of the atoms resulted in the formation of the structure of equiaxed grains, characteristic of the monolithic material.

The dependence of the critical thickness of the multilayer coating of Co/TiN on the

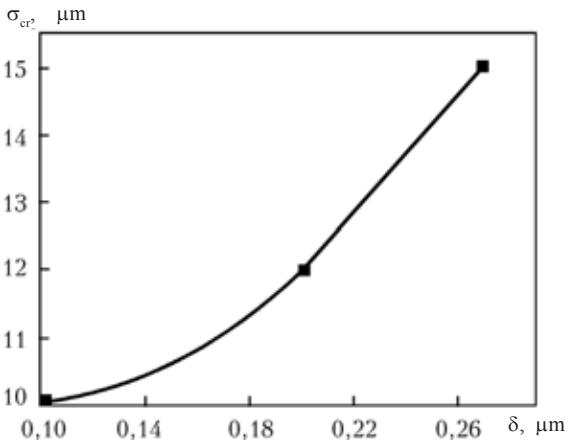

Fig. 9. Dependence of the critical thickness δ_{cr} of the Co/TiC multilayer coating produced at a substrate temperature of 400°C, the thickness of of the cobalt interlayers.

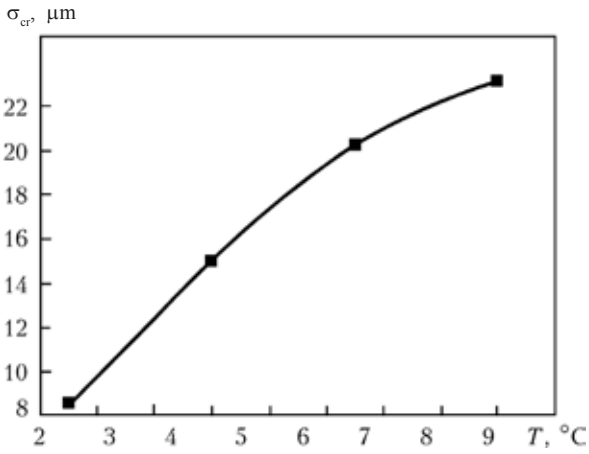

Fig.10. Dependence of the critical thickness δ_{cr} of the multilayer coating of Co/TiN on the substrate temperature at which the coating was deposited.

substrate temperature at which deposition takes place is shown in Fig. 10. The graph indicates that the dependence is not linear. The strongest effect is exerted by this parameter at a temperature close to 400°C. At a substrate temperature of 450° C and higher the effect of this parameter is weaker. At the same time, the curve does not show any distinctive saturation at temperatures close to 500°C.

The physical–mechanical properties of the multilayer coatings of Co/TiC were studied. This was carried out, as in previous investigations, on the 20×10×1.5 mm sheets of Cr18Ni9Ti stainless steel, with the deposition of a multilayer coatings based on TiC with cobalt interlayers.

The multilayer coating of Co/TiC was produced by layer spraying of the next layer after opening the chamber and analogue of the specimen with the given number of the layers for further investigations.

The remaining specimens were subjected to the following spraying cycle: the next layer of the TiC coating was deposited after eating the specimens by ion bombardment to (400±20) °C and the deposition of a soft cobalt interlayer. The thickness of the latter was 0.3 μm, and the hardness of the hard erosion-resisting TiC layer was 3.4 μm.

The specimens produced by this procedure with different numbers of the layers of the Co/TiC multilayer coating were subjected to nanoHardness measurements. Prior to the measurements, the upper layer of the TiC coating was polished to reduce the surface roughness at the values acceptable for testing in the nanoindentor.

Table 2. Physical properties of titanium nitride coatings

Co/TiC coating (thickness, μm)	Elasticity Modulus, GPa	Mean elasticity modulus, GPa	Nanohardness, GPa	Mean nanohardness, GPa
Single-layer (3.40	384.3	384.8	32.7	32.7
Two-layer (6.80)	381.2 421.5 442.8	415.2	33.4 37.1 38.5	36.3
Four-layer (13.7)	408.3	408.3	35.8	35.8

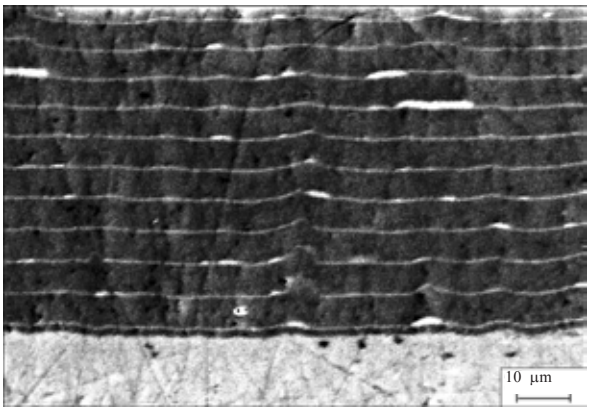

Fig. 11. Typical microstructure of the multilayer coating based on TiCN with ductile cobalt interlayers (the total thickness of the coating 30 μm).

Investigations of the nanohardness were carried out in equipment Nano Indenter-II, MTS Systems Corp., Oak Ridge, USA the hardness was tested in a Berkovich triangular inden tor. After testing the hardness was determined on the basis of the depth of indentations under load, and the elasticity modulus was determined using the unloading curve.

The results of investigations of the nanohardness and elasticity modulus for the Co/TiC multilayer coatings, deposited at a temperature of (400±20) °C, are presented in Table 2.

A typical multilayer microstructure is shown in Fig. 11.

It is interesting to note that in multilayer deposition of the coatings based on titanium carbide the nanohardness of the coating reached in individual cases 38.5 MPa which is considerably higher than the microhardness of the identical single-layer coatings. The load and indentation depth of the coating in these tests are comparable with the conditions of the effect on the coating in erosion wear and, consequently, the higher physical-mechanical properties of the multilayer coating confirm the efficiency of its deposition on the components as a shielding erosion-resisting coating.

Thus, the modernised equipment described in this article provides new technical and apparatus possibilities for depositing detective erosion-resisting coatings in the multilayer variant with a total thickness of 30 μm and more, including for protection of the compressor blades of gas turbine engines against erosion wear. This increases the service characteristics and service life of these components.

References

1. Movchan B.A. and Malashenko I.S., Creep-resisting coatings, deposited in vacuum, Naukova Dumka, Kiev, 1983.
2. Besso G.G., Methods of vacuum deposition of coatings and comparative analysis, Seminar by Alcatel, Moscow, 1982, 15–18.
3. Danilin B.S. and Syrchin V.K., Magnetron sputtering systems, Radio i svyaz', Moscow, 1982.
4. Andreev Yu.N., et al., Electric arc sputtering of metals and alloys in vacuum, LatNIINTI, Riga, 1982.
5. Rakhovskii V.I., Physical fundamentals of switching of electric current in vacuum, Nauka, Moscow, 1970.
6. Lyubimov T.A. and Rakhovskii V.I., Usp. Fiz. Nauk, 1978, No. 4, 665–706.
7. Laferty G., Vacuum arcs, theory and applications, Mir, Moscow, 1982.
8. Lunev V.M., et al., Zh. Tekh. Nauk, 1977, No. 7, 1491–1495.
9. Bondar' I.V., The relationships governing the formation of metal coatings on diamond powders in vacuum sputtering, Dissertation, Kiev, 1991.
10. Dabizha E.V., et al., Sovremen. Elektrometall., 2005, No. 4, 34–40.
11. Popescu A., et al., J. of Optoelectronics and Advanced Materials, 2002, No. 1, 115–120.
12. Golovchenko O.L. and Dabizha V.E., Patent 6804 Ukraine, MPC S 23 S 14/22Multilayer wear-resisting coatings, produced by the ion-plasma method, 16.05.2005.
13. Movchan B.A. and Demchishin A.V., Fiz. Met. Metalloved., 1969, No. 4, 653–660.
14. John A., J. Vac. Sci. Tech., 1986, No. 6, 3059–3065.

Advances in Electrometallurgy 2010 ***8*** *(1) 31–38*
Translated from Sovremennaya Elektrometallurgiya 2010 ***8*** *(1) 28–33*

Using nanostructured coatings for reducing the dynamic stress state of constructional machine components

A.I. Ustinov, A.P. Zin'kovskii, I.G. Tokar' and V.S. Skorodzievskii

E.O. Paton Electric Welding Institute, Kiev
Institute of Problems of Strength, National Academy of Sciences of Ukraine, Kiev
Institute of Metals Physics, National Academy of Sciences of Ukraine, Kiev

The results of experimental investigations carried out to determine the effect of the characteristics of the structure on the physical–mechanical properties of materials of coatings and damping capability of design elements with coatings taking into account factors such as as temperature, stress frequency and amplitude, are described.

Introduction and formulation of the problem

The development of engineering imposes stringent requirements on the reliability and longevity of both individual structural members and machines as a whole. Since the majority of these systems are used in the conditions of the wide spectrum of dynamic loading which may cause failure and malfunction of structural members, one of the key problems of ensuring the reliable functioning throughout the required service life is to ensure the sufficiently high dynamic strength of these components.

This problem is especially acute in the case of aviation gas turbine engines (AGTE) in which the majority (more than 60%) of defects, detected in design, starting up and service, are determined by the insufficient strength of the sections and structural members, especially the working blades. Approximately 70% defects are caused by vibrations.

One of the most important technical and economic parameters of the quality of engineering components is to ensure their vibration reliability. However, in the majority of cases, as a result of the high density of the frequency of intrinsic and forced oscillations in service of the investigated objects it is not simple to prevent the formation of dangerous resonance regimes. Therefore, various design and technological methods are used to reduce the detrimental effect of consequences of these regimes, especially the increase of the damping capacity as a means of restricting the maximum resonance stresses of the most heavily stressed structural members.

With special reference to the working blades of the compressors of the aviation gas turbine engines, produced from high strength titanium alloys with low dissipative properties, one of the most efficient methods of increasing the vibrational reliability is the deposition of high-damping coatings on the blade [1]. Since these alloys are sensitive to surface damage, the coatings should also be characterised by the required physical–mechanical characteristics, i.e., high parameters of hardness, longevity, corrosion resistance and others, i.e., they should be capable of ensuring simultaneously the reliable resis-

tance to the effect of the conditions in which the structural components are used.

At the moment, there is a large amount of experience with the formation of such coatings which satisfy the conditions of production and service of the aviation gas turbine engines [2]. At the same time, it should be mentioned that the parameters of these characteristics of the materials which can be used as the high-damping coatings are insufficiently high and the increase of these characteristics by alloying or thermomechanical treatment usually reduces the dissipation properties.

Taking into account the tendency for the development of advanced aviation engine construction, reflected in the increase of the gas temperature and amplitude of the dynamic stresses, the expansion of the frequency spectrum of external loading, it is necessary to develop new materials for coatings. The latter include the nanostructured vacuum condensates (condensates), developed at the E.O. Paton Electric Welding Institute, Kiev, [3], deposited on the structural elements from the vapour phase by the technology described in [4].

An important task from the viewpoint of using the materials of these coatings in the production of working blades of the compressors of the advanced aviation gas turbine engines is the determination of the optimum parameters of the structure of the material and the deposition conditions for increasing the damping capacity of the blades in service. This is also the aim of the present work.

Materials of the coatings and production methods

In this study, the parent material of the coating was in the form of the quasi-crystalline alloy Al–Cu–Fe, characterised by higher hardness (10–11 GPa) and corrosion resistance [5, 6] and also pure copper with iron additions (up to 4%). The last two materials can be used as the binding sublayer characterised by a high level of adhesion with the material of the structural member and the coating. In addition to this, the presence of copper in the composition of the coating increases the extent of scattering of energy in the vibrational system because in the nanostructured condition these materials belong to the group of high-damping materials [7].

The coatings with a thickness of 50–150 μm produced on the selective materials were prepared by the technology of electron beam evaporation and deposition in vacuum [4]. Deposition was carried out on bar-shaped specimens of VT1-0 titanium alloy, characterised by the low dissipation properties at temperatures up to 450°C [8]. The starting blanks for the coatings were in the form of ingots of iron and copper, and also tablets of the pressed mixture of the powders of aluminium, iron and iron. In the deposition of the Cu–Fe coatings of the metals were evaporated from two targets simultaneously. The surface of the specimen was cleaned in the vacuum furnace with the argon ion beam. The rate of deposition of the coatings was 2–3 μm/min, and the structural condition of the coatings was varied by varying the temperature of the specimen in the range 160–600°C.

The deposition of the coatings on the compressor blades of the aviation gas turbine engines to ensure the homogeneity throughout the entire surface was carried out in the rotation conditions. For this purpose, the blades were secured to a horizontal shaft rotating during the formation of the coating.

The structure of the coatings was investigated by the methods of scanning and electron microscopy (equipment CamScan 4), and the microhardness of the coatings were measured on the cross sections of the specimens using the Vickers method with an optical microscope PolyvarMet at a load of 0.05N, testing time 10 s.

Main assumptions of the methods of investigating the dissipation properties of the coating materials and the damping capacity of structural members

The characteristics of the scattering of the energy of the material the coatings were

determined by the calculation–experimental method. Initially, the results of the tests of the console-constrained specimens with the coating in equipment, described in [9], in the conditions of damping oscillations, were used to obtain the amplitude dependences of the logarithmic decrement of the oscillations. Subsequently, the data were used, on the basis of the calculation procedure described in [10], to determine the amplitude dependences of the true logarithmic decrement for the coating material, i.e., the characteristics of energy scattering of the material in the uniform stress state.

The damping capacity of the structural members was determined using the experimental system, developed at the Institute of Problems of Strength of the National Academy of Sciences of Ukraine, for the investigation of the dissipative properties of the materials and structural members at both room and elevated temperatures [11], ensuring the minimisation of the energy losses in the sections, not connected with the hysteresis losses in the materials of the tested object and the coating. The logarithmic detriment of the oscillations was determined by the method of the resonance curve [1].

The tested object was the console specimen with the rectangular cross-section ($h \times b \times l$ = 4×12×150 mm). The coating was deposited only on one surface of the working section of the specimen along the entire width of the section b, starting from the root section. The length of the latter was constant, 50 mm. Tests were carried out on the specimens at the constant thickness h = 4 mm, with the decrease of the length of the working section l from 150 to 50 mm for obtaining the required frequency of the oscillations.

In accordance with the formulation of the problem, the following range of the variation of the test parameters was used: oscillation frequency 150–1000 Hz, temperature 20–400°C (on the whole, these parameters correspond to the service conditions of the working blades of the compressor of the aviation gas turbine engine).

Structure and properties of the coating materials

The structure of the copper coatings was varied by varying the deposition temperature T_c in the range 160–600°C. Consequently, the grain size D (crystallite) of the columnar grains decreased from 4–5 μm (T_c = 600°C) to 0.3–0.4 μm (T_c = 160°C). This was accompanied by qualitative changes in the substructure of the crystals.

Figure 1 shows that a decrease of deposition temperature results in changes of the internal structure of the crystals reflected in the formation of an interlayer of twinned

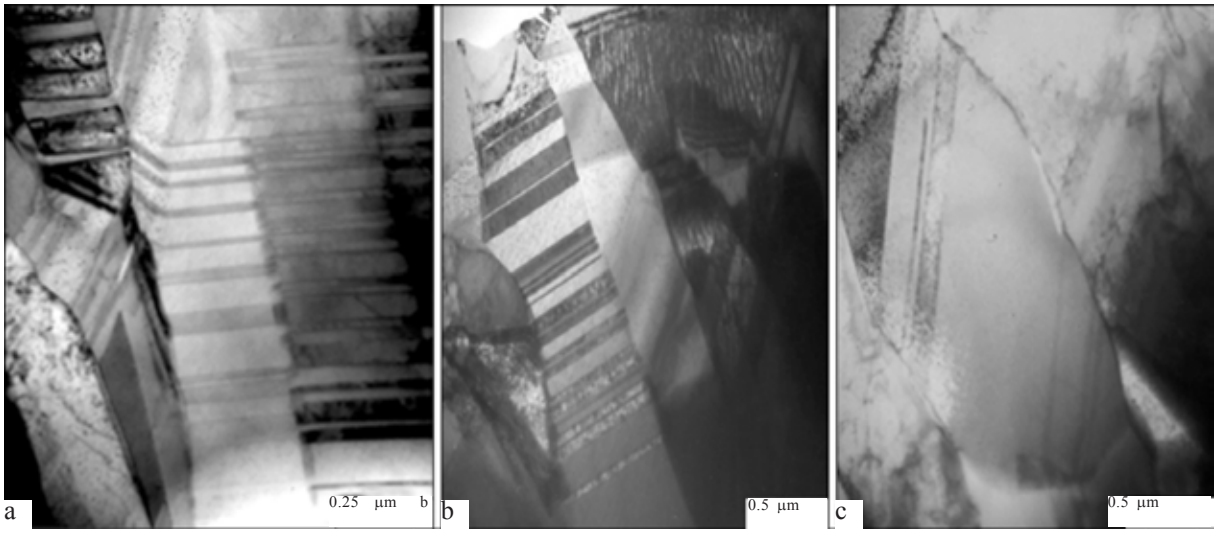

Fig. 1. Electron microscopic images of the cross-section of copper condensates deposited on a specimen at temperatures of 170 (a), 230 (b) and 350 (c); a) × 4000, b, c) × 2000.

domains, distributed mainly parallel to the front of crystal growth (Table 1). The number of these twins rapidly increased with the decrease of the deposition temperature, starting at $T_c \approx 350$°C [7]. With a further decrease of temperature, the number of these twins increases, leading to the formation of a polydomain nanotwinned substructure in the crystals (Fig. 1a).

The transition to the nanotwinned structural state of the copper coatings results in a large increase of the microhardness of the coatings from 0.8 to 1.5 GPa [7], and also in a qualitative change of the characteristics of energy scattering. This is reflected in a large decrease of the amplitude dependences of the logarithmic detriment, typical of the coarse-grained copper, with the retention of high values under heating (Fig. 2). In addition, in contrast to the coarse-grained copper, the characteristics of energy scattering of these coatings remain unchanged after multiple cyclic deformation.

The additional increase of the microhardness of the coatings (up to 2 GPa) is obtained as a result of adding 2–4% iron and copper. The energy scattering characteristics of such Cu–Fe coatings this case decrease at high stress amplitudes. At the same time, they remain sufficiently high and cyclically stable at the test temperature of 20–350°C. The results show that the curves obtained during cyclic deformation of the specimens at a temperature of 250°C are in almost complete agreement with the initial curve.

The variation of the mechanical and dissipative properties of the coatings produced from the copper condensates and Cu–Fe during the formation of the nanotwinned substructure is determined by the considerable weakening of the role of intragranular dislocations both in the process of plastic deformation and during scattering of mechanical energy.

At the dimensions of the structural elements of approximately 100 nm the generation of 'fresh' dislocations in the metals is no longer possible [12]. On the other hand, with the decrease of the grain size of the role of the grain boundary surfaces become smaller important and, consequently, the dominant mechanism in the nanostructured materials becomes the mechanism of scattering of energy, associated with the thermally activated rearrangement of the atomic configurations at the grain boundaries.

Figure 3 shows the results of investigation of the effect of the grain size on the energy scattering characteristics of the coatings of the Al–Cu–Fe composite alloy. In the coatings deposited at $T_c = 650$°C the mean grain size D was 580 nm. When the deposition temperature was reduced to 350 and 270°C the mean grain size decreased to 270 and 30 nm, respectively. For the coatings with the grain size of 580 and 270 nm the parameters of the energy scattering characteristics

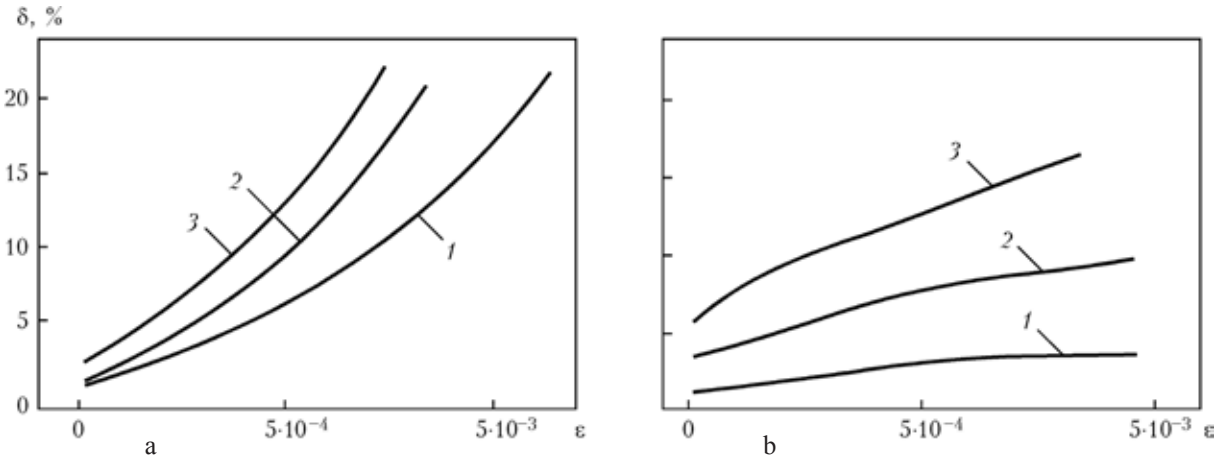

Fig. 2. Amplitude dependences of the logarithmic decrement of oscillations for a copper condensate with a grain size of 2.5 μm (a) and with a polydomain nano twinned substructure (b) at temperatures of 20 (1), 250 (2) and 350 (3) °C.

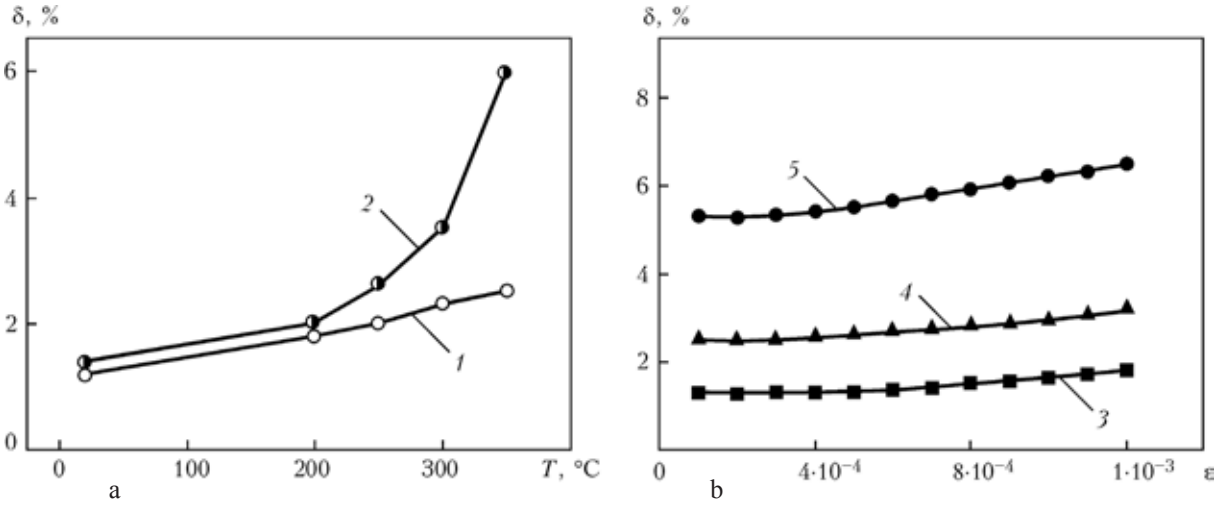

Fig. 3. Dependence of the logarithmic decrement of oscillations of the specimen with a coating of the Al–Cu–Fe alloy on temperature (a) at the relative strength amplitude of $\varepsilon = 5 \cdot 10^{-4}$ for the grain size of 580 (1) and 30 (2) nm and on the relative strength amplitude (b) at the grain size of 30 nm and different temperatures: 3) 20; 4) 300; 5) 350°C.

in the temperature range 20–400°C were low but with the decrease of the grain size to 30 nm there was a rapid increase of the decrement of oscillations at a temperature of 250–400°C (Fig. 3).

A special feature of the investigated nanostructured coatings is the amplitude-Independent nature up to the amplitudes of relative strain of $\varepsilon = 1 \cdot 10^{-3}$. This is important from the practical viewpoint. It is also important to note the high hardness of these coatings (15 GPa) and lower elasticity modulus (177 MPa) in comparison with the coating of the same composition with the grain size of 270 and 580 nm and the elasticity modulus of 207 and 210 MPa, respectively.

Thus, the experimental results show that by selecting the appropriate conditions of electron beam deposition on the surface of structural elements it is possible to produce nanostructured coatings with the higher level of dissipative and mechanical properties.

Results of determination of the damping capacity of structural members with coatings and analysis of the results

Analysis was carried out on three types of coatings of these materials, with the characteristics presented in Table 1.

The determined amplitude–frequency characteristics of the specimens were used to determine their logarithmic decrement of oscillations and the corresponding dependence on the amplitude of maximum stresses max during the variation of the frequency of oscillations and test temperature for different values of the parameters of the coatings. It should be mentioned that at the resonance tested is not possible to ensure the same frequency of oscillations of these specimens. However, since this difference is small, it does not have any significant effect on the analysis of the test results.

For the comparative analysis of the effect of factors on the damping capacity of the specimens with the selected coatings, preliminary tests were carried out to determine the amplitude dependences of the decrement of oscillations for the specimens without a coating in the given oscillation frequency range at room temperature (20°C), with the results show in Fig. 4a. The results show that the dependences are linear and the effect of the frequency of oscillations of the value of the oscillation decrement is small at low stress amplitudes and slightly increases with increase of the amplitudes.

The results of the tests will be investigated from the viewpoint of the effect of the fre-

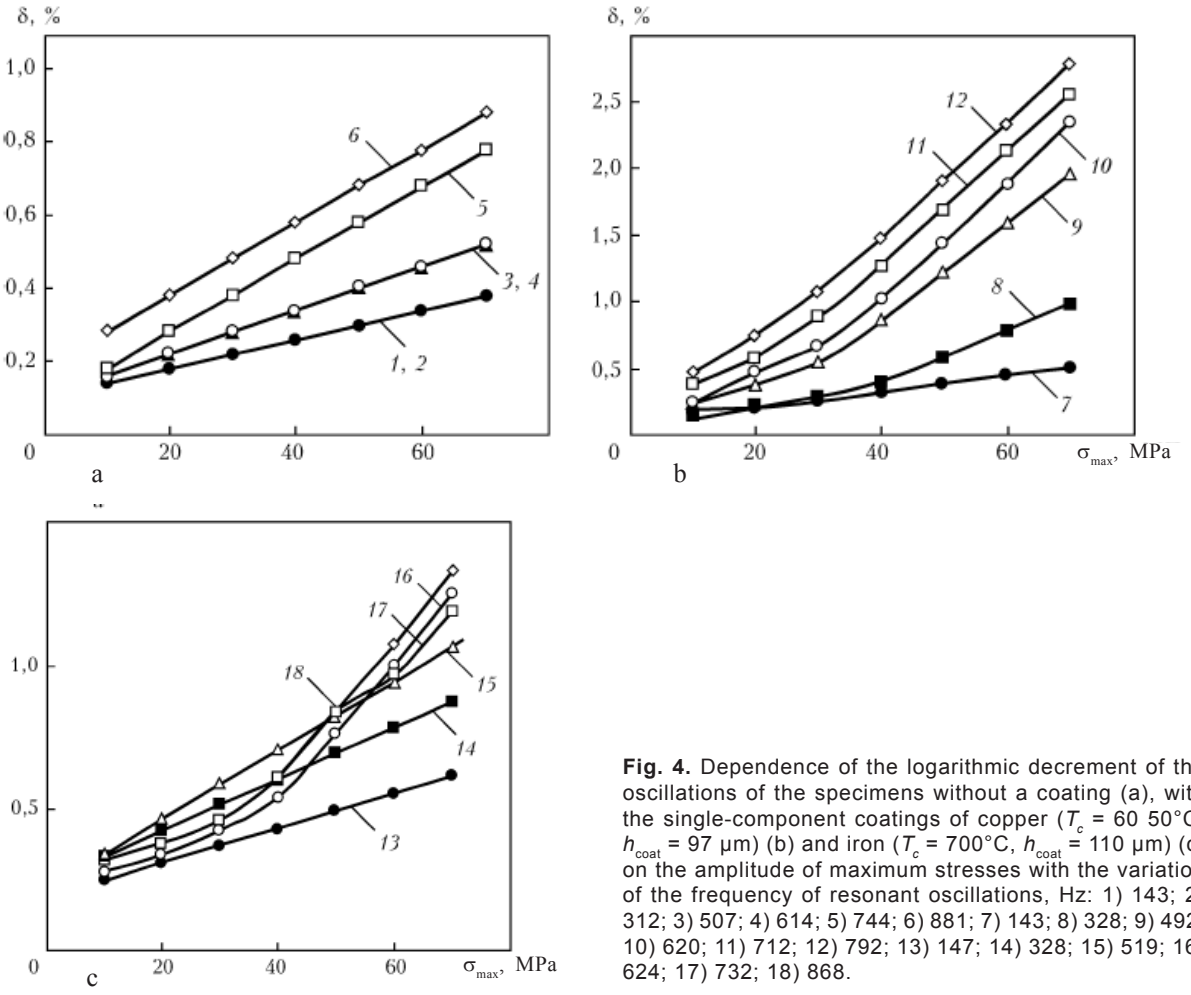

Fig. 4. Dependence of the logarithmic decrement of the oscillations of the specimens without a coating (a), with the single-component coatings of copper (T_c = 60 50°C, h_{coat} = 97 μm) (b) and iron (T_c = 700°C, h_{coat} = 110 μm) (c) on the amplitude of maximum stresses with the variation of the frequency of resonant oscillations, Hz: 1) 143; 2) 312; 3) 507; 4) 614; 5) 744; 6) 881; 7) 143; 8) 328; 9) 492; 10) 620; 11) 712; 12) 792; 13) 147; 14) 328; 15) 519; 16) 624; 17) 732; 18) 868.

quency of oscillations on the damping capacity of the specimens with the selected coatings.

The analysis of the amplitude dependences of the decrement of oscillations of the specimens with the single-component coatings (specimens 1–9, obtained at room temperature), corresponding to the specific structural state (Fig. 4b, c), show that in this case the effect of the frequency of oscillations on the value of the decrement depends on the type of coating. For example, the most significant frequency dependence of the decrement of oscillations characteristic of the copper coatings, especially at higher amplitudes of maximum stresses. The dependence is less distinctive for the specimens with the iron coating.

The effect of frequency on the decrement of oscillations of the specimens is clearly indicated by the frequency dependences of the decrement which for the amplitude of the maximum stresses (σ_{max} = 50 MPa) are presented in Fig. 5. Here the abscissa gives the mean frequency of oscillations taking into account that in the tests it is not possible to ensure the same values of the frequency.

The results of the tests show that the damping capacity of the specimens depend strongly on the characteristics of the microstructure.

On the whole, on the basis of the experimental results it may be concluded that the frequency dependence of the logarithmic decrement of the oscillations of the specimen is more characteristic in the deposition of the copper coating. The rate of growth of the coating is more distinctive for the coatings with the large grains and higher values of the amplitude of maximum stress. For the specimens with the iron coating this dependence of the logarithmic detriment on the frequency of oscillations have not been

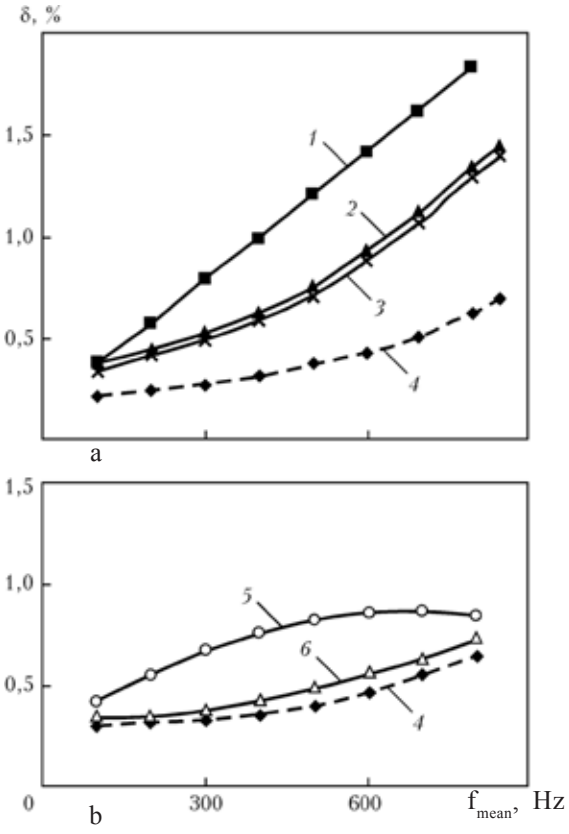

Fig. 5. Dependence of the logarithmic decrement of oscillations at the amplitude of the maximum stresses of 50 MPa of the specimens with the single-component coatings of copper (a) and iron (b) and the mean frequency fm of the resonance of oscillations for different parameters of the coating: 1) T_c = 605°C, h_{coat} = 97 μm; 2) 350°C, 150 μm, 3) 245°C, 170 μm, 4) the specimens without a coating: 5) 700°C, h_{coat} = 110 μm; 6) 340°C, 102 μm.

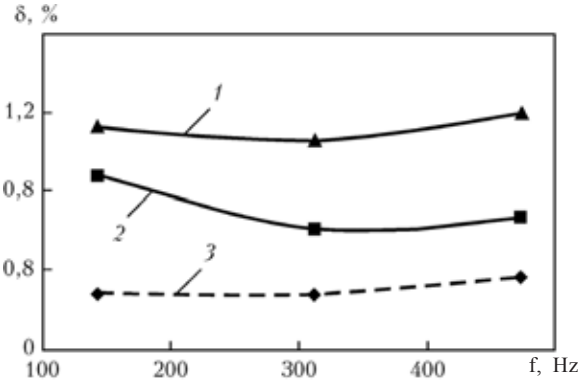

Fig. 6. Diagram of the variation of the logarithmic decrement of the oscillations of the specimen with a coating of the Al–Cu–Fe alloy (T_c = 500°C, h_{coat} = 62 μm) and frequency *f* of resonant oscillations at the amplitude of the maximum stresses of 45 MPa and a test temperature of 350 (1) and 20 (2) oC; 3) the specimen without a coating.

recorded, especially with a decrease of the amplitude of maximum stress.

In accordance with the tasks of the investigations, the results of investigations carried out to determine the combined effect of the frequency of oscillations and service temperature on the damping capacity of the specimens with the coating will be analysed. The solution of the problem is investigated on the example of the coating of the quasi-crystalline Al–Cu–Fe alloy (as the more suitable alloy) in comparison with the single-component coatings, for application in practice, especially for the working blades of compressor of aviation turbine engines.

Tests were carried out on the specimens with the variation of the same technological and service factor was investigated for the single-component coatings, and also the service temperature. As for the homogeneous coatings, the amplitude dependences of the logarithmic decrement of the oscillations on the amplitude of the maximum stress were obtained and the results of analysis of the relationships shows that the damping capacity of the specimens with the investigated coating can increase by a factor of three or more at elevated temperatures.

The resultant amplitude dependences of the logarithmic decrement were used for constructing the diagram of the variation of the decrement in relation to the frequency of the resonant oscillations of the specimen (Fig. 6). As indicated by the results, the frequency of oscillations has almost no effect on the damping capacity of the specimen with the multicomponent coating of the Al–Cu–Fe quasi-crystalline alloy.

Evaluation of the cyclic strength of titanium blades with the coatings of nanostructured copper

The high level and cyclic stability of the energy scattering characteristics of the nanostructured condensates based on copper, and also efficient adhesion of the condensates to the titanium alloys enable the investigated condensates to be proposed as the possible

component of the intermediate layer of the composite shielding coatings for the blades of aviation gas turbine engines.

The test results were used to determine the technological conditions of the position of the coatings of copper on titanium blades with the nanostructured state. Special attention was given to the effect of these coatings with a thickness of 5–10 μm on the resistance to fracture of titanium blades of VT3-1 alloy. For comparison, copper coatings with the micron grain size were deposited on the other part of the blades. The tests were carried out at a temperature of 20°C and the oscillation frequency of 530 Hz. The cyclic fatigue strength of the blades was estimated by the accelerated method in the conditions of the discrete increase of the amplitude of stresses after each of the $5 \cdot 10^6$ oscillation cycles [13].

The positive effect on the vibrational fatigue of the blades, having the coatings with the micron grain size, was recorded for 50% of the specimens. However, in the case of the nanostructured coatings positive results were obtained for all specimens, and 50% of the specimens did not fail up to the end of the tests.

The results confirm the assumption according to which the condensates based on nanostructured copper can be used as the components of composite coatings, for example, binding layers between the structural element and the main part of the coating.

Conclusions

1. The experimental results show that the damping capacity of the specimens with the coatings depend strongly on the structure and production parameters of the coatings, primarily on the deposition temperature of the coating and also the oscillation frequency.

2. It was also found that the logarithmic decrement of the bending oscillations of the specimens with the nanostructured coatings at elevated temperatures may increase by a factor of 3 or more, in comparison with the values at room temperature.

3. It is necessary to carry out further search for the optimum nanostructures of the coatings and production parameters to ensure the maximum dump capacity of the structural elements of the machines of the type of working blades of compressors of aviation gas turbine engines in the service conditions.

References

1. Matveev V.V., Damping of oscillations of the deformed solid, Naukova Dumka, Kiev, 1985.
2. Yakovlev A.P., Dissipative properties of heterogeneous materials and systems, Naukova Dumka, Kiev, 1985.
3. Ustinov A.I., et al., Probl. Prochn., 2008, No. 2, 149–159.
4. Paton B.E. and Movchan B.A., Welding and surfacing, 1991, No. 2, 43–64.
5. Sales M., et al., Surf. and Coat. Tech., 2007, No. 201, 6206–6211.
6. Milman Yu.V., et al., ibid, 5937–5943.
7. Ustinov A.I., et al., Acta Materialia, 2008, No. 56, 3770–3776.
8. Pisarenko G.S., et al., A handbook of the strength and materials, Naukova Dumka, Kiev, 1988.
9. Ustinov A.I., et al., Probl. Prochn., 2001, No. 4, 55–61.
10. Ustinov A.I., et al., Probl. Prochn., 2007, No. 6, 134–143.
11. Lebedev A.A., et al., Strength of materials and structures, Akademkniga, Kiev, 2005.
12. Kaschner G.C., et al., Acta Materialia, 2002, No. 50, 653–662.
13. Matokhnyuk L.E., Accelerated fatigue tests in high–frequency loading, Naukova Dumka, Kiev, 1988.

Advances in Electrometallurgy 2010 ***8*** *(1) 39–42*
Translated from Sovremennaya Elektrometallurgiya 2010 ***8*** *(1) 34–36*

Electron beam equipment for melting of molybdenum

V.O. Mushegyan

Paton Armeniya Scientific and Technical Centre, E.O. Paton Electric Welding Institute, Kiev

MV-1 industrial electron beam equipment is described. The technical characteristics of the installation are given. Functional peculiarities of such installation components as: working chambers, technological fixture, electron guns are described.

The melting of molybdenum is a complicated technical task as a result of the high melting point (2617°C) and stringent requirements on the purity of metal as regards the content of impurities [1]. In the world practice, molybdenum ingots are melted by vacuum-arc or electron-beam remelting in which the shielding medium is represented by vacuum and concentrated energy sources (electric arc and the electron beam).

Vacuum-arc remelting in a rarefied atmosphere of the inert gas is characterised by limited possibilities as regards the removal of harmful impurities and gases from the initial molybdenum material and, consequently, this method requires high purity charge materials. Electron beam melting is carried out in higher vacuum ensuring a high degree of purification of metal [2].

The method of electron-beam remelting with an intermediate container (EBIC) is especially efficient [3]. As a result of the spatial separation of the processes of melting, refining and solidification of the metal, this method makes it possible to keep the metal melt in the intermediate container for the period of time required for refining to the required purity level.

To achieve the maximum effect from the application of the EBIC method in the area of melting of refractory metals, it is necessary to develop new industrial systems combining the high productivity of the vacuum system with the high specific power of the electron beam. The E.O. Paton Electric Welding Institute, Kiev has accumulated a large amount of experience in the construction of these systems.

Armenia has large reserves of molybdenum which is extracted in copper–molybdenum ore deposits. Metallic molybdenum in the form of the reduced powder is produced at the Chistoe Zhelezo company (Erevan) in the form of briquettes according to TU RA28-54-529-61-661-2007. Melting equipment was required for further purification of molybdenum to remove impurities and produce high-quality ingots, suitable for deformation to semifinished products.

For this purpose, the Paton Armeniya Scientific and Technical Centre of the E.O. Paton Electric Welding Institute, Kiev, constructed electron beam equipment MV-1 (Fig. 1), capable of melting efficiently the refractory metals and alloys of these metals.

Equipment consists of a melting chamber, a loading chamber, and an ingot chamber. All the elements of the structure are produced with hollow walls in which water circulates for forced cooling during melting and cooling

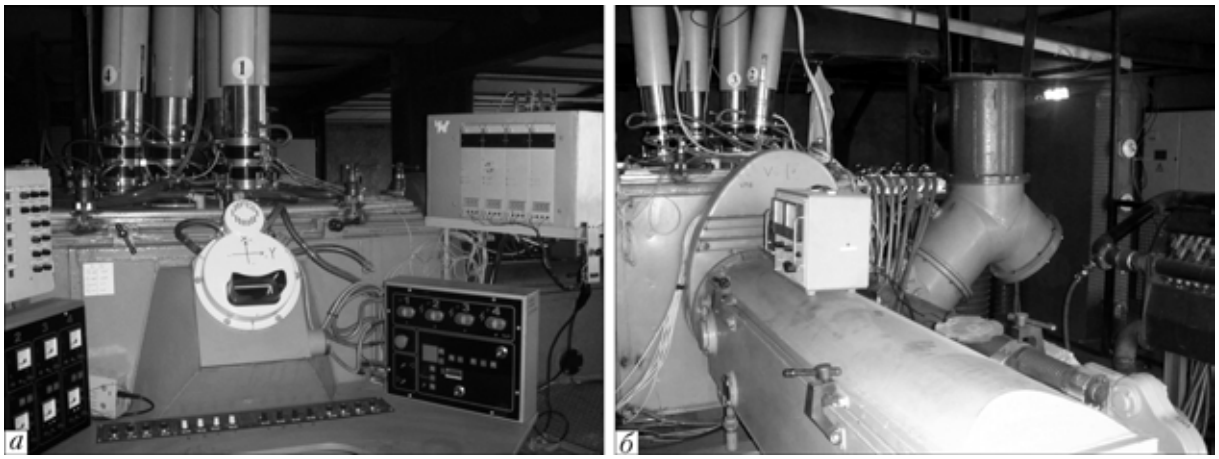

Fig. 1. MV-1 electron beam equipment: a) the operator panel; b) the view from the side of the loading chamber.

of the ingot. In addition to this, equipment is fitted with a power unit for electron beam heaters, control and stabilisation systems of the electron beams, and a vacuum system. The main technical parameters of equipment are:

Technical characteristics of MV-1 electron beam equipment

Maximum power, kW	480
Accelerating voltage, kV	30
Number of guns	4
Largest dimensions of the billets, m:	
length	2.2
cross-section	0.5 × 0.45
Largest dimensions of ingots, m:	
length	2.0
diameter	0.13
rectangular cross-section	0.2 × 0.3
Productivity of the high vacuum pumping system, l/s	15 000
Working vacuum in the melting chamber, Pa	$1 \cdot 10^{-2}$
Maximum consumption of cooling water, m^3/h	40
Dimensions of equipment, m	5×7×5

The melting chamber is the central part of equipment and is used for melting. It has the form of a vertical rectangle with the size of 1.5×0.9 m, covers with vacuum-tight lids and the top part on the bottom. The wall thickness of the chamber completely prevents the penetration of secondary x-ray radiation from of the chamber. The radiation is caused by the deceleration of electrons on the remelted material.

Inside the chamber, there is a technological device consisting of an intermediate container, a ??? and a solidification mould (Fig. 2). The electron beam guns VTR are placed on the upper cover (4 guns)

Technical characteristics of VTR gun

Nominal power, kW	100
Working scan frequency, Hz	50
Maximum current intensity, A	4
Angle of reflection of the beam from the axis of the gun, deg	0...10
Working gas	mixture of hydrogen and oxygen
Maximum flowrate of the gas, l/h	1.0
Diameter of the spot in the gun focus, mm	10-20

During inspection and operations, the upper plate can be moved using a shop crane for cleaning the upper surfaces of the cover and the guns to remove deposits settled there during melting.

The ingot chamber is connected with the inspection orifice in the lower cover. The cooling water is supplied through the nozzles in the side wall of the chamber into the components of the technological system using copper nozzles.

The side wall of the chamber contains an inspection system (stroboscopic) for the operator. Opposite the operator is the DU400 nozzle into the chamber wall through which the melting chamber is connected with the pumping system to a vacuum gate. To the

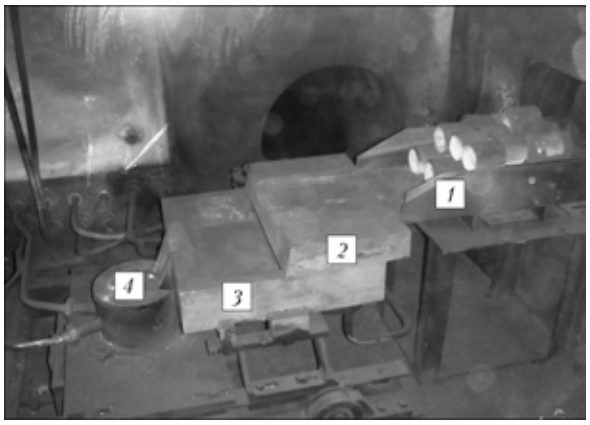

Fig. 2. Processing chamber with rigging; 1) the box with the charge (molybdenum briquettes); 2) the top plate; 3) the intermediate container; 4) the solidification mould.

right of the operator the melting chamber is connected with the loading chamber, also using a DU 400 vacuum gate.

The loading chamber has the form of a hollow parallelepiped with the cover fitted with a vacuum seal. The total length of the loading chamber is 2.2 m. For loading the charge, these sections of the chamber are separated after releasing the clamps situated on the ceiling perimeter and, subsequently, the cover is opened for loading the charge. The loading chamber contains the mechanism for feeding the charge which can be used to supply the entire blank, the consumable box with charge materials, pieces of charge and bulk materials (for example, the powder of reduced molybdenum).

In the first cases, a roller table is placed on the guides and the pusher transfers the blank into the melting zone. If the charge is separated into sections, the nonconsumable box is placed on the guides. The width of the box does not exceed the size of the back wall of the intermediate container, and the pusher uniformly transfers the charge materials into the intermediate container.

The ingot chamber has the form of a hollow rectangle with the size of 0.7×0.7×2.2 m which is secured to the lower cover of the chamber using a flange. A bar is introduced into the ingot chamber through the vacuum seal at the bottom, and a copper water-cooled base plate is placed on the upper part of the bar. The baseplate is secured in the ingot chamber using two traverse, connected together with screw bars.

On the outside of the ingot chamber there is a drive which transfers, through the screw bars, vertical displacement of the bar for withdrawing the ingot during melting. The drive consists of an electric motor and a reduction gear.

In the lower part of the ingot chamber there is a window for access to the internal part of the withdrawal mechanism. Through this window plates are placed on the baseplate prior to melting and the completed ingot is released after melting prior to extraction from equipment.

The technological system in which electron beam remelting takes place consists of an intermediate container, a bottom plate and a solidification mould. The intermediate container (cold base) has the form of a copper watercooled surface restricted by the walls, with one of the walls containing an orifice for the discharge of liquid metal (pouring spout). In the container, the charge supplied from the loading chamber is melted using the electron beams.

The intermediate container is used for averaging of the chemical composition, refining the melt to remove impurities (including gas impurities) and inclusions [3]. During melting, a skull forms on the bottom of the intermediate container and protects the walls and the bottom against interaction with the molten metal.

From the intermediate container, the metal is poured into the solidification mould having the form of a hollow close contour, whose internal part, which is in contact with the ingot metal, is produced from watercooled copper. The intermediate container, the bottom plate in the solidification mould form a single section assembled on a steel frame, secured in the melting chamber.

The attachment system is such that the section inside the chamber can be efficiently replaced (change to other dimensions of the ingot).

The vacuum system of MV-1 equipment

includes vacuum mains, gates and pumps: mechanical, the vapour jet and diffusion. The mains consists of steel pipes, connecting the pumps with each other and also with the melting chamber, the guns, and ensure the required flow sections for the maximum utilisation of the productivity of the ions.

The evacuation of the internal cavities of the chambers of equipment from the atmospheric pressure is carried out with AVZ-125D mechanical pump. The productivity of the pump is such that the residual pressure of $3 \cdot 10^4$ Pa can be produced in the chamber within 10 min. For further evacuation removal of the gases of metal vapours during melting, the system contains the main vacuum mains consisting of the following pumps:

AVZ-125	2
2DVN1500	1
2NVBM400	2

The vacuum system of equipment MV-1 produces rarefaction in the volume of the melting chamber ($1 \cdot 10^{-2}$ Pa) for breakdown-free operation of the electron beam guns and the required degree of refining of the melted metal throughout the entire technological process.

The main technical special feature of MV-1 electron beam equipment is the stability of melting refractory metals – high specific power of electron beam heating in elation to the volume of the melting chamber and the design solution of the rigging, resulting in efficient degassing and melting of the initial materials.

The presence of four VTR guns with a total power of 480 kW ensures the specific power of the electron flux in the intermediate container of approximately $2 \cdot 10^6$ W/m^2, and in the zone of melting of the briquettes of reduced molybdenum powder $3 \cdot 10^7$ W/m^2, which is fully sufficient for refractory metals.

If necessary, the equipment produces electron bombardment in a point with the specific power $5 \cdot 10^8$ W/m^2. To increase the productivity of electron beam melting of refractory metals, the initial charge must be degassed [4].

For this purpose, the technological rigging in MV-1 electron beam equipment is fitted with a copper watercooled plate (base) of a considerable length on which the molybdenum briquettes are preheated and partially melted under the effect of electron beams.

Equipment is fitted with a stroboscopic system for inspecting the melting process using an external drive so that visual inspection can be carried out and the inspection system can be serviced without interrupting the process.

The MV-1 electron beam equipment is a high-productivity industrial system for melting metals and alloys with an intermediate container. The charge materials include both the whole consumable blank or pieces of waste and bulk materials. The high specific power of the electron beams enables effective melting of the refractory metals and alloys based on these metals. Since it is possible to replace efficiently the rigging, equipment can be used for melting both circular and right angled sections ingots.

References

1. Emel'yanova V.S. and Evtyukhin A.I., Molybdenum in nuclear power engineering, Atomizdat, Moscow, 1977.
2. Movchan B.A., et al., Electron beam melting and refining of metals and alloys, Naukova Dumka, Kiev, 1972.
3. Paton B.E., et al., Electron beam melting, Naukova Dumka, Kiev, 1997.
4. Paton B.E., et al., Electron beam melting of refractory and high-reactivity metals, Naukova Dumka, Kiev, 2008.

Advances in Electrometallurgy 2010 ***8*** *(1) 43–46*
Translated from Sovremennaya Elektrometallurgiya 2010 ***8*** *(1) 37–39*

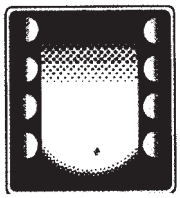

VACUUM-INDUCTION MELTING

A melting-pouring ladle with induction heating

V.A. Shapovalov, F.K. Biktagirov, A.P. Ignatov, V.I. Kolesnichenko, O.V. Karuskevich, Yu.A. Nikitenko, V.V. Yakusha, A.V. Glatushenko and A.N. Gnizdylo

E.O. Paton Electric Welding Institute, Kiev

The results of development of a portable melting-pouring module are given. The principal feasibility of creation of units of a ladle-furnace type with induction heating for melting, treatment and transporting of molten steel is shown.

In metallurgical production, the steel melted in a specific system for finishing and refining is treated in the ladle-furnace type equipment. The heat losses in the process of this and subsequent treatments (vacuum treatment, transport, casting) are compensated by arc heating in which the heat is transferred by the upper metal layer.

Therefore, to average-out the temperature over the height of the ladle, it is usually necessary to use bottom blowing of metal with argon with the appropriate technical facilities (argon mains, porous inserts, regulating and controlling apparatus, etc).

A special feature of arc heating is local subelectrode superheating of the melt, resulting in the burn-out of alloying elements and also the high level of thermal load on the arc and on the upper belt of the ladle, causing premature wear of the lining.

To fulfill the pouring conditions and ensure high quality of the steel billets, the temperature of metal in the steel pouring ladle must be maintained in a specific range (relatively narrow). The excessive reduction of the metal temperature in the ladle results in clogging up of the pouring vessel, and the superheating of the metal above the pouring temperature reduces the service life of the ladle and leads to unjustified energy losses.

Taking into account the special features of arc heating, it is relatively difficult to ensure the uniform and required temperature of the metal throughout the entire volume of the ladle. From this viewpoint, it is preferred to use induction heating in which the heating power can be efficiently regulated, and the metal in the ladle is efficiently mixed as a result of electromagnetic forces, ensuring the uniformity of the temperature field.

In addition, in induction heating it is possible to combine in time the heating and vacuum treatment operations and this has a positive effect on the production costs in metallurgy.

As regards the formation of a refining slag in the ladle during induction heating, this can be carried out using the same electric

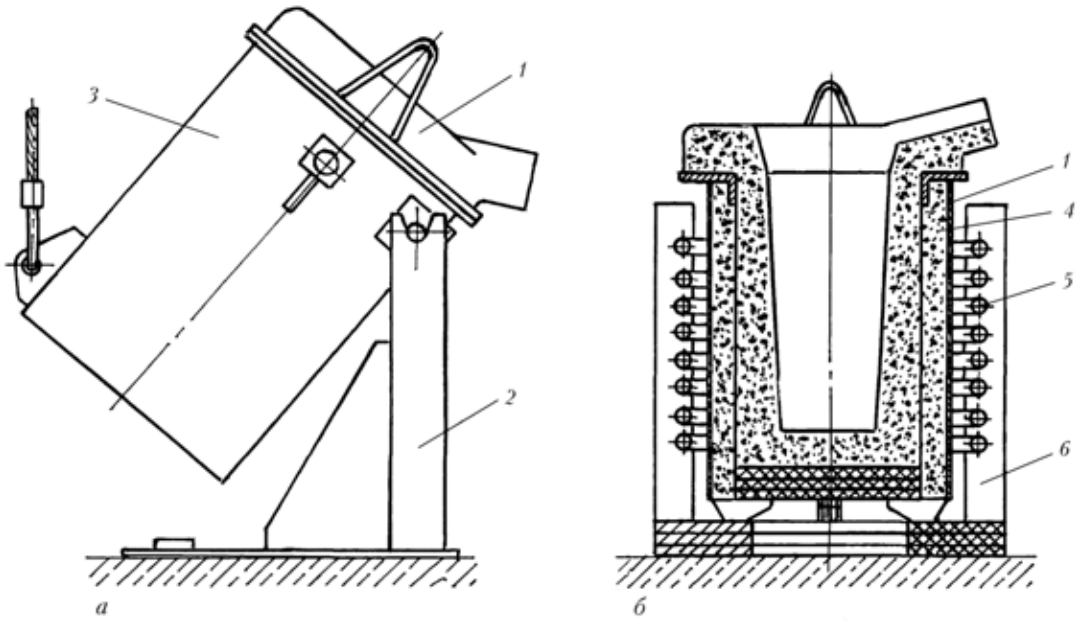

Fig. 1. Laboratory melting-pouring module (a) with induction heating of metal in the ladle-furnace (b): 1) ladle, 2) tilting mechanism, 3) 'vessel', 4) lining, 5) the induction coil, 6) columns for securing the induction coil.

arc electroslag heating procedures, but the power in this case is considerably lower in comparison with purely electric arc heating of the entire volume of the ladle, and gas heating, including with the so-called flame-slag torches, is also used [1].

The ladle-furnace with the induction or hybrid heating system can be used to treat steels with the required heating rate, shorten the treatment time, and maintain the metal temperature in the strictly specified range. Induction heating can also be used for operation of the steel pouring ladle in the 'mixer' regime, for example, when expecting transfer to the pouring position or if the pouring cycle is disrupted.

To develop such a system, it is necessary to design a ladle which can be transported from position to position, i.e., with the separation of the 'induction crucible furnace' classic scheme into two independent units – a stationary heater and a mobile ladle. In this case, the body of the ladle with no water cooling should be 'transparent' for the electromagnetic field. The currently available designs provide for the manufacture of the body from metallic non-magnetic materials, for example, stainless steel or titanium. However, this results in a large increase of the cost of the ladle and does not eliminate partial screening of the electromagnetic field and also power losses.

The patent [2] proposes that the body of an induction ladle, with the exception of the bottom and top parts, should be produced from non-metallic materials (refractory concrete). However, the ladles of this type can be used preferentially in pouring of low-melting metals and are not suitable for steel melting production. Therefore, it was important to develop a melting-pouring module with induction heating which would make it possible to separate the heater and the ladle and would be characterised by the high service strength of the body.

Design was based on the structure of the body of a ladle in the form of a metallic frame of the 'squirrel wheel' type. The individual elements of this structure have the form of packets of electrically insulated strips of non-magnetic steel, rigidly connected together, with a thickness smaller than the depth of penetration of current, induced by the induction heater.

The space between the metallic frame is filled with a refractory material forming the crucible of the ladle. As a result of the

presence of the metallic frame, this ladle is characterised by high strength and the body itself does not screen the electromagnetic field of the induction coil [0].

Laboratory equipment was developed for verification of the efficiency of this ladle (Fig. 1). The following geometrical parameters of the ladle were selected taking into account the available power source (machine converter with a frequency of 8 kHz, power 100 kW): internal diameter 120–150 mm, height 400 mm, lining – packed magnesite lining; the thickness of the lining 30–50 mm; the liquid metal mass up to 30 kg. The ring-shaped multi-turn induction coil was produced from copper pipe in the form of a spiral. The induction coil is not connected with the ladle and is secured to the load-carrying columns. In the laboratory conditions, the metal is discharged from the ladle through a spout and by tilting in a special pouring module with the tilting mechanism placed in the 'vessel' of the ladle under the angle of 90° (Fig. 1b). The general view of this melting-pouring module is shown in Fig. 2.

During service, the ladle filled with the molten metal is placed inside the induction coil. Power is supplied to the coil and the metal is heated to the required temperature with simultaneous alloying and refining.

After reaching the required temperature and completing technological operations the power supply to the induction coil is disconnected, the ladle is withdrawn from the coil and transported to the pouring position where the metal is poured into an ingot mould. If necessary, slag is removed prior to pouring.

The results of the tests with the variation of the heating conditions and the grade of treated steel showed high efficiency and safety of the system. The technological procedure and equipment can be used not only for treating the melt at a specific temperature to carry out metallurgical operations but, taking into account the power range of the induction source, can melt the charge without reducing the load-carrying capacity of the ladle [4].

Thus, in future it would be possible to introduce various variants of the design of the ladle and the induction coil, depending on volume. Preliminary calculations show that for ladles with the capacity of 10–20 t it is preferred to use a stationary ring-shaped induction coil, and for ladles with a capacity greater than 50 t a stationary system of the magnetic circuit with individual induction coils (Fig. 3). To make contact between the magnetic circuits in the body of the ladle it is recommended to use special 'windows' transparent for the electromagnetic field.

In addition, the body of the ladles with induction heating can be pear-shaped to reduce the heat losses, including the losses from the metal surface, and improve the efficiency of mixing of the metal bath. The pear-shaped form is also preferred from the viewpoint of distribution of the stresses in the jacket of the ladle.

Induction heating can be applied to maintain the required temperature of metal in the intermediate ladle (Fig. 4) and it is also proposed to separate the heated section and the stationary induction coil.

On the basis of the investigations and analysis of the sources it may be concluded that the application of induction heating of the portable ladle–furnace system makes it possible to average-out and regulate smoothly the metal temperature in the entire volume; halve the treatment time of the metal; combine the operation of heating with vacuum and slag treatment of the metal; carry out blowing with the gas, refining and additional

Fig. 2. General view of the melting-pouring module: 1) induction coil; 2) ladle; 3) pouring module.

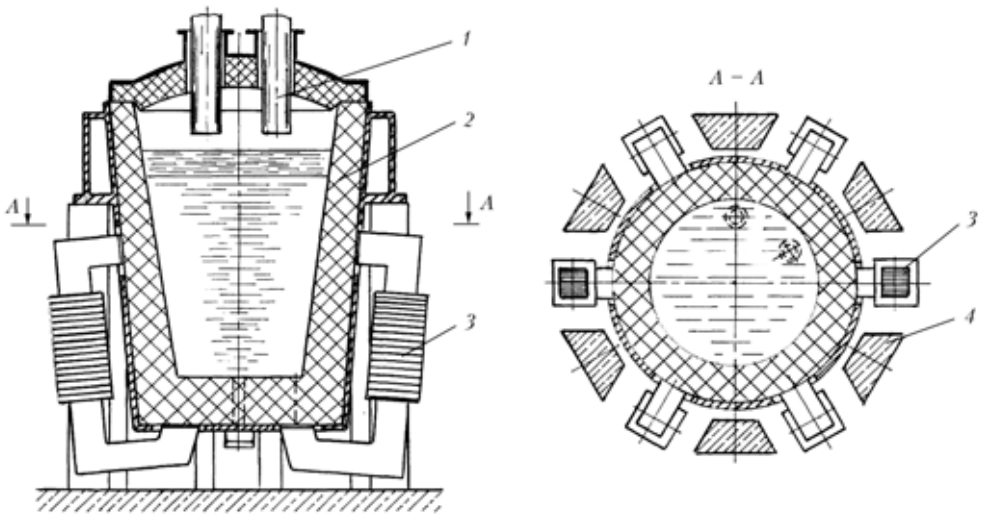

Fig. 3. Diagram of a hybrid induction ladle–furnace with magnetic circuits: 1) arc heater, 2) ladle, 3) magnetic circuit, 4) ladle support.

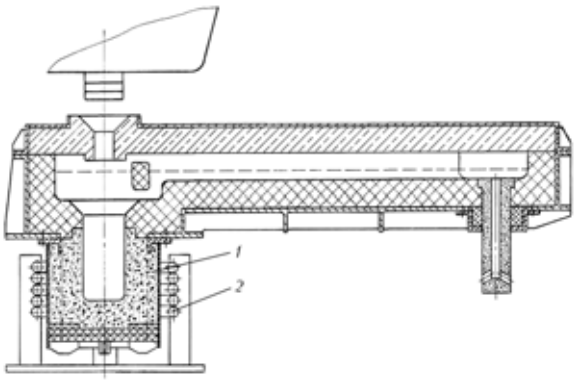

Fig. 4. Diagram of induction heating in the intermediate ladle: 1) heating section, 2) induction coil.

alloying; reduce the burn-out of the metal and alloying elements as a result of preventing local superheating of the metal; reduce the consumption of electrical energy for additional superheating of the metal; extend the service life of the ladle and save refractory materials; reduce technogenous loading on the surrounding atmosphere.

References

1. Dudko D.A., et al., Complete improvement of the quality of steel billets, Tekhnika, Kiev, 1969.
2. Larson H.G., et al., Ladle or tundish, US Patent 4618964, MPC N 05 V 5/16, 21.10.1976.
3. Paton B.E., et al., Patent 36318, Ukraine, MPC V 22 D 41/005, 27.10.2008, Equipment for heating, transport and pouring of molten metal,
4. Shapovalov V.A., et al., Key problems of the development of electrometallurgy, Proceedings of the Second international scientific and technical conference, Kiev, 2009, 44.

Advances in Electrometallurgy 2010 ***8*** *(1) 47–55*
Translated from Sovremennaya Elektrometallurgiya 2010 ***8*** *(1) 40–46*

GENERAL PROBLEMS OF METALLURGY

Modelling stationary regime of the reaction of self-propagating high-temperature synthesis in nanolayered materials (phenomenological model)

1. Single-stage reaction

T.V. Zaporozhets, A.M. Gusak and A.I. Ustinov

B. Khmel'nitskii Cherkask National University
E.O. Paton Electric Welding Institute, Kiev

The simplified and self-consistent (with respect to the temperature profile) analytical models of the stationary mode SHS in multilayer nanostructures based on the application of kinetics of reaction growth of phases in thin films under non-isothermal conditions are proposed.

Recently, the processes of self-propagating high-temperature synthesis (SHS) have been studied quite extensively on the nanolevel not only in the powder systems [1] but also in multilayered structures. The interest in these structures is determined by the fact that they can be used as intermediate layers in the formation of permanent joints in low-weldability materials, for example, composites or intermetallics [2, 3].

As a result of the generation of a large amount of heat during the SHS reaction in multilayered systems based on intermetallic-forming components they can be used as local heat sources in brazing [4]. It is also promising to use these systems as the initial material in the production of thin intermetallic foils.

To ensure the required parameters of the solid-phase reactions in the multilayered structure, it is necessary to take into account a number of factors, such as the chemical and concentration compositions of the foils, the thickness of the foils and the period of the multilayer, the spraying conditions of the foil (the degree of non-equilibrium of defects, the presence of intermediate phases and the probability of formation of these phases), and the reaction initiation parameters (temperature and ignition time).

The experimental solution of this problem requires the formulation of a large number of experiments. One of the methods of simplifying the problem is the construction of theoretical models which make it possible to predict the characteristics of the combustion front in the SHS process in relation to the experimental conditions.

In a general case, the SHS reaction should be studied in the non-stationary conditions,

because the systems in which they take place are usually characterised by the complex phase diagrams. In this case, the phases can grow both simultaneously or successively and, consequently, there is competition between exo- and endothermic processes with changing local temperature which in turn predetermines the course of evolution of phase formation. The behaviour of the system becomes difficult to predict and because of the large number of the varied parameters it is necessary to find the required SHS conditions.

According to the authors, this problem can be solved by the construction of a simulation model of the self-consistent solution of heat conductivity and diffusion equations taking into account the phase characteristics changing discretely in time and in space.

This is due to the fact that the diffusion parameters of the phases and their thermodynamic stimuli of transformation depend, on the one hand, on the temperature and concentration fields and, on the other hand, affect them as a result of exo- or endothermic reactions. A preparatory stage of the construction of such a model is the development of a series of simple phenomenological models for describing the partial cases of the structure of the combustion front of the SHS reaction.

Since the diffusion transfer of the combustion products in the direction of propagation of the front is almost completely negligible [1], during the diffusion process in the direction normal to the propagation of the combustion front, the front itself travels the distance $\sqrt{a^2 / D} \sim 10^3$ greater (a^2 is the thermal diffusivity coefficient, D is the diffusion coefficient). Consequently, the profile of the combustion front can be divided into the required number of the intervals to ensure that in each interval the temperature is regarded as constant, the diffusion process is isothermal and the duration of passage of the front is sufficient for the formation of the final product of solid-phase combustion.

For example, the Al/Ni system is characterised in most cases by a sequence of the formation of equilibrium phases with the increase of the nickel content and the generation of heat in the condition of the presence of a sufficiently large number of reagents both for mutual diffusion in the bulk specimens [5] and in interaction in thin films [6–8]. If it is assumed that external heat removal and the losses of heat in melting of aluminium are small, the resultant final phase will be determined by the initial composition of the foil.

The aim of the present work is the phenomenological description of the stationary propagation of the flat front as a result of the formation of a single intermediate phase. The model should be capable of predicting the main parameters (the speed of propagation of the front and the temperature of the front) on the basis of the characteristics of the multilayer structure (the period of the multilayers, the ratio of the number of the components, the degree of nonequilibrium of the structure). The solution of the inverse problem makes it possible to determine the optimum parameters of the structure for obtaining the required rate, temperature of the front and (if necessary) products of the SHS reaction with the required properties.

The construction of the model of processes in the nanolayered structure enables us to use directly the laws of mutual and reaction diffusion with a correction for the spatial nonuniformity of the temperature field [9], whereas in the case of the powder systems it is necessary to use the general equations of chemical kinetics with some fitting coefficients (the interpretation of these coefficients is not always unambiguous).

We examine a nanolayered two-component foil in the form of alternating M layers of the components A and B (Fig. 1), the width and the period of the multilayer $4l$, where l corresponds to half the thickness of the layer of the same component (the thicknesses of the layers A and B are identical).

In contrast to the mutual diffusion approach, used in [9], it is assumed that the heat does not generate in the entire volume and only on the moving interphase boundaries. The model of propagation of the front is constructed using the reaction diffusion equations. This

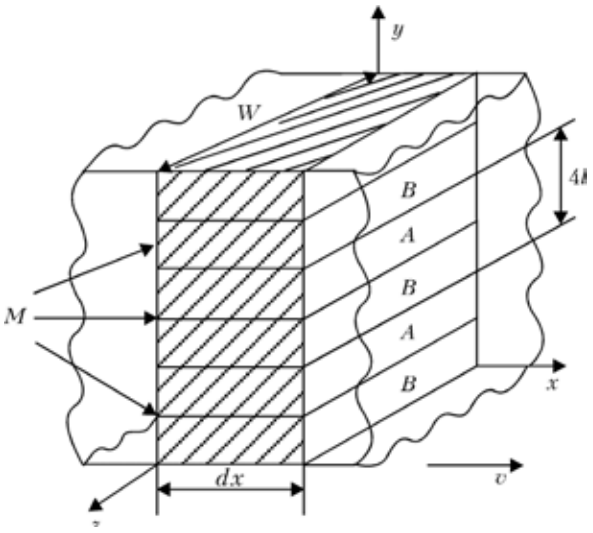

Fig. 1. Geometry of the specimen of a multilayer binary film.

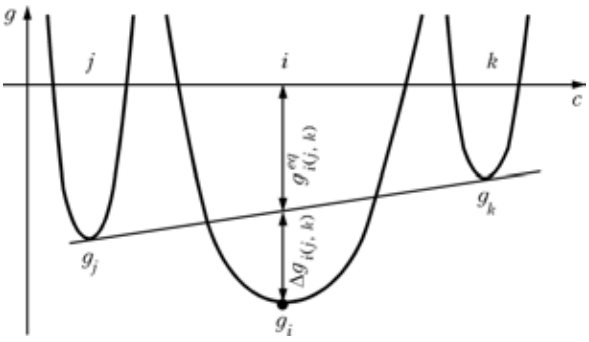

Fig. 2. The thermodynamic stimulus: $\delta g_i(j,k)$ is the free energy released in calculation for the atom during the formation of the phase *i* from phases *j* and *k* in accordance with the law of conservation of matter; it is calculated as the difference between the Gibbs potential (per atom) of the *i*-th phase *g* and the potential $g^{eq}_{i(j,k)}$ of a mixture of the adjacent phases *j*, and also *k* of the appropriate composition.

is more efficient in the formation of intermediate compounds with narrow regions of homogeneity in the SHS process.

The following main assumptions of the phenomenological model can be defined:

–the propagation front of the reaction is flat and stationary;

–as regards the concentration and temperature, all the phase boundaries correspond to the equilibrium diagram;

–a single phase forms during the passage of the front;

–the diffusion flows in the front are directed mainly normal to the direction of front propagation (on the condition that the width of the combustion front is considerably greater than the period of the multilayer);

–the resultant phase is characterised by a narrow homogenising range with similar values of the concentrations c_{left}, c_{right} $(\Delta c \equiv c_{right} - c_{left} << 1)$ at the boundaries x_{left}, x_{right}. In this case, we can use the constant flow equation [10], i.e., the densities of the flows J_{left} and J_{right} on the left and right boundaries are approximately the same and equal to the density of the flow inside the phase. This flow density is determined by the integration, i.e., from the mean value the concentration dependence of the diffusion coefficient $\bar{D}$ (c):

$$j_{left} \sim j_{right} \sim j = -\frac{\frac{1}{\Omega}\int_{c_{left}}^{c_{right}} D(c)dc}{\left|x_{right} - x_{left}\right|} = -\frac{\frac{1}{\Omega}\bar{D}\Delta c}{x_{right} - x_{left}}, \quad (1)$$

where Ω is the atomic volume;

–there is no heat removal through the external surfaces of the multilayer.

The investigated the growth of the intermediate δ-phase between the α-phase (solid solution based on *A*) and the ζ-phase (solid solutions on the basis of *B*) with the thermodynamic stimulus per atom $\Delta g_{\delta(\alpha,\zeta)}$ (Fig. 2) [11]. The thermodynamic stimulus depends on temperature but in calculations it is assumed to be constant because of the insufficient number of the actual data. Since the foil has a periodic structure, we select the minimum period with thickness 2*l*, where *l* is the 1/4 period of the multilayer; Δy_0 is the initial thickness of the layer of the phase formed prior to the SHS reaction (Fig. 3).

In the thin section *dx*, normal to the direction of propagation of the front, the formation of the phase during time *dt* takes place in the interlayer $d\Delta y_\delta(x)$, containing $d\Delta y(x)$ dxW/Ω atoms (Fig. 4). The generated heat $\Delta g_{\delta(\alpha,\zeta)} d\Delta y_\delta(x) dxW/\Omega/dt$ is used for heating the interlayer *dx* throughout the entire thickness 2*l*. Thus, the variation of temperature in the section *dx* is:

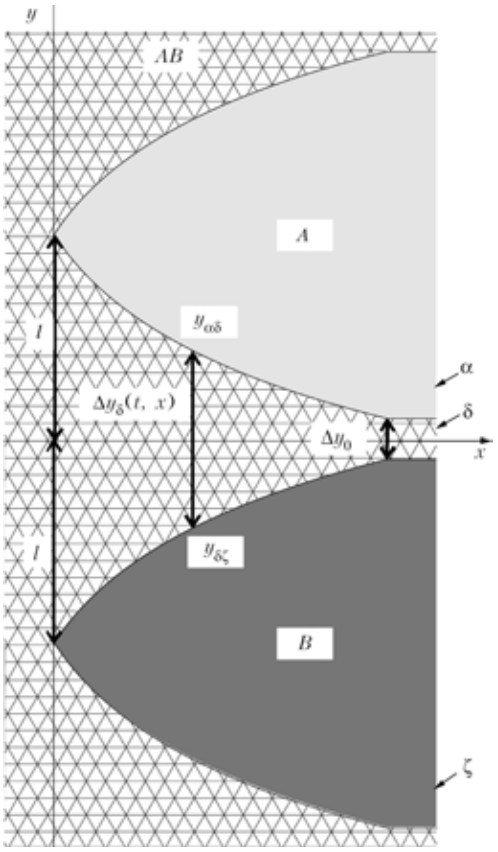

Fig. 3. The geometry of the model of growth of the intermediate δ-phase.

$$q\delta(x) = \frac{\Delta g\delta(\alpha,\xi) d\Delta y\delta(x)\, dx W / \Omega / dt}{c_p \rho 2l\, dx W} = \frac{\Delta g\delta(\alpha,\xi)\, d\Delta y\delta(x)}{2lc_p \rho \Omega dt}, \quad (2)$$

where c_p is the specific heat capacity, ρ is density.

In the stationary combustion regime each point of the front moves with constant speed v and is characterised by temperature $T(x)$, the width of the phase formed $\Delta y(x)$ between two layers, heat generation per atom during unit time $q_\delta(x)$. It is evident that the diffusion characteristics depend on temperature, determined by heat generation which in turn depends on the efficiency of the diffusion process. Thus, the solution of the problem is the determination of self-consistent profiles $T(x)$, $\Delta y(x)$ and $q(x)$. For this purpose, it is necessary to use the iteration procedure which is stopped when these profiles are stabilised.

To construct the self-consistent model,

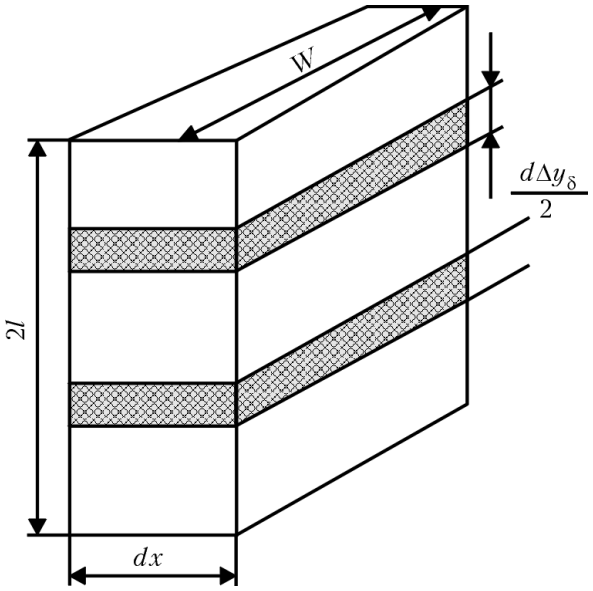

Fig. 4. The interlayer $d\Delta y_0$ from which the heat is generated during the period *dt*.

requiring numerical calculations, we determine the profile of the width of the resultant δ-phase. For this purpose we write the equation of the balance of matter for the moving interphase boundary $y_{\alpha\beta}$ (component *A*/intermediate phase) and for the moving interphase boundary $y_{\alpha\zeta}$ (intermediate phase/component *B*), using the approximation (1):

$$\begin{cases} (c_\delta - 0)\dfrac{dy_{\alpha\delta}}{dt} = -\dfrac{D_\delta \Delta c_\delta}{y_{\delta\xi} - y_{\alpha\delta}} \\ (1 - c_\delta)\dfrac{dy_{\alpha\delta}}{dt} = +\dfrac{D_\delta \Delta c_\delta}{y_{\delta\xi} - y_{\alpha\delta}} \end{cases}, \quad (3)$$

where c_δ is the mean concentration in the δ-phase; D_δ is the diffusion coefficient in the δ-phase; Δc_δ is the homogeneity range of the δ-phase.

After relatively simple mathematical transformations we obtain:

$$\frac{d\Delta y_\delta^2(t,x)}{dt} = \frac{2}{c_\delta(1-c_\delta)} D_\delta^W, \quad (4)$$

here $y_{\delta\xi} - y_{\alpha\delta} = \Delta y_\delta(t,x); D_\delta^W = D_\delta \Delta c_\delta -$ is the

diffusion permeability of the phase which depends on temperature (the function of time and coordinate) and is the combination of diffusion D_δ*(A), D_δ*(B) of the marked atoms *A*, *B* and the thermodynamic stimulus of the transformation $\Delta g_{\delta(\alpha,\,\zeta)}(T)$ [12]:

$$D_\delta^W(T(t,x)) = (c_\delta D_\delta^*(A) + (1-c_\delta)D_\delta^*(B)) \times \times \Delta g_{\delta(\alpha,\xi)}(T(t,x)) / k_B T(t,x), \quad (5)$$

where $c_\delta D_\delta^*(A) + (1-c_\delta)D_\delta^*(B) = D_{0\delta}^* \exp(-Q_\delta / k_B T(t,x)), D_{0\delta}, Q_\delta$ is the pre-exponential multiplier and the activation energy of diffusion, respectively; k_B is the Boltzmann constant.

After integrating equation (4) it must be taken into account that the interlayer $\Delta y_\delta(t,\, x)$ contains the layer Δy_0 with diffusion permeability D_0^{W} in which the reaction took place even prior to the start of the SHS:

$$\Delta y_\delta^2(t,x) - \Delta y_0^2(t,x) = \frac{2}{c_\delta(1-c_\delta)} \int_{-\infty}^{t} (D_\delta^W(T(t',x)) - D_0^W) dt', \quad (6)$$

where *t* is the time at which the interlayers of the new δ-phase come into contact.

We transfer to new variables

$$\xi = x - \upsilon t', t' = \frac{x-\xi}{\upsilon}, dt' = -\frac{d\xi}{\upsilon}$$ so that

$$\tilde{x} = x - \upsilon t, \begin{cases} \tilde{x} < 0 - after\ front \\ 0 < \tilde{x}\ in\ front \end{cases}$$

Consequently, at $\tilde{x} = 0$ the interlayers come together $\Delta y_\delta(t,\, 0) = 2l$ and the solution of (6) has the following form

$$\Delta y_\delta^2(\tilde{x}) \Delta y_0^2 + \frac{2}{c_\delta(1-c_\delta)} \frac{1}{\upsilon} \int_{\tilde{x}}^{+\infty} (D_\delta^W(T(\xi)) - D_0^W) d\xi, \quad (7)$$

and the speed of propagation of the stationary front is

$$\upsilon = \frac{1}{4l^2 - y_0^2} \frac{2}{c_\delta(1-c_\delta)} \int_0^{+\infty} D_\delta^W(T(\xi)) - D_0^W) d\xi. \quad (8)$$

In the heat conductivity equation, we transfer to the introduced variable $\tilde{x}$:

$$-\upsilon \frac{\partial T}{\partial \tilde{x}} - a_\delta^2 \frac{\partial^2 T}{\partial \tilde{x}^2} = = \begin{cases} 0 \quad \tilde{x} < 0, \Delta y(\tilde{x}) = 2l - after\ front \\ q_\delta(x) 0 < \tilde{x}, \quad \Delta y_0 < \Delta y(\tilde{x}) in\ front \end{cases}. \quad (9)$$

Equation (2) is substituted into equation (9), followed by preliminary substitution $dt = d\tilde{x}/\upsilon$, and we obtain the equation describing the dissipation of heat in the front ($0 < \tilde{x}$):

$$-\upsilon \frac{\partial T}{\partial \tilde{x}} - a_\delta^2 \frac{\partial^2 T}{\partial \tilde{x}^2} = \frac{\Delta g_{\delta(\alpha,\xi)(T(\tilde{x}))}}{2lc_p \rho \Omega} \upsilon \frac{d\Delta y_\delta(\tilde{x})}{d\tilde{x}}. \quad (10)$$

The formal solution of equation (9) leads to the following integral equation:

$$T(\tilde{x}) \begin{cases} T_0 + \frac{1}{\upsilon} \int_0^\infty q_{\delta(\alpha,\xi)}(T(\xi)) d\xi, \tilde{x} < 0 \\ T_0 + \frac{1}{\upsilon} \int_{\tilde{x}}^\infty q_{\delta(\alpha,\xi)}(T(\xi)) d\xi + \\ + \frac{1}{\upsilon} \int_\infty^{\tilde{x}} q_{\delta(\alpha,\xi)}(T(\xi)) \exp\left(\frac{\upsilon}{a_\delta^2}(\xi - \tilde{x}) \right) d\xi, 0 < \tilde{x} \end{cases} \quad (11)$$

which can be solved using the iteration self-consistent procedure of the simultaneous determination of the profile of variation of temperature (11) and speed (8).

In order to avoid using the described iteration procedure, the proposed model can be simplified by obtaining simple analytical estimates of the maximum temperature in the front T_f and the speed of the front υ. This requires another assumption: when solving the heat conductivity equation (but not the diffusion equation!) it is necessary to ignore the heat generated as a result of the formation of the new phase. Consequently, in the quasi-stationary approximation $\frac{\partial T}{\partial t} = -\upsilon \frac{\partial T}{\partial x}$ the heat conductivity equation has the form $-\upsilon \frac{\partial T}{\partial t} = a^2 \frac{\partial^2 T}{\partial x^2} = 0$ with the solution of

$$\frac{\partial T}{\partial x} = \left(\frac{\partial T}{\partial x} \right) \exp\left(-\frac{\upsilon}{a^2} x \right) \sim \exp\left(-\frac{x}{L} \right),$$

where the width of the front is

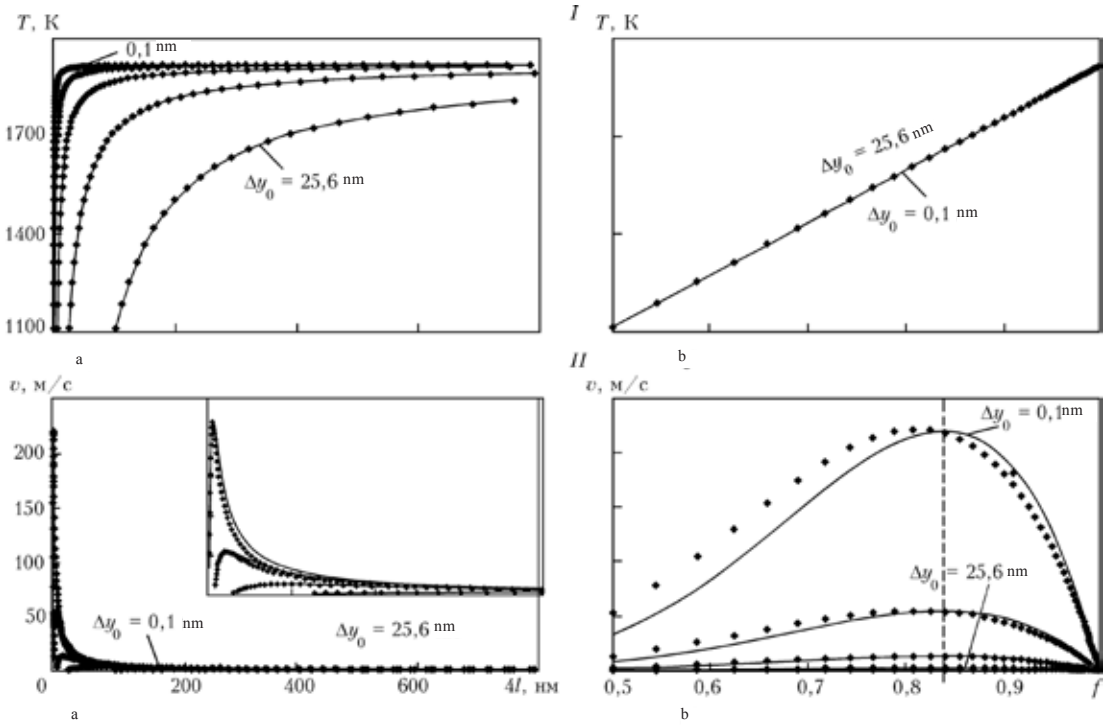

Fig. 5. Dependences of maximum temperature in the front T_f (I) and the speed of the front υ (II) on the period of the multilayer $4l$ (a) and the coefficient of efficiency of the interlayer f (b) at different values of the width of the initial phase y_0 as a result of formation of a single intermediate phase during calculations using the self-consistent model (lines) and analytical evaluation (points). The broken line passes through the maximum values of the speed at different values of y_0.

$$L = \frac{a^2}{\upsilon}. \tag{12}$$

During the time $\tau \sim \frac{L}{\upsilon} = \frac{a^2}{\upsilon^2}$ of passage of the front through the width L the δ-phase with the equilibrium concentration c_δ should close up as a result of reaction diffusion

$$\frac{2}{c_\delta(1-c_\delta)}\int_0^\tau D(T(t))dt \approx (2l)^2 - (\Delta y_0)^2, \tag{13}$$

where

$$D(T) = D_{0\delta}\exp\left(-\frac{Q_\delta}{k_B T}\right)\frac{\Delta g_P \delta(\alpha,\xi)}{k_B T}.$$

As a result of the integration of the equation (13) using quite simple but cumbersome mathematical transformations we obtain the expression for the speed of propagation of the stationary front:

$$\upsilon = \sqrt{\frac{2}{c_\delta(1-c_\delta)}\frac{\alpha^2 D_0 \delta \Delta g_{\delta(\alpha,\xi)}}{4l^2 - \Delta y_0^2}\frac{T_0(k_B T_f + Q_\delta)}{Q_\delta^2 (T_f - T_0)}\exp\left(-\frac{Q_\delta}{k_B T_f}\right)}, \tag{14}$$

where T_f is the maximum temperature at the front. It is estimated using equation (10). Since the maximum temperature is reached during the time of passage t of the reaction throughout the entire thickness of the effective interlayer $2l–\Delta y_0$, the variation of temperature is

$$T_f - T_0 = \int_0^t q_\delta(x)dt' = \frac{\Delta g_{\delta(\alpha,\xi)}(2l - \Delta y_0)}{2lc_p\rho\Omega}. \tag{15}$$

It is evident that as the thickness of the initial interlayer y_0 increases, the maximum temperature T_f at the front decreases. At $y_0 = 0$ the maximum temperature $T_{\max} = T_0 + \frac{\Delta g_{\delta(\alpha,\xi)}}{c_p\rho\Omega}$. is reached.

The proposed analytical estimate does not take into account the effect of heat generation on the temperature profile (zero in the right-hand part of the heat conductivity equation), i.e., this model is not self-consistent.

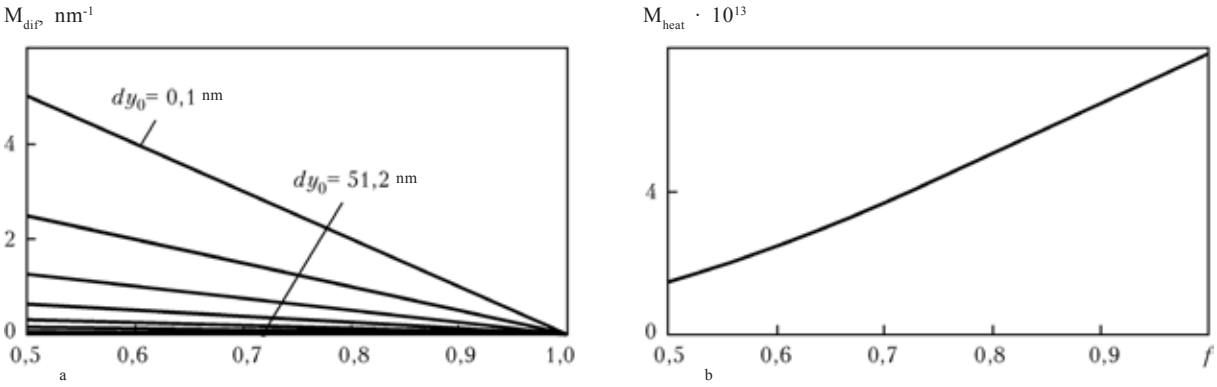

Fig. 6. Competing factors M_{dif} (a) and M_{heat} (b); the superposition of these factors determines the non-monotonic form of the dependence of the speed of the front on the coefficient of efficiency of the interlayer f ($Q = 1.35 \cdot 10^{-19}$ J).

The quantitative estimates of the proposed models with one intermediate phase were obtained using the parameters described in [9]: $c_\delta = 0.5$; $D^*_{0\delta} = 1.5 \cdot 10^{-5}$ m²/s; $Q_\delta = 2.7 \cdot 10^{-19}$ J; $a^2_\delta = 7.451 \cdot 10^{-5}$ m²/s; $T_0 = 300$ K; the thermodynamic stimulus of the formation of the δ-phase $\Delta g_{\delta(\alpha,\zeta)} = 7.36549 \cdot 10^{-20}$ J was determined from the equation (15) at $\Delta y_0 = 0$ and $T_f = 1919$ K.

The results can be efficiently analysed using the parameter $f = (2l - y_0)/(2l)$, which determines the fraction of the interlayer which has not reacted in the process of production of the multilayer foil where a phase can form in the process of SHS. This means that f shows the efficiency of the SHS reaction (at $f \cong 1$ the temperature of the front reaches the maximum value $T_f = T_{max}$) and may have values from zero (phase formation took place throughout the entire thickness of the interlayer) to 1 (the multilayer film consists of pure components without intermediate phases). Therefore, the introduced parameter f is referred to as the coefficient of efficiency of the interlayer. In computer calculations, the value of this coefficient is in the range $0.5 \leq f < 1$, because the multilayer foil with $f < 0.5$ is not used efficiently in the SHS processes.

The quantity l (a quarter of the period of the multilayer) varied from Δy_0 ($f = 0.5$, half the interlayer has reacted) to 200 nm (the maximum value in spraying), and the thickness of the interlayer Δy_0, which interacted prior to the passage of the combustion front, varied from 0.1 nm ($f \cong 1$, smaller than the interplanar spacing) to 100 nm ($f = 0.5$, half the maximum thickness of the interlayer in spraying). The graphs show the results for Δy_0, having the values of 0.1; 0.4; 1.6; 6.4; 25.6 nm.

In the computer calculations the maximum temperature at the front (Fig. 5, I) was fixed; the speed of the front was calculated from equation (8) (Fig. 5, II). The results were compared with the estimates obtained from the simplified analytical model: for the speed of the front using equation (14), for the maximum temperature at the front from equation (15). The speeds of the front were in qualitative agreement. For quantitative agreement, it was sufficient to introduce an adjustable multiplier p in the equations (12) and (14):

$$L = p\frac{a^2}{\upsilon}, \tag{12*}$$

$$\upsilon = \sqrt{p\frac{2}{c_\delta(1-c_\delta)}\frac{\alpha^2 D_0 \delta \Delta g_{\delta(\alpha,\xi)}}{4l^2 - \Delta y_0^2}\frac{T_0(k_B T_f + Q_\delta)}{Q_\delta^2 (T_f - T_0)}\exp\left(-\frac{Q_\delta}{k_B T_f}\right)}, \tag{14*}$$

$$\text{Where } T_f = T_0 + (T_{max} - T_0)f. \tag{15*}$$

The points in Fig. 5, II show the profiles of the speed of the front υ at the optimum adjustable multiplier $p = 4.04$ (determined for the maximum value of the dependence $(4l)$ at $\Delta y_0 = 0.1$ nm).

Since the results of the proposed models are in qualitative agreement, the resultant

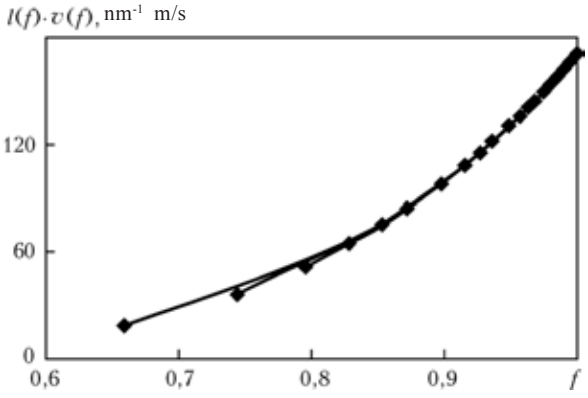

Fig. 7. Dependence of the product $l(f)\upsilon(f)$ on the period of the coefficient of efficiency of the interlayer f with the variation of the values of the width of the initial phase Δy_0 and the fixed values of l (50, 75, 100, 125, 150, 175 nm) as a result of calculations using the self-consistent model.

relationships will be analysed using the analytical expressions (14) and (15). Equation (15) shows that the maximum temperature at the front depends on the thermodynamic stimulus of the formation of the new phase.

The dependence of temperature on the period of the multilayer $4l$ and the thickness of the initial interlayer of the new phase Δy_0 is determined by the coefficient of efficiency of the interlayer f and is linear (Fig. 5, I, b). At fixed Δy_0, the asymptotic value of temperature at the front is reached when the unit of the multilayer become sufficiently long for heating taking into account Δy_0: as the thickness of the initial interlayer increases, the period of the multilayer $4l$ at which the maximum temperature in the front is reached, becomes greater (Fig. 5, I, a).

The non-monotonic form of the dependence of speed on the period of the multilayer correlates not only with the analytical estimates for solid-phase [9] and gas-phase [13] combustion but also with the experimental results obtained for the TiAl system [14]. In the range of low values of l the coefficient of efficiency tends to the value 0.5, which indicates slow heating of the multilayer is which, according to the authors of [14], is caused by the 'increase of the specific surface of the interlayer boundaries per unit volume'.

The reasons for the non-monotonic dependence of the speed of the front on the period of the multilayer will now be analysed from the mathematical viewpoint. If the temperature of the front in equation (14*) is assumed to be the function of the coefficient of efficiency (15*) and $\frac{1}{4l^2-\Delta y_0^2}$ is regarded as $\frac{1}{4l^2 f(2-f)}$, the speed of the front can be described by a function of two variables:

$$\upsilon(l,f)=\frac{1}{l}\sqrt{const\,\frac{1}{f(2-f)}\,\frac{(k_B T_f(f)+Q_\delta}{(T_f(f)-T_0)}\exp\left(-\frac{Q_\delta}{k_B T_f(f)}\right)}, \quad (16)$$

i.e., the speed is determined by two such competing factors (without taking into account the constant quantities);

– the diffusion factor, inversely proportional to the period of the multilayer $M_{\text{dif}}\,(l) = 1/l$ and associated with the parabolic growth of the new phase (as the value of l increases, the diffusion path becomes longer); decreasing with increasing f (Fig. 6a);

– the thermal factor, which depends on the temperature of the front as a function of the coefficient of efficiency

$$M_{heat}(l,f)=\sqrt{\frac{1}{f(2-f)}\,\frac{(k_B T_f(f)+Q_\delta}{(T_f(f)-T_0}\exp\left(-\frac{Q_\delta}{k_B T_f(f)}\right)},$$

and increases with increasing f (Fig. 6b).

In this case, the maximum speed is obtained for the same value of f, regardless of the period of the multilayer structure (Fig. 6, II, b). In turn, the position of the maximum is determined by the activation energy of diffusion for the given phase: at $Q = 2.7\cdot 10^{-9}$ J the maximum speed corresponds to the value $f = 0.85$; at $Q = 1.35\cdot 10^{-19}$ J the maximum is displaced to $f = 0.675$.

The decrease of the speed of the front at f close to 0.5 can be explained by the controlling effect of the thermal factor M_{heat} which decreases at a considerably higher rate than the rate of increase of the diffusion multiplier M_{dif}, i.e., an increase of the period of the multilayer is accompanied by an increase of the diffusion path of the atoms, extending the heating time and, correspondingly, making it less effective.

In addition, equation (16) shows that the product of the speed in the period of the multilayer is determined by the coefficient of efficiency $l(f)\upsilon(f)$ = Func(f). To verify this relationship, determined on the basis of the simple analytical model, the dependence $l(f)\upsilon(f)$ was constructed and the variation of the value of Δy_0 at fixed values of l for the results obtained for the self-consistent model (Fig. 7). The curves coincide (small differences are caused by the errors of linear extrapolation in the determination of the speed for the fixed value of l from the dependences $\upsilon(l)$ at the fixed value of Δy_0 (Fig. 6a). The results against confirm the adequacy of the simple evaluation procedure.

Since the multilayer foils are non-equilibrium objects, it is not guaranteed that the diffusion and thermodynamic parameters of the model discussed here can be taken from the tables of physical quantities. This relates especially to the stimulus for the transformation and the activation energy of diffusion. It is proposed to interpret them as adjustable parameters in the equation (14*). It should be mentioned that the derivative ln $l(f)\upsilon(f)$ with respect to f (taking into account (15*)) depends on only on the single parameter Q_δ:

$$\frac{d\ln(l(f)\upsilon(f))}{df} = \frac{1}{2}\ln\left(\frac{1}{f^2(2-f)}\frac{Q_\delta}{(T_{\max}-T_0)}\right) - \frac{Q_\delta}{k_B T_f(f)}.$$

Comparison with the experimental curves can be used for the single-parameter adjustment of the value Q_δ. The adjustable value Q_δ may be used for determining the second free parameter $D_{0\delta}\Delta g_{\delta(\alpha,\xi)}$.

Conclusions

1. A phenomenological approach was used for describing the stationary regime of the process of SHS, controlled by reaction diffusion. The proposed models can be used for evaluating the effect of phase formation on the parameters of the combustion front.

2. Comparison of the results, obtained from the simple analytical evaluation, with the results of numerical calculations using the more complicated self-consistent scheme enables the adjustable parameter to the selected. The use of this parameter in equation (14*) can be used for a simple evaluation of the speed of the combustion front.

3. A self-similarity was detected in the behaviour of the multilayer system at the fixed value of the proposed efficiency parameter f.

4. The scaling relationships, determined using simple phenomenological models, can be used for evaluating the diffusion and thermodynamic parameters of the system, and also for adjustment (calibration) of the computer calculations of temperature and the speed of the combustion front to the experimental data.

5. The correlated model, adequately describing the actual experiments with SHS in thin films may be used for predicting the course of the SHS reactions in a wide range of the characteristics of the multilayer foils (the thickness and period of the multilayer, concentration composition, number of defects, etc). Consequently, it is possible to optimise the parameters of the course of the SHS reaction in thin foils without carrying out a large number of experiments.

References

1. Merzhanov A.G., Solid flame combustion, ISMAN, Chernogolovka, 2000.
2. Ishchenko A.Ya., et al., Avt, Svarka, 2007, No. 7, 5-9.
3. Ustinov A.I., et al., Intermetallics, 2008, volume 16, 1043-1045.
4. Shishkin A.E., et al., Metallofizika Noveish. Tekhnol., 2009, No. 9, 1179–1188.
5. Larikov L.N., et al., Diffusion in ordered alloys, Naukova Dumka, Kiev, 1975.
6. Colgan E.G., Mater. Sci. Rep., 1990, vol. 5, 1–44.
7. Ma E., et al., J. Appl. Phys., 1989, vol. 65, 2702–2712.
8. Ustinov A.I., et al., Sur. Coat. Technol., 2008, vol. 202, 3832–3838.
9. Mann B., et al., J. Appl. Phys., 1997, vol. 82, 1178–1188
10. Gusak M. and Yarmolenko M.V., Jibid, 1993, vol. 73, 4881–4884.
11. Gusak A.M., et al., Models of solid-phase reactions, ChNU, Cherkassy, 2004.
12. Gusak A.M. and Tu K., Acta Mater., 2009, vol. 57, 3367–3373.
13. Strunin V.A. and Manelis G.B., Fiz. Goreniya Vzryva, 2004, No. 3, 22–27.
14. Rogachev A.S., et al., ibid, 2004, No. 2, 45–51.

Advances in Electrometallurgy 2010 ***8*** *(1) 56–60*
Translated from Sovremennaya Elektrometallurgiya 2010 ***8*** *(1) 47–50*

ELECTROMETALLURGY OF STEEL AND FERROALLOYS

Effect of technological factors on the nitrogen content of steel melted in a superpowerful arc furnace

E.L. Korzun, A.G. Ponomarenko, A.V. Kodak and E.M. Yudenkov

Donetsk State Technical University

The effect of application of carbon powder for slag foaming in steel melting in a superpowerful furnace on the nitrogen content in metal is considered. The statistical dependence of the change of the nitrogen content in molten metal on the rate of adding of carbon materials in the finishing period is obtained. The double role of added carbon is outlined. The conditions of producing steels with ultra-low and regulated content of nitrogen are discussed.

Nitrogen is the subject of special attention because of its strong effect on the service properties of final components, the constantly increasing requirements on the quality of metal and the development of steel melting technology. The maximum permissible nitrogen content for many types of steel products is certified below 50 ppm, and for some types below 20 ppm [1, 2]. The complicated and in many aspects unique behaviour of nitrogen in the conditions of the steel melting process has been the subject of a large number of investigations, both general theoretical [3–5], and technological, relating to the specific melting conditions [6–9].

This article is concerned with describing the attempts for the generalisation of the publications and also some of the results obtained by the authors for the dynamics of nitrogen in melting of steel in a superpowerful arc furnace.

The unique behaviour of nitrogen during melting in open furnaces is manifested mainly by the fact that the nitrogen content of the metal always remains considerably lower (by approximately an order of magnitude) and the equilibrium content in relation to the furnace atmosphere and, most importantly, continues to decrease monotonically during melting [4, 6–9]. This means that nitrogen transfer takes place in the direction of the gradient (increase) of its chemical potential which at first sight contradicts the loss of thermodynamics and diffusion kinetics.

In handbooks dealing with the kinetics of metallurgical processes the investigation of the interaction of flows is usually restricted to a brief description of thermal diffusion, thermal EMF and Sorre effect. Therefore, the only explanation of this phenomenon in the literature is the removal or nitrogen by the bubbles of CO formed during carbon oxidation.

However, the extensive literature data, relating to the behaviour of gases in open furnaces working by conventional technology

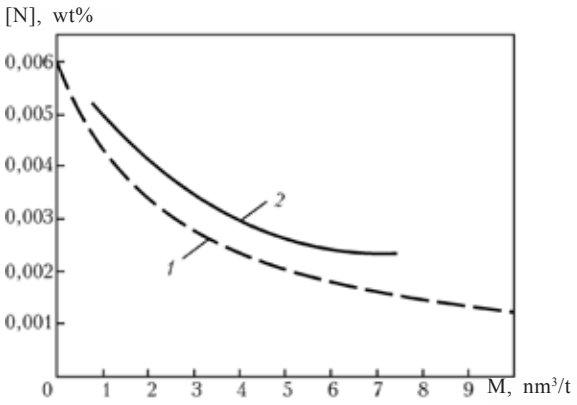

Fig. 1. Comparison of the results of calculations of the amount of the gas–carrier for the removal of nitrogen from the steel melt with the experimental data [12] at the initial nitrogen concentration of 0.006 wt.%: 1) calculations, 2) experiments, M is the consumption of the carrier gas.

(from open-hearth furnace to superpowerful arc furnaces) indicates that the complete interaction of oxidation of carbon in the reduction period of melting is not reflected to a large extent in the process of removal of nitrogen [6,10]. The nitrogen content continues to decrease even after introduction of the deoxidation agents. At the same time, simple calculations, based on the combined solution of the following two equations:

the Sieverts law for the solubility of nitrogen in metal

$$[N] = K_N - P_{N2}^{1/2} \quad (1)$$

and the pressure of gases in the bubble

$$P_b = P_{CO} + P_{N2,} \quad (2)$$

where [N] is the nitrogen content of metal, K_N is the equilibrium constant of the reaction of dissolution of nitrogen in metal, P_{N2} is the partial pressure of nitrogen in the bubble, P_{CO} is the pressure of carbon monoxide in the bubble (the formula proposed by Geller [11], calculations carried out by Yavoiskii et al [7], etc) shows that the 'bubble' mechanism of removal of nitrogen is effective only at a relatively high nitrogen content of the steel even at complete saturation of the rising bubbles with nitrogen.

If the kinetic delay which rapidly increases with a decrease of the nitrogen concentration is taken into account, the actual efficiency of the mechanism is even lower. Practical experience with degassing of the furnace and experimental investigations [12] show that the removal of nitrogen by the CO bubbles or bubbles of some other gas is almost completely interrupted when reaching the level of approximately 0.0024 wt.% even in blowing with a flow rate of 6–7 nm³/t (Fig. 1). Nevertheless, in the open hearth process conditions, the nitrogen content at the end of melting is often lower than 0.002 wt.% [4, 6].

There is a large number of examples indicating the existence of a nitrogen flow directed to the gradient of its chemical potential and the absence of any relationship between this phenomenon and carbon boiling of the metal. This is especially distinctive in the alloys with a high nitrogen solubility, in particular when melting low-carbon ferrochrome (approximately 80% Cr, 0.06% C, 1% Si) in the open arc ore–thermal furnaces.

The melting process in these furnaces is cyclic and in general features identical as regards the period of melting in the arc steel melting furnace: charging–melting–finishing–discharge; charge–ore, and limestone (in approximately the same amount), a reduction agent–silicon (silicochrome).

In the investigations carried out in this study, the furnace arch was not present. The solubility of nitrogen in the previously mentioned alloy was approximately 3% (almost 2 orders of magnitude higher than in argon) so that it was possible to investigate in detail the dynamics of behaviour of nitrogen in a wide concentration range.

According to the data in [13], nitrogen in the metal samples taken from the furnace at the end of melting was usually expressed in ten thousandths of a percent, regardless of the high affinity of chromium for nitrogen and the fact that the furnace atmosphere consisted mostly of nitrogen.

In the experiments with the development of technology of producing cast nitrided ferrochrome briquettes of vacuum-thermal nitrided ferrochrome (approximately 7 wt.%

of nitrogen) were loaded on the bottom of the furnace (prior to charging) to produce, in the completed alloy, the nitrogen content close to saturation. However, in this case, almost the entire amount of nitrogen added prove to be displaced into the atmosphere at the end of melting. Denitriding of metal and its independence of the process of carbon oxidation in electroslag remelting of steels and alloys have been shown in [14, 15].

At the same time, experiments carried out in specific conditions showed the active displacement of nitrogen into the metal from the furnace atmosphere during melting. Plasma-arc remelting is accompanied by a rapid nitriding of exposed metal in the region of the plasma 'spot' and 'nitrogen boiling' at the periphery. Consequently, the nitrogen content may decrease to equilibrium.

Similar phenomenon was reported in [16] in investigating the dynamics of the nitrogen content of the metal in the initial period of melting in an acid arc remelting furnace. During the passage of the electrode through the 'blocks' in the solid charge when the exposed film of running down liquid metal in the area of the arcs is in direct contact with the atmosphere, the nitrogen content increases by almost an order of magnitude, and at the end of melting decreases to the usual value.

The 'naked' metal, i.e., the metal not coated with the slag, may be rapidly saturated equilibrium both in the laboratory and industrial conditions in air or in a commercial nitrogen atmosphere. When the metal was separated from the furnace atmosphere by the slag layer, and the gas phase content even very small amounts of nitrogen, the situation greatly changed – nitrogen started to be transferred rapidly into the atmosphere. 'Nitrogen boiling' of the slag was clearly visible in the laboratory melts of ferrochrome.

The gas phase of the open furnaces always contains nitrogen and, consequently, the surface layer of the slag is oxidised to a higher degree than the layer which is in contact with the metal. The gradient of the chemical potential of oxygen causes diffusion flow of oxygen in the volume of the slag directed to the metal. In particular, this flow supplies oxygen to the steel melting bath during 'pure boiling' and is clearly manifested in the entire pattern of the material flows in the slag, up to changes of the direction of some of these flows towards the gradient (increase) of their chemical potential. These processes are sometimes referred to as 'pumping'.

The total drop of the degree of oxidation of the slag layer can be easily estimated by expressing it through the equilibrium partial pressure of oxygen P_{O2} on the upper and lower boundaries. In the case of the open furnaces of this value is approximately 10 kPa (air) and approximately $1 \cdot 10^{-3}$ Pa (the iron oxidised to the maximum extent that 1600°C). Consequently, using the calculation procedure described in detail in [17–19] we can calculate the thermodynamic limit of possible denitriding and obtain a large number of quantitative estimates relating to other flows. This procedure has also been used as a basis for the development in practice of a large number of technological measures for controlling the gas saturation of metal.

In the majority of the currently available superpowerful arc melting furnaces melting of steel is carried out by blowing a large amount of carbon powder in the final stage of melting (10... 15 min) in order to maintain the regime of 'immersed' arcs and carry out additional reduction of iron from the slag. Boiling of the slag which takes place in this case should, on the one hand, intensify the mass exchange processes in the volume of the slag, including the removal or nitrogen and, on the other hand, deoxidation of the surface with carbon reduces the dip in the degree of oxidation and they should have the directly opposite effect on the final nitrogen content.

In [19, 20] the results show the increase of the mean nitrogen level in the final period of melting with ejection in the individual melts to 0.015–0.020%. The replacement of operation of deoxidation of the slag with coke completely prevents these ejections and stabilises the nitrogen content at the end of melting on the level of approximately 0.005 wt.% [19]. Since the oxygen pressure

equilibrium with solid carbon and 600°C is approximately $1 \cdot 10^{-6}$ Pa, the dense coating of the surface of the slag with a carbon powder can not only reduce the gradient of the degree of oxidation in the slag layer but also change its direction.

The placing of coke on the surface of the slag (the so-called diffusion deoxidation) was widely used in open-half and arc furnaces operating by standard technology, but there is no mention of any relationship of this operation with the nitrogen content in the technical literature. Experimental investigation show [18] that the nitrogen content in the metal in deoxidation of the surface of the slag with carbon materials depend strongly on the conditions of the operation (added material, dispersion of the material, etc).

Therefore, of certain interest is the classification of this problem with special reference to the conditions of melting steel in superpowerful arc furnaces. Investigations were carried out at the electric steel melting section of the Donetsk Electrometallurgy Plant in a DSP-2 furnace. The nominal capacity of the furnace is 120 t, nominal power of the transformer 87 MV·A. The nitrogen content of the metal at discharge from the furnace was relatively stable in the range 0.004–0.009, with the mean content of 0.0063 wt.%.

The experimental procedure can be described as follows. During melting in the arc steel melting furnace the first sample for the nitrogen content was taken simultaneously with the first sample of the metal for melting the last charge, the second sample – just prior to discharge of the metal from the furnace. The nitrogen content of the metal samples was analysed by standard procedures of reduction melting in the flow of a carrier gas in a TC-300 gas analyser (LECO). The relative error of determination of the nitrogen content was 0.5%.

The results of determination of the nitrogen content in the metal were analysed together with certificates for the melts and the results of analysis of the chemical composition of the metal, with the samples for this analysis taken simultaneously with the samples of metal to determine the nitrogen content. On the whole, the nitrogen content was determined in 26 melts.

Analysis of the effect of the feed rate of carbon powder for foaming of the slag during finishing on the variation of the nitrogen content in the metal during the period between taking the samples showed the presence of a weak relationship between these parameters (Fig. 2, Table 1). Regardless of the low value of the determination coefficients, the effect of the rate of supply of the carbon powder on the variation of the nitrogen content of the metal ($R^2 = 0.077$) and of the coefficients of the regression dependence (Fig. 2) is strong (Table 1), with the confidence level of 90%, and the dependence is inversely weak ($-0.5 < R = -0.337 < 0$).

Thus, in the working conditions of DSP-2 furnace at the Donetsk Electrometallurgy Plant the increase of the rate of supply of the carbon powder for foaming the slag in the process of finishing in the arc remelting surface reduces the nitrogen content of the metal.

Conclusions

1. It has been shown that the addition of carbon powder in foaming of the slag has the contradicting effect on the variation of the nitrogen content of the metal. On the one hand, the oxidation of carbon particles

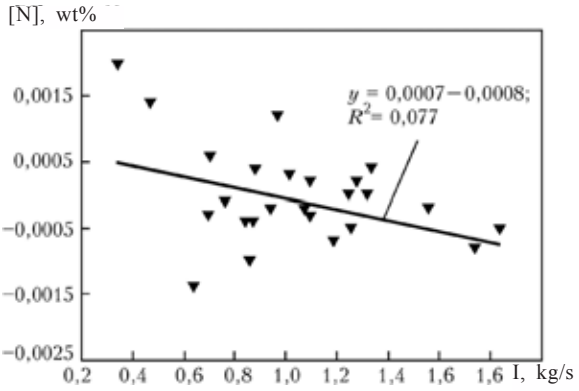

Fig. 2. Effect of the rate of supply *I* of the carbon powder for foaming the slag in the oxidation period on the variation of the nitrogen content of metal.

Table 1. Results of correlation analysis of the effect of the rate of supply of the carbon powder on the variation of the nitrogen content of metal

Regression coefficient in equation $y = a+b\ x$	Regression coefficient	Standard error of regression coefficient	Student criterion
A	0.000744	0.000508	1.4648
B	— 0.000814	0.000464	— 1.7532

Comment. 1. Here x is the rate of supply of carbon powder, kg/s; 2. Number of observations 24; 3. Correlation coefficient R = -0.337; determination coefficient R^2=0.077; more accurate determination coefficient R^2 = 0.077; value of F-criterion F(1.24) = 3.0736; significance of hypothesis $p < 0.09234$.

in the slag causes extensive mixing of the slag and intensifies therefore the 'pumping' effect reducing the nitrogen concentration of the metal. On the other hand, the supplied of an excessive amount of carbon on the slag surface results in a large increase of the scatter of the values of the final nitrogen content in the metal with an increase of its mean level [19].

2. All the steel melting processes with a long duration of holding the molten metal and the liquid slag (open-half melting, melting of steel from scale in an arc furnace with a continuous supply into the liquid pool) are characterised by the low nitrogen content of the metal in the ladle in melting and this is the consequence of the natural removal of nitrogen from the metal has a result of the 'pumping' effects.

3. It has been shown that the nitrogen concentration of the metal at the end of melting is independent of the nitrogen content in the initial materials, used for melting.

4. To control the nitrogen content of the steel melting processes, it is necessary to take into account the interaction of the flows of the components in the gas–slag–metal system and, in particular, the effect of the oxygen flow on the flows of other components of the system.

References

1. Zhang L. and Thomas B.G., ISIJ International, 2003, No. 3, 271–291.
2. Lule R., et al., AISTech 2009 Proc., 2009, vol. 1, 489–498
3. Pel'ke R.D. and Elliott G.F., Probl. Sovremen. Elektrometall., 1960, No. 6, 3–28.
4. Morozov A.N., Hydrogen and nitrogen in steel, Metallurgiya, Moscow, 1960s.
5. Svyazhin A.G., et al., Izv. AN SSSR, Metally, 1974, No. 5, 24–35.
6. Yavoiskii V.i., Gases in the pools of steel melting furnaces, Metallurgizdat, Moscow, 1952.
7. Luzgin V.P. and Yavoiskii V.I., Gases in steel and the quality of metal, Metallurgiya, Moscow, 1983.
8. Yanke D., Chernye Metally, 1992, No. 2, 3–11.
9. Debra W., et al., Arch. Metall. Materials, 2008, No. 2, 523–529.
10. Kramarov A.D., Production of steel in electric furnaces, Metallurgiya, Moscow, 1964.
11. Knyuppel' H., Deoxidation in vacuum treatment of steel. Part one: Thermodynamic and kinetic special features, translated from the German, Metallurgiya, Moscow, 1984.
12. Knyuppel' H., Deoxidation in vacuum treatment of steel. Part two: The fundamentals and technology of ladle metallurgy, translated from the German, Metallurgiya, Moscow, 1984.
13. Bezobrazov S.V., Theoretical fundamentals and technology of production of high-quality ferrochrome, Dissertation, Moscow, 1984.
14. Klyuev M.M and Volkov S.E., Electroslag remelting, Metallurgiya, Moscow, 1984.
15. Latash Yu.V. and Medovar B.I., Electroslag remelting, Metallurgiya, Moscow, 1970.
16. Pilliod C.F., et al., Trans. American Foundrymen's Society, 1992, No. 8, 23–25.
17. Ponomarenko A.G. and Kozlov Yu.E., Izv. VUZ, Chern. Metall., 1975, No. 5, 20–25.
18. Kodak A.V., Removal of hydrogen from steel during electroslag remelting, Dissertation, Donetsk, Moscow, 1985.
19. Korzun E.L., Elektrometallurgiya, 2001, No. 11, 3–8.
20. Molinero J., et al., in: 6th Eur. Elec. Steelmak. Conf., Dusseldorf, 1999, 51–57.

20.

Advances in Electrometallurgy 2010 ***8*** *(1) 61–73*
Translated from Sovremennaya Elektrometallurgiya 2010 ***8*** *(1) 51–60*

ENERGY AND RESOURCES SAVING

Periodic supply of magnesium portions in magnesium thermal production of $TiCl_4$

D.A. Listopad and I.F. Chervonyi

Zaporozh'e State Engineering Academy

The results of experimental investigations of the process of reduction of titanium tetrachloride in reactors with portion-periodic adding of magnesium under the layer of reaction mass are described. It was found that during this process its rate of reduction is growing at the initial period due to intensification of gas-phase reactions, the duration of high-temperature holding is reduced and the effectiveness of vacuum separation of the produced experimental block of reaction mass is increased.

Titanium is characterised by a valuable combination of the high mechanical properties and comparatively low density (4.5 g/cm^3). Titanium components have high heat resistance and especially high specific strength at temperatures of up to 600°C, in comparison with the main grades of steel and other metals for constructional publications, high specific creep strength, biocompatibility and the controlled structure and properties [1–3]. This advantage of titanium is especially evident in the case of titanium alloys whose specific strength can be increased 1.5–2.0 times and remains high at elevated temperatures, whereas many other structural materials greatly soften [4, 5].

At present, the world capacity in the production of titanium sponge is 181 900 t/year [6]. The main producers of titanium sponge and the fraction of production of these producers in the world production capacity in 2009 are shown in Fig. 1.

Recently, titanium has been used in chemical industry, medicine, in the manufacture of sports and different consumer goods, electronics, architecture, vehicle construction and engineering, aviation and space system components. In ferrous metallurgy, titanium is used as an alloying element of steel for reducing the grain size and as a deoxidation agent, for reducing the carbon content of stainless steel, and also in many other branches and applications.

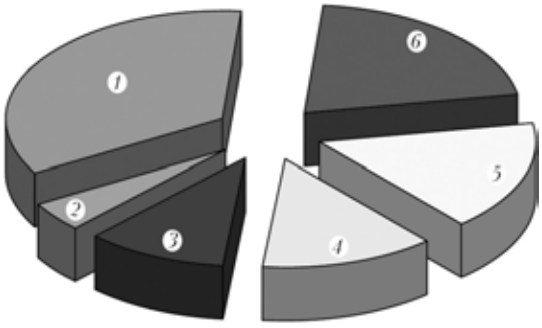

Fig. 1. Main world producers of titanium sponge and the fraction of production in the world production capacity in 2009:1) 34% China 67 000 t; 2) 4% Ukraine (ZTMK, 8500 t; 3) 11% USA (Alta, ATI and Allvac, Timet), 20400 t; 4) 13% Kazakhstan (UKTMK), 25000 t; 5) 17% Russia (VSMPO-AVISMA), 32 000 t; 6) 21% Japan (Sumitomo, Toho), 40 000 t.

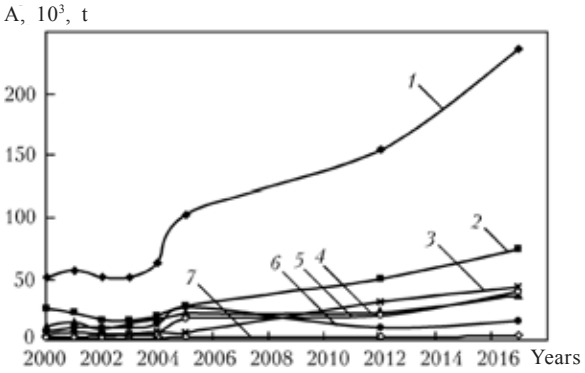

Fig. 2. Dynamics of world demand for titanium A: 1) total, 2) USA, 6 (European Union, 4) China, 5) Japan, 6) Russia, 7) Ukraine.

The requirement on titanium throughout the world is shown in Fig. 2 [7].

At present, the industrial production of titanium sponge is concentrated in magnesium thermal production of titanium tetrachloride (Kroll method). Regardless of the attempts to develop other technologies [8] (FFC–Cambridge [9], sodium-, calcium-, zinc- and alumothermal, electrolytic, hydrogen production and other variants), the Kroll method remains the main method in the production of primary titanium in countries – producers of titanium sponge. The reduction of $TiCl_4$ with magnesium is used at ZTMK (Zaporizh'e, Ukraine), ywo US plants (Titanium Metals Corp and Oregon Metallurgical Corp), two Japanese plants (Osaka Titanium and Toho Titanium Co Ltd), in Russia (VSMPO-AVISMA, Berezniki) and Kazakhstan (Ust'-Kamenogorsk, UKTMK) and also in China.

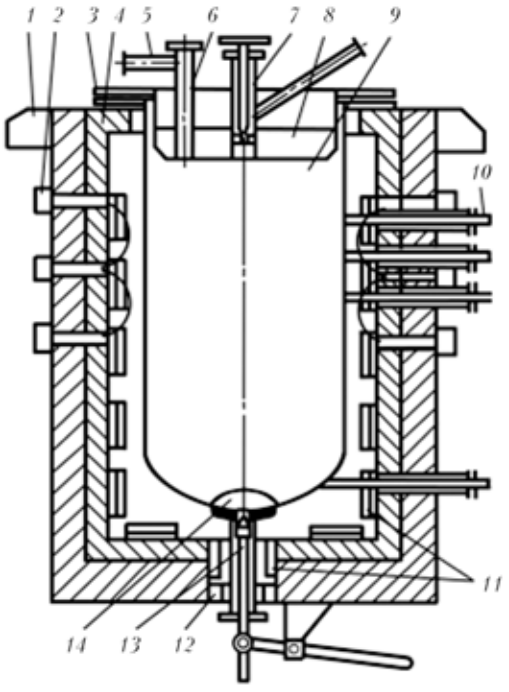

Fig. 3. Reduction equipment with lower discharge, placed in a furnace [10]: 1) the furnace support; 2) collectors for supplying and removing air; 3) water-cooled flanged joint; 3) vacuum treatment nozzle and the nozzle for supplying argon; 6) section 4 point magnesium; 7) the section for feeding titanium tetrachloride; 8) the cover of the reactor; 9) the reactor; 10) contact monitors (thermal sensors); 11) heaters; 12) sand gate; 13) the bar of the discharge device; 4) false bottom.

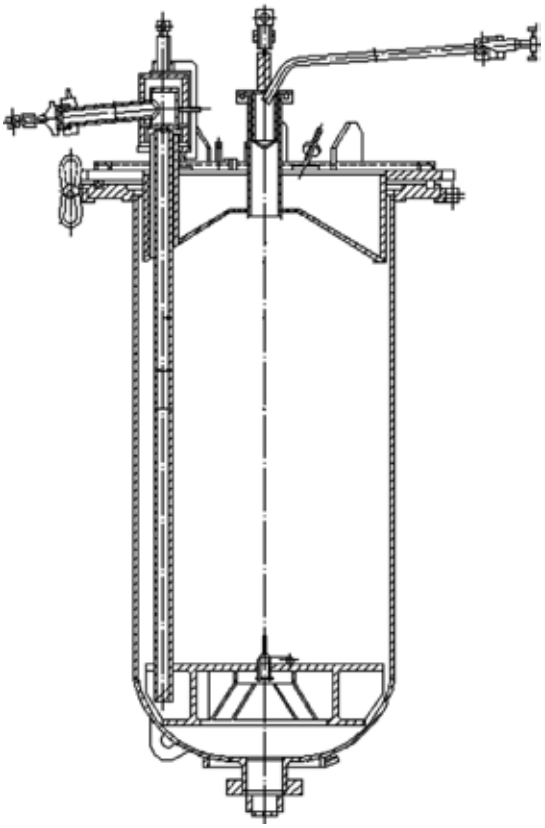

Fig. 4. The reactor for the reduction of titanium tetrachloride with upper discharge.

Equipment for producing titanium sponge by the magnesium–thermal method consists of an electric shaft furnace, a reduction reactor, the system for supplying $TiCl_4$, argon, water, and process control and regulation devices (Fig. 3). The internal surface of the furnace lining contains nickel–chromium heating elements distributed in the individual heating zones. The furnace also contains a system for cooling the reactor for supplying cold

and removing hot air.

The main element of the reduction reactors (Fig. 4) is a cylinder made of 12Cr18Ni10Ti stainless steel with a thickness of 15–25 mm with spherical dished ends and a water-cooled flange. The cover of the reactor is used for sealing the reactor. It contains the sections for the supply of initial substances and inert gas into the reactor, and also a device for discharging the magnesium chloride collected in the reactor.

Purified titanium tetrachloride is transferred into the hermetic reactor, filled with argon and purified magnesium. The reduction of titanium from its tetrachloride by magnesium is a complicated heterogeneous process accompanied by the generation of a large amount of heat and also by the continuous variation of the surface area of the resultant reaction mass (RM). The process and the nature of formation of the reaction mass are regulated by changing the rate of introduction of titanium tetrachloride, the production process temperature and the regime of discharge of magnesium chloride to produce products with controlled composition.

The resultant titanium has the form of a sponge (reaction) mass in which the pores are filled with magnesium chloride and unused magnesium. Titanium is purified by the process of vacuum separation, carried out in vacuum in equipment with temperatures of up to 1020°C. The heating rate of the block of reaction mass and of condensation of sublimated products [11] in the initial period are the main factors determining the rate of the vacuum separation process.

The sublimated and condensed (in the reversed flow retort) components of the reaction mass (condensates) are directed into circulation for use in the subsequent reduction process. Titanium in the form of a sponge block is pressed out from the retort.

The structure and physical characteristics (specific surface, porosity) of titanium sponge reflector the overall effect of individual parameters both during reduction and vacuum separation. The quality of the sponge block differs in individual parts and, therefore, it is necessary to carry out differentiated separation and grading. For this purpose, peripheral sections (skull, bottoms) rich in impurities are removed from the block. Subsequently, the titanium sponge is crushed and graded. The resultant material is the commercial product.

The Kroll method has been adopted because of the favourable combination of the properties in the Ti–TiCl4–Mg–$MgCl_2$ system. Magnesium is characterised by a considerably higher chemical affinity for chlorine in in comparison with titanium. Titanium, magnesium and magnesium chloride are mutually insoluble. The ratio of the melting and boiling points of magnesium and magnesium chloride is favourable for the process of production in a wide temperature range from 720 to 1410°C.

However, the maximum temperature is a restricted by the stability of steel equipment because at temperatures below 1000°C the contact of titanium with a steel of the reactor may result in the formation of an eutectic and burning-through of the reactor wall, and also in the transfer of iron and nickel into the adjacent sponge layers in the vicinity of the wall to a depth of approximately 20–40 mm followed by contamination [12, 13].

The mechanism of the processes of reduction and formation of the titanium sponge has been studied in considerable detail and described in [14–18]. The main relationships and limiting stages of the process can be characterised as follows:

–the reduction of titanium tetrachloride by magnesium is a complicated physico–chemical process in which several reactions take place simultaneous or consecutively. For example, in the actual conditions of industrial production, the reduction process is discrete (not continuous), and the conditions of the reactions in individual stages and even in different zones of the reactor constantly change, like the nature of the process:

–the rate of the reduction process is determined by both the rate of supply of $TiCl_4$ into the reactor and by the transfer (diffusion) the sensors of magnesium into the reaction zone and magnesium dichloride from the zone, and also by the associated heat transfer processes.

As the feed rate of $TiCl_4$ increases the rate of the process also increases but the rate of reduction is limited by both the rate of supply of magnesium into the reaction zone and by the rate of removal of heat from the zone in the reaction products;

–keeping the free titanium in the pores of the sponge, especially at the end of the process, restrict the rate and the efficiency of the reduction process and, consequently, the coefficient of utilisation of magnesium in the industrial conditions does not exceed 60–65%;

–with increasing temperature the rate of the process increases by the increase of temperature above 850°C leads to the formation of a fine-grained structure which complicates the process of vacuum separation, and also to the formation of local superheating and melting of the reactor wall as a result of the formation of a low-melting eutectic;

–the reduction reaction takes place with the decrease of the rate and pressure in the volume of the reactor as a result of a decrease of the open surface of magnesium and the variation of the phase composition of the reacting substances;

–the rate of the reduction process has a strong effect on the structure of the titanium sponge block and its porosity and this influences the vacuum separation process. The high rate of the reduction process of formation of a titanium sponge block with a large amount of fine pores, complicating the process of vacuum separation and production of titanium sponge with the required amount of chlorine, nitrogen, oxygen and other admixtures. Therefore, to intensify the process of production of titanium tetrachloride and vacuum separation of the reaction mass it is necessary to determine the optimum conditions of the feed rate of titanium tetrachloride, discharge of magnesium chloride from the retort, and also the process of separation of the reaction mass.

At the same time, the magnesium–thermal method has the following shortcomings:

–insufficient efficiency of the utilisation of the volume of the reduction reactor because all the main reactions of reduction of titanium tetrachloride (and of initial materials and lower titanium chlorides as intermediate products) takes place in the upper part of the reactor – on the surface of the magnesium melt, the resultant titanium dendrites and in the gas phase. All the remaining volume at the start of the process is occupied by the magnesium melt which is later displaced by the resultant titanium sponge and magnesium dichloride. Prior to each discharge of magnesium dichloride the reaction zone travels upwards along the height of the reactor, and if the discharge of magnesium chloride is not carried out efficiently, the reaction zone may move even below the cover resulting in premature failure and interruption of service as a result of corrosion. In addition, the constant positioning of the reaction zone in the upper part of the reactor supports high-intensity high-temperature corrosion of the reactor material in the zone because of the presence of titanium and magnesium chloride. This reactor zone is subjected to additional static loading at 820–850°C under the effect of the reactor mass, loaded magnesium and the resultant titanium sponge and magnesium dichloride. Consequently, the high-intensity reduction process results in the formation of a nonuniform thermal fields in the upper part of the reactor along its height – a large amount of heat is generated in the upper part, and in this zone must be often cooled with an air flow, and the lower part must be additionally preheated with nickel–chromium heating elements, situated in the appropriate zones of the furnace. This list of the formation of scale on the external surface of the reactor. All these factors cause premature failure of the expensive retorts and additional contamination of the titanium sponge with the alloying components of the reactor material;

–long low-productivity vacuum separation process. The total production cycle in the reactor results in the formation of the reaction mass in the form of the titanium sponge block saturated with magnesium and magnesium chloride. These compounds are removed from the block by vacuum separa-

tion, based on sublimation of the vapours of magnesium and magnesium chloride from the reaction mass into the reciprocal retort in vacuum. This process consists of three stages: degassing and heating of the reaction mass; high-intensity evaporation from the surface of the reaction mass and large symbol or the of magnesium and magnesium chloride; evaporation mainly of magnesium chloride and the remaining amount of magnesium in the fine pores. This is the longest process, representing 65–75% of the total duration of the separation process. The duration of the third period depends on the path length of the magnesium chloride vapours. The longest path is that of the vapours of Mg and $MgCl_2$ from the central zone of the industrial block. Therefore, the sublimation of the last 2–2% $MgCl_2$ is the stage of the process of vacuum separation with the highest energy requirement and the longest duration. For example, the separation of 1 t of titanium sponge requires theoretically 1500 kW h of electrical energy, and the consumption in practice is 3–4 times higher [19];

–the need to carry out labour-intensive and long operations with the separation of the titanium sponge block, with the variation of the shape, dimensions and the weight of the sponge blocks, produced in the equipment of the same dimensions, and also nonuniform strength of the titanium sponge blocks in different zones and the heterogeneity of the shape, especially in the upper part. Preliminary separation of the block takes place in hydraulic presses about because of the slipping of the block from below the tool, with the block lying freely on the press stable, disintegration is possible after removal of relatively large pieces, thicker than 0.3 m. The duration of the operations with the orientation of the pieces of titanium sponge on the press amounts up to 15% of the total processing time. More than 80% of the total time in the process is used for the preparatory operations: feeding the sponge under the blade of the press stable, idling direct and reversed movement of the blade. The efficient utilisation of the press power does not exceed 5% [20]. All these difficulties form as a result of the nonuniform structure of the titanium sponge block – the density of titanium sponge in the individual zones of the block varies in the range 1–3 t/m^3, decreasing from bottom to top and from centre to periphery. The blocks of the same dimensions can be characterised by different mean density, depending on the conditions of metal thermic production. The large blocks in most cases are characterised by the highest density in the lower part. The height and mass of the blocks, produced in the reactor's of the same standard size, may differ by 5–10% from the mean level [20].

The aim and tasks of experiments

Investigations were carried out into the process of magnesium–thermal reduction of titanium tetrachloride in portions–periodic feeding of magnesium and the layer of the produced reaction mass taking into account the possibilities of eliminating the shortcomings of the Kroll method.

To solve this problem, it was necessary to fulfil the following tasks:

–design of equipment for melting and loading magnesium, ensuring the supply of magnesium portions discharge of magnesium chloride during the production of titanium tetrachloride;

–develop a procedure for the operations and conditions of reduction of titanium tetrachloride during portional feeding of magnesium, ensuring the optimum rate of reduction and vacuum separation, and also the high quality of the produced titanium sponge;

–determine the effect of the method of loading magnesium on the special features of the process of reduction of titanium tetrachloride and subsequent vacuum separation of the produced reaction mass;

Experimental procedure

The experimental equipment is shown in Fig. 5. Equipment consists of two main systems: the reduction (reactor) system and the system for melting and supplying magnesium.

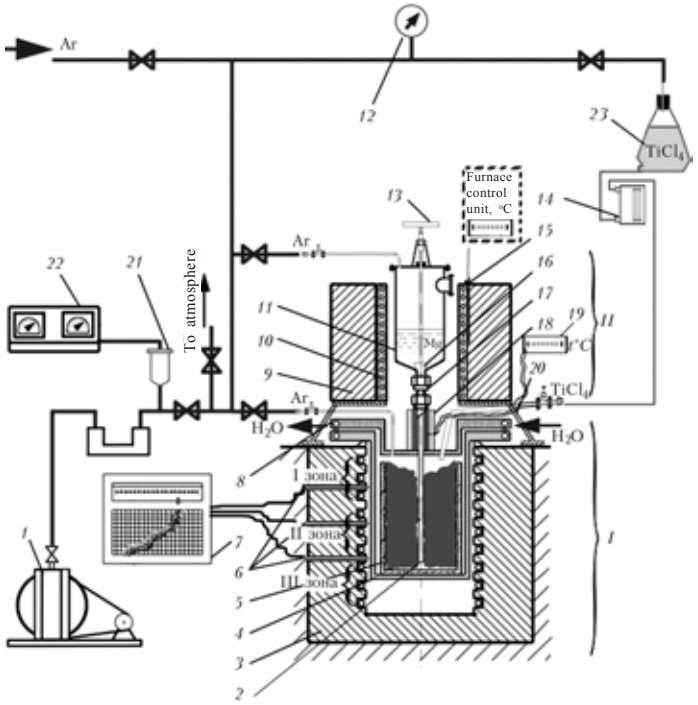

Fig. 5. Experimental equipment for producing titanium sponge by magnesium–thermal reduction of titanium tetrachloride with portional–periodic supply of the magnesium melt into the reactor: I) the reduction equipment, II) equipment for melting magnesium; 1) VN-461 vacuum pump; 2) loading pipe; 3) the electric furnace; 4) the reactor; 5) the reaction vessel; 6),-alumel thermocouple is; 5) the cover; 8) KSP-4 potentiometer; 9) electric furnace for melting magnesium; 10) of the heaters of the melting furnace; 11) the melting device; 12) OBMV1-100 vacuum pressure metre; 13) the valve of the closing bar; 14) RS-3A flow meter; 15) chromel-alumel thermocouple of the melting furnace; 16) the closing bar; 17) the section for securing the melting device to the loading system of the reactor; 18) the tubular heaters; 19),-alumel potentiometre; 20) the base of the melting furnace; 21) thermoelectric converter PMT-2; 22) V IT-1A vacuum metre; 23) discharge container for titanium tetrachloride.

The former is produced from 12Cr80Ni10Ti stainless steel and consists of a reactor was a water-cooled flange hermetically sealed with a cover. The reduction process is realised in the reaction vessel with the internal diameter amounted to millimetre and a height of to 50 mm into which the first magnesium charge is loaded prior to the start of the experiments. To maintain the required temperature of the losses of reduction the reactor is placed in a shaft electrical furnace. The supply of liquid titanium tetrachloride into equipment takes place from a discharge container. The shielding atmosphere in the system is generated by supplying argon through a nozzle in the cover of the reactor.

The system for melting magnesium, produced from stainless steel, is placed in a tubular electric furnace. The charge of magnesium pieces is fed into the melting systems through a loading window, sealed with heat resisting rubber. Molten magnesium is supplied into the reduction reactor through a gate device and a loading pipe. The melting systems is secured to the loading time using a fixing section, and is heated (to avoid solidification of magnesium) with a tubular heating element.

The investigations were carried out using purified titanium tetrachloride, grade OChT-0, MG-0 magnesium, gaseous argon of the first sort (GOST 10157-79). Measurements of the content of impurities in the produced titanium sponge from the experimental processes were taken in accordance with GOST 9853.24-96.

Four reduction and vacuum separation processes were carried out in accordance with the experimental procedure, and a single process by traditional (basic) technology.

For the production processes, a charge of 85 g of magnesium was loaded into the reaction vessel and placed in the reactor. The

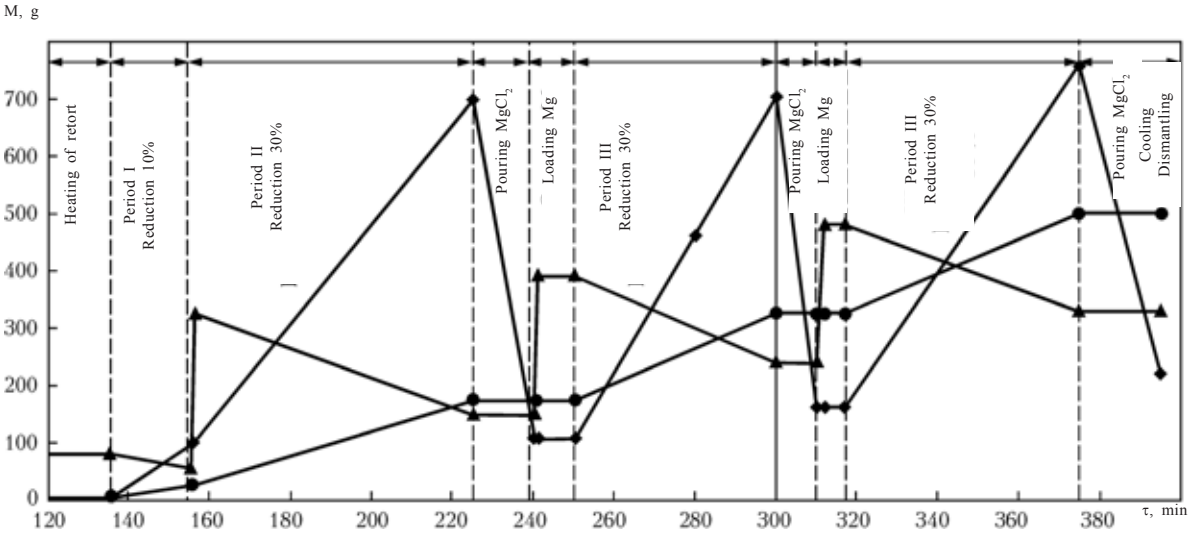

Fig. 6. Graphs of the variation of the mass M of substances in the experimental Reactor during the production process: ▲) magnesium; ●) titanium; ◆) magnesium dichloride.

reduction apparatus was assembled, placed in the furnace and evacuated to 50 Pa, with water is supplied for cooling the flanges. This was followed by heating of the furnace.

After drying at 120°C with simultaneous evacuation, the reduction apparatus was filled with argon up to 120 kPa, and after melting magnesium (after reaching the temperature of 800°C) titanium tetrachloride was supplied into the apparatus. The feed rate of titanium tetrachloride was regulated in ending on the stage of the process and pressure in the apparatus. It was 0.104–0.170 g/cm^2·min (62.4–102 kilograms/m^2 h).

During this period, the next portion of magnesium (255 g) was melted in the melting system. After loading into the apparatus the calculated amount of titanium tetrachloride (in accordance with the accepted coefficient of utilisation of magnesium of 60%), the feeding of titanium tetrachloride was interrupted, magnesium was poured from the melting systems through the loading pipe into the reaction vessel, and the reduction process was restarted.

Prior to feeding the third and subsequent portions of magnesium, the melting system was dismantled, the discharge device was assembled, and the processed melt of magnesium dichloride was supplied through the loading pipe under the excess pressure of argon.

The total load of the magnesium in the process reached 850 g, and the portions consisting of the first portion of 85 g and three 225 g portions, i.e., initially 10% of the required amount was loaded and this was followed during the process by additional pouring of three times of 30% of the total load. A total of 1990 g was supplied. After subsequent discharge of magnesium dichloride, the system was cooled down at, dismantled into the separation equipment and this was followed by vacuum separation of the produced reaction mass.

Figure 6 shows the graph of the variation of the mass of substances in the reactor during the reduction process which shows clearly the dynamics of formation and use of these substances. The arrests in the figure corresponds to the periods of pouring magnesium and discharging magnesium dichloride. The origin of the time counting axis was 120 min which was associated with the duration of sealing, drying and heating of the reduction system to the required temperature. The graph shows that with the buildup of titanium, the zone of reduction which takes place on the surface of the resultant sponge, gradually moved along the height of the reaction vessel during the experiments. Correspondingly, the volume of the gas space above the surface of the melt under sponge, amounting to 90%

of the beginning of the process, gradually decreased and at the end of the process equal to 10–20% of the reaction volume. At the end of the production process, the reaction mass occupied 80–90% of the volume of the reaction vessel. The height of the titanium sponge block, produced after vacuum separation, reached 170–200 mm, weight 480–490 g.

The maximum loading rate of titanium tetrachloride for the reactor of the given design (102 kg/m^2 h) was limited by the conditions of evaporation of titanium tetrachloride in the reaction vessel. A further increase of the rate resulted in the partial displacement of the reaction zone under the cover and clogging of the cover of the system.

The stability of loading the portions of the molten magnesium and the layer of the reaction mass formed in the experiments is of the utmost importance in the reduction technology. The experiments show that this operation is feasible.

During pouring the reaction agent, the pressure in the reduction equipment was lowered, and excess argon pressure was generated in the melting system of the molten magnesium. The maximum excess pressure of argon in supplying the final portion of magnesium was 165 kPa. This ensured relatively fast displacement of molten magnesium into the reduction system.

The graph of the discharge of magnesium dichloride and the increase of the level of the dichloride in the reaction were calculated and organised to avoid of the losses of residual magnesium from the system and improve the conditions of transport of the reduction agent to the reaction zone to the surface of the growing sponge when supplying the next portions of magnesium.

The graphs of variation of the temperature of the furnaces of the reduction in melting systems in the experiments are shown in Fig. 7.

The temperature in the reaction vessel was maintained in the range 800–850°C. This was controlled by the deposition of the vessel in relation to the furnace zones and automatic regulation of temperature in the individual zones.

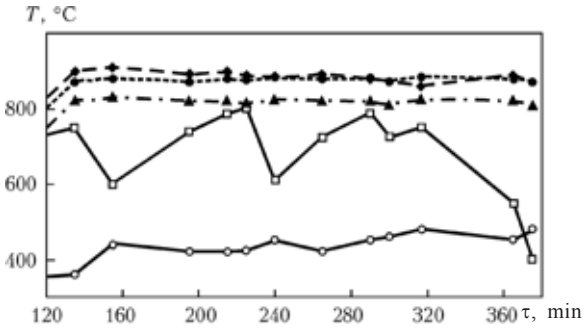

Fig. 7. Graph showing the variation of temperature in the furnaces of the reduction equipped bent and the melting system during the experiments:▲) the first zone; ●) the second zone; ●) the third zone; ○) the temperature to which the mains is heated; □) the temperature in the melting furnace.

The gradual variation and lifting of the front of the reduction process in the reaction vessel, accompanied by the generation of the excess amount of heat in the thermal chemical reaction, was recorded on the basis of the variation of the duration and frequency of activation of the heaters of the individual zones.

The reduction process was realising a quick and the pressure in the range 105–125 kPa and, if necessary, the pressure was corrected by feeding in argon the small rising of the pressure level took place at the start of the process in initial feeding of titanium tetrachloride, and also in the final stage of the process after loading the final portion of magnesium.

Consequently, it was necessary to reduce the feed rate of titanium tetrachloride in these periods to 62.4–84.0 kg/m^2 h. The pressure in the reactor also increased during the consumption of the calculated amount of magnesium (55–60%) after each pouring in, since the amount of the evaporated titanium tetrachloride started to exceed the amount used for production.

After feeding the final portion of titanium tetrachloride the reduction equipment was dismantled, sealed end cooled to the temperature of the environment, followed by vacuum thermal purification of the produced reaction mass. The cover of the system with the loading pipe was dismantled, a thermal screen

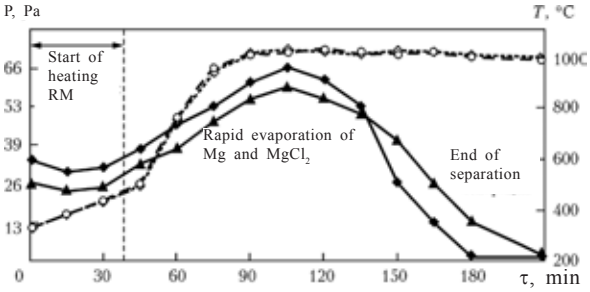

Fig. 8. Variation of pressure P and temperature in the reaction during vacuum separation of the experimental and conventional blocks: ◆, ▲) the pressure in the experimental equipment and comparison system, respectively; ○, ◇) the temperature of the furnace in the experimental process and the comparison process, respectively.

was positioned at a water-cooled condenser was installed above the reduction reactor. The separation equipment was placed in the shaft electrical furnace, the argon supply system was activated together with water cooling and evacuation, and the process of heating and vacuum treatment of the reaction mass started.

Preliminary pumping was carried out using a AVZ–20 mechanical vacuum pump. When the pressure and the outlet from the separation equipment dropped to 30 Pa the booster pump VN-461 for deep vacuum pumping was activated. The pressure of the outlet from the separation equipment was measured using thermocouple vacuum metres VIT-1A and VT-2A. High-temperature holding was performed at 980–1020°C and completed when the pressure reached 3.5–3.0 Pa. Leakage of equipment was checked after five min and the results show that there was no leakage.

Figure 8 shows the graph of the variation of temperature and pressure in the equipment during vacuum separation. The start of the increase of pressure during continuous pumping was detected at temperatures higher than 600°C and is associated with the start of rapid sublimation of Mg and $MgCl_2$.

The yield of the skull sponge in the experiments was 5–12%, which is approximately half the value in the conventional method. Evidently, this is caused by the fact that the transport of magnesium into the reaction zone in the final stage of the process is almost completely limited by the capillary processes in the sponge, and the distribution of the capillaries in the cross-section of the block was relatively uniform.

The examination of the titanium sponge, purified by vacuum separation, shows that the titanium sponge block has a laminated structure with the dimensions of the layers in the lower part of the block relatively proportional to the portions of the welded magnesium. The structure of the sponge, produced in the experiments, is shown in Fig. 9.

The laminated structure of the produced blocks is determined mainly by the change of the mechanism and of the rate of the reduction reaction during the process. The nature and distribution of the large pores (more than 500 μm) corresponds to the direction of movement of the rising flows of magnesium and descending flows of the resultant magnesium dichloride.

The main size range of the finer pores was 50–200 μm, and the total porosity of the sponge reached 20–50% at a density of

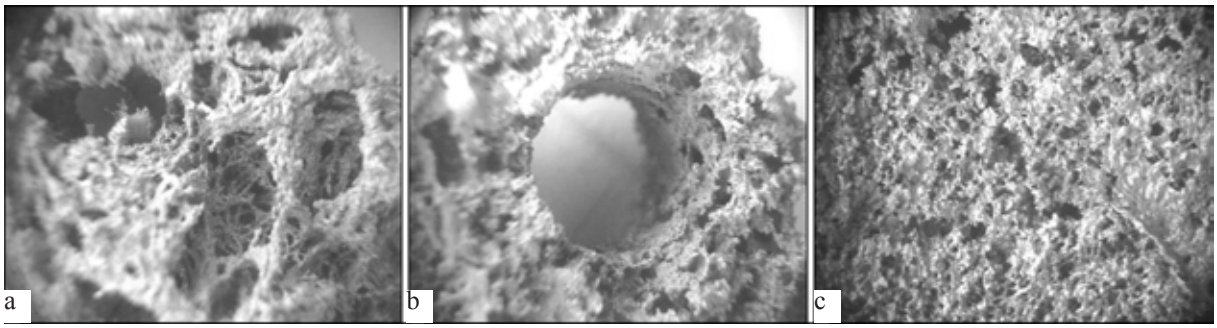

Fig. 9. Structure (×5) of titanium sponge produced in the experimental equipment: a) the centre of the block; b) the hole left by the pipe; c) the surface of the block.

1.2–2.5 g/cm^3. The structure of the block reduces the duration of high-temperature holding in the process of vacuum separation of the block of the reaction mass.

The mass fraction of the main impurities in the produced sponge is as follows, %: 0.020–0.046 Fe; 0.032–0.037 Ni; 0.040–0.050 O; 0.01–0.02 N; 0.023–0.050 Cl, which corresponds to the content of these elements in the commercial titanium sponge, grades TG-90-TG-120.

Experimental results and discussion

The supply of the first auction of magnesium and titanium tetrachloride into the reactor results in the start of the reduction reaction. The initial titanium dendrites are used as a refining adsorbent of the impurities from magnesium which combines with them, and settling on the bottom of the reactor, forms, in the bottom part of the block, brittle structures of the compounds of titanium with impurities.

When supplying the next portion of magnesium through the bottom part of the block refining takes place on the titanium dendrites in the bottom part of the block. The already refined magnesium and testy reactions on and ensures the high rate of the reduction process and of the formation of high-quality sponge.

The mechanism of the process of reduction in portional-periodic feeding of magnesium and delay of the reaction mass may be described as follows. In the initial period of reduction, the mechanism is characterised by a high rate, and the increase of the volume of the gas phase above the surface of the magnesium melt makes it possible to double the intensity of the gas phase reactions, formation of localised and active centres of the start of the process. These reactions are shown in Fig. 10.

In the experimental processes the rate of supply of titanium tetrachloride and the rate of reduction in the initial period (for the first and second magnesium charge) is 1.2–1.5 times higher than the rate of requirement of titanium tetrachloride for the basic process, and the duration of the incubation period of the process is shortened (Fig. 6).

Further, with the development of the surface of the resultant titanium sponge, the mecha-

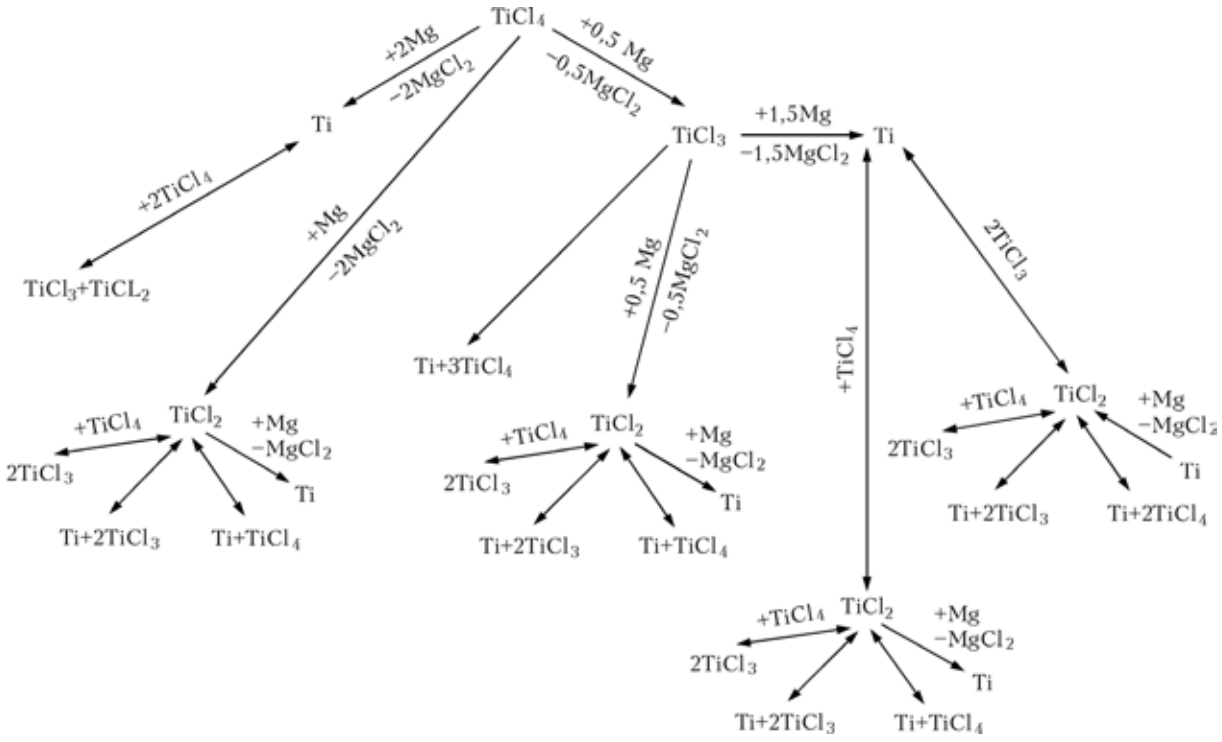

Fig. 10. Diagram of gas-phase reactions, taking place above the melt surface.

nism of the experimental process does not differ greatly from the conventional process.

Special attention has been given to the processes of formation of titanium on the surface of the sponge and also on the walls of the reactor and the loading pipe wetted by molten magnesium and magnesium dichloride. The high rate of formation of the lower titanium chlorides may cause a slight reduction of the quality of the magnesium dichloride melt.

However, as shown by the experiments, the titanium content of the discharged magnesium dichloride didn't exceed the permissible level (0.005%), and there was no clogging of the loading pipe with the sponge. This confirms that a relatively extensive additional reduction of the lower titanium chlorides took place during the process. This additional reduction usually takes place on the surface and in the capillaries of the sponge (through the adsorption stage), on the surface of the magnesium melt and in the magnesium dichloride melt during its counter flow phase separation with magnesium.

Since the experiments resulted in the formation of a coarser crystalline sponge, it is evident that additional reduction took place preferentially through the stage of the solution of titanium dichloride in molten magnesium dichloride.

A special feature of the mechanism of the reduction process in portional-periodic supply of magnesium is the important role of the magnesium dichloride in transport of the reduction agent of the reaction zone in the final stage of the process. The presence of the titanium block and a small volume of the final charge of magnesium requires incomplete discharge of magnesium dichloride and the formation of a 'cushion' of the $MgCl_2$ melt which makes it possible, as a result of delamination, to accelerate the transport of the magnesium-reduction agent through the capillaries into the reaction zone.

The process of reduction using the entire calculated mass of the reagents (magnesium and titanium tetrachloride) resulted in the formation of blocks of reaction mass which were subjected to vacuum separation. Comparison of the grouse of the valuation of residual pressure in separation of blocks (Fig. 8), produced by the experiments and basic reduction technologies, indicates the intensification of the process in the case of the experimental block of the reaction mass.

The experimental block of the reaction mass (Fig. 11a) differs from the block of the reaction mass produced by the basic logic (Fig. 11b) by the fact that it contains a continuous hole in the centre of the block.

Since the rate of evaporation of the volatile components of the reaction mass is proportional to the evaporation surface, the presence of a continuous hole in the centre of the block after extracting the loading pipe increases the rate of evaporation process in the first stage of vacuum separation.

In the second stage of the separation process, the presence of a continuous hole intensify is the diffusion processes whilst reducing the length of the path of the magnesium dichloride vapours through the capillaries in the titanium pipe. This resulted not only in many reduction of the duration of separation for the experimental reaction mass by 10–15% (30 min) but also reduce the residual content of the chlorine ion in the produced titanium sponge.

The rate of evaporation from the capillary in the titanium sponge block depends on the position of the meniscus of the magnesium

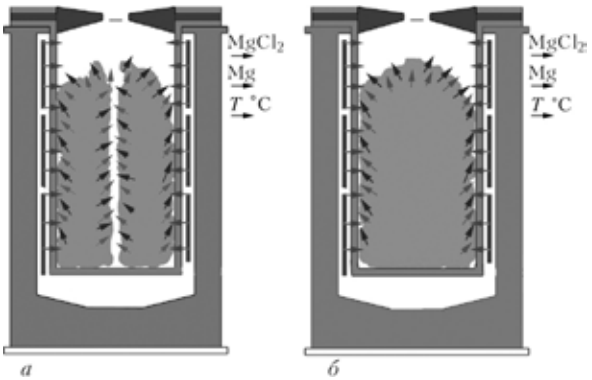

Fig. 11. Diagram of vacuum separation of the reaction mass produced in portional-periodic supply of magnesium under the melt layer (a) and in traditional charging of the magnesium melt (b).

melt and magnesium chloride in relation to the edge of the capillary.

The mass density of the flow of the vapours of the substance is determined by the following equation:

$$M = \frac{P_0 D\mu}{RTl} \ln\left(\frac{P_0 - P_1}{P_0 - P_S}\right)$$

where M is the mass density of the vapour flow, g/(s cm^2); l is the distance from the surface of the melt to the edge of the capillary, cm; μ is the molar mass of the vapour, g/mole; R is the universal gas constant, J/(mole K); P_0 is the total pressure in the system, Pa; P_1 is the partial vapour pressure, Pa; P_S is the saturated vapour pressure, Pa; D is the diffusion coefficient, cm^2/s; T is temperature, K.

The rate of evaporation of the substances is described by the following equation:

$$v = \frac{M}{\rho}$$

where ρ is the density of the evaporated substance, g/cm^3.

The distance from the evaporation surface of the titanium sponge block (the length of the capillary) is assumed to be equal to l and, consequently, the length of the capillary in the titanium sponge block, produced by the experimental technology, is 0.5 l. This is explained by the fact that the hole formed by the loading pipe is situated in the centre of the experimental block, and the distance which must be travelled by the separated magnesium and magnesium chloride is equal to half the radius (it is assumed that magnesium and magnesium dichloride evaporated from the cylindrical pipe of the reaction mass block). Consequently, if all other conditions of vacuum separation of the experimental and conventional blocks of the reaction mass car the same, and also the characteristics of substances in the amount of the substances in the reaction mass is the same, the difference in the mass density of the vapour flow from the experimental block M_{exp} in comparison with the conventional block M_0 is:

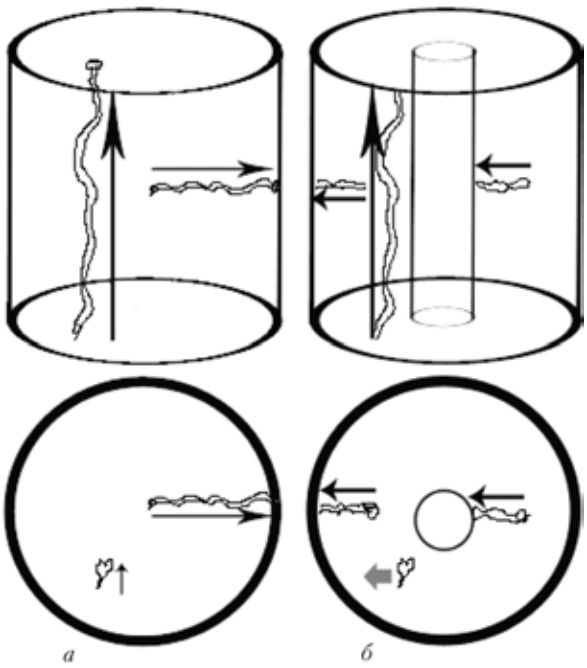

Fig. 12. Diagram of evaporation (separation) of magnesium and magnesium dichloride from the titanium sponge blocks produced by the conventional (a) and experimental (b) technologies.

$$\frac{M_{exp}}{M_0} = \frac{1}{0.5}$$

i.e., the mass density of the vapour flow from the experimental block is twice the mass density of the vapour flow from the conventional block ($M_{exp} = 2M_0$).

The creation of suitable conditions for the formation of open or continuous capillaries in the reaction mass block ensures a large increase of the rate of separation and reduces the duration of the processes of production of titanium sponge. The proposed process is shown in Fig. 12.

Conclusions

1. It has been sure possible to supply portions of magnesium below the layer of the resultant reaction mass during the production process.

2. The process of refining of magnesium

has been intensified and the extent of refining increased to the maximum value.

3. The efficiency of the vacuum separation of the reaction mass in the process of portional-periodic supply of magnesium has been increased.

4. The productivity of equipment in the initial stage of the reduction process has been increased as a result of the intensification of the gas-phase reactions above the melt surface.

5. The duration of high temperature holding during vacuum separation of the blocks, produced in the process of portional-periodic supply of magnesium, has been shortened.

6. Titanium sponge was produced with a high yield of annual production as a result of reducing the degree of contamination with the impurity elements transferred from the reactor material.

References

1. Garmata V.A., et al., Metallurgy of titanium, Metallurgiya, Moscow, 1966.
2. Garmata V.A., et al., Metallurgy of titanium, Metallurgiya, Moscow, 1983.
3. Pol'kin I.S., et al., Using titanium in various branches of industry, Ti-2006 in CIS, Institute of Physics of Metals, Kiev, 2006, 28–38.
4. Pol'kin I.S., Hardening heat treatment of titanium alloys, Metallurgiya, Moscow, 1984.
5. Kolachev B.A., et al., Physical metallurgy and heat treatment of nonferrous metals and alloys, Moscow Institute of Steel and Alloys, Moscow, 1999.
6. Aleksandrov A.V., Development of the titanium market in the CIS, Proceedings of the international conference, Institute of Physics of Metals, Kiev, 2009.
7. Hart A. and Perre W., Prospects for consumption of titanium, in: International conference 'Titanium', San Diego, October 2006, 109–112.
8. A new methods of production of Ti sponge uwing SOM technology, Shanghai Metals, 2005, No. 2, 40–43.
9. Krivoruchko N.P., et al., Zb. Nauk Prats' Zaporiz. Derzh. Inzh. Akad. Ser. Metalurgiya, 2004, No. 10, 59–64.
10. Mal'shin V.M., et al., Metallurgy of titanium, Metallurgiya, Moscow, 1991.
11. Yatsenko A.P., et al., Ti-2008 in CIS, Proc. Int. Conf., St Peterburg, 2008, Proceedings of the international conference, Institute of Physics of Metals, Kiev, 2008, 149–157.
12. Chervonyi I.F., et al., Titan, 2007, No. 1, 5–12.
13. Teslevich S.M., et al., Advances in Electrometallurgy, 2004, No. 2, 45–48.
14. Sandler R.A., ZhPKh., 1960, No. 5, 1013–1017.
15. Vlasov V.V., et al., Tr. VAMI, 1966, No. 57, 208–217.
16. Pampushko A.N., Tsvetn. Metallurg., 1988, No. 9, 21–23
17. Ogurtsov S.V., Titan and Ti alloys, 1961, No. 6, 3–13.
18. Listopad D.O., et al., Visti Akad. Inzh. Nauk Ukraini, 2008, No. 2, 25–34.
19. Sergeev V.V., et al., Metallurgy of titanium, Metallurgiya, Moscow, 1979.
20. Sandler R.A., et al., Processing of titanium sponge blocks, in: Problems in nonferrous metallurgy, Metallurgiya, Moscow, 1987.